

Aus dem Bereich Physiologie
Theoretische Medizin und Biowissenschaften bzw. Klinische Medizin der
Medizinischen Fakultät
der Universität des Saarlandes, Homburg/Saar

Odorant responsiveness of mouse olfactory sensory neurons

Dissertation zur Erlangung des Grades eines Doktors der
Naturwissenschaften der Medizinischen Fakultät
der UNIVERSITÄT DES SAARLANDES
2016
(entsprechend dem Jahr der mündl. Prüf.)

vorgelegt von: Bassim TAZIR
geb. am: 18.01.1982 in Ain Berda, Algeria.

_____ * alternativ

Aus der-Klinik,
Universitätsklinikum des Saarlandes, Homburg/Saar
(fakultativ zusätzlich: Direktor: Prof. Dr. Dr. Frank Zufall)

Table of Contents

1 ABSTRACT	9
2 INTRODUCTION.....	11
2.1 Evolutionary aspect of the olfactory system.....	11
2.2 Organization of the mouse olfactory system	12
2.2.1 Main olfactory epithelium.....	12
2.2.2 Vomeronasal organ	14
2.2.3 The septal organ of Masera	16
2.2.4 Grueneberg ganglion.....	17
2.3 Physiological properties of olfactory sensory neurons	18
2.3.1 Membrane properties of olfactory sensory neurons	18
2.3.2 Odorant-induced currents.....	19
2.4 Transduction pathway signaling	20
2.4.1 cAMP signaling.....	20
2.4.2 Additional signaling pathways	22
2.5 Trace amine-associated receptors.....	22
2.6 Spontaneous activity of olfactory sensory neurons.....	23
2.7 Mechanical response of olfactory sensory neurons	23
2.8 Ca ²⁺ activated Cl ⁻ channel (TMEM16b, Ano2).....	24
2.9 The voltage-gated sodium channel Nav1.7.....	25
2.10 Progress in olfactory receptor-ligand identification.....	27
2.11 Olfactory receptor responsiveness.....	29
2.12 Axon guidance.....	30
2.13 Aims of the thesis	32
3 MATERIALS AND METHODS	33
3.1 Animals	33
3.2 Electrophysiology experiments	34
3.2.1 Dissecting the olfactory epithelium.....	34
3.2.2 Visualizing fluorescent dendritic knobs	35
3.2.3 Patch clamp recordings.....	35
3.2.4 Odorant stimulation	37
3.3 Genotyping.....	40
3.3.1 Genomic DNA extraction.....	40
3.3.2 Polymerase chain reaction	40
3.3.3 Agarose gel electrophoresis	40
3.4 Immunohistochemistry	42
3.5 X-gal staining	44
3.6 Data analysis and statistics.....	45
4 RESULTS	46
4.1 The MOR256-17 mouse strain tagged with GFP	46
4.2 Electrophysiology of MOR256-17-IRES-tauGFP and SR1-IRES-tauGFP olfactory sensory neurons.....	48
4.2.1 Monitoring the state of the cells during recordings.....	48
4.2.2 Spontaneous activity analysis	49
4.2.3 Current-induced activity analysis.....	51
4.2.4 Extremely broad responsiveness of MOR256-17 OSNs.....	52
4.2.5 Similar odorant responses of MOR256-17 neurons in the MOE and the SO	57

4.2.6 Comparison of odorant response profiles of MOR256-17 OSNs and SR1 OSNs	59
4.2.7 Differences in odorant response properties between SR1 and MOR256-17 OSNs	64
4.2.8 Dose-response curves	65
4.3 Nav1.7 Knockout in specific subpopulation M71 OSNs	67
4.4 Tm16b Knockout in specific subpopulation M71 OSNs	71
5 DISCUSSION	73
5.1 Intrinsic membrane properties of SR1 and MOR256-17 neurons	74
5.2 Extremely broad odorant responsiveness of MOR256-17 OSNs.....	75
5.3 Discrepancies with heterologous systems	80
5.4 Why does the mouse olfactory system employ broadly responsive ORs?	82
5.5 Neural activity and axonal guidance	84
5.6 Summary.....	86
6 REFERENCES.....	87
7 PUBLICATIONS AND ACKNOWLEDGMENTS	101
7.1 Publications.....	101
7.2 Acknowledgments	101
8 CURRICULUM VITAE	ERROR! BOOKMARK NOT DEFINED.

List of figures

Figure 2.1. Mouse olfactory subsystems	12
Figure 2.2. Olfactory epithelium	13
Figure 2.3. Axonal wiring of vomeronasal neurones	15
Figure 2.4. Morphology of Grueneberg ganglion	17
Figure 2.5. cAMP transduction pathway	21
Figure 3.1. Dissection of the main olfactory epithelium	34
Figure 3.2. Epiemental setup used for patch clamping	36
Figure 3.3. Detection of GFP OSNs	36
Figure 3.4. Preparation of the stimulation pipette	37
Figure 3.5. PCR protocol for genotyping	41
Figure 4.1. The olfactory system of MOR256-17-IRES-tauGFP mouse strain	46
Figure 4.2. Axonal wiring of MOR256-17-IRES-tauLacZ	47
Figure 4.3. Monitoring the neurons during recordings	48
Figure 4.4. Spontaneous activity of MOR256-17 and SR1 OSNs	49
Figure 4.5. Spontaneous activity analysis of MOR256-17 and SR1 OSNs	50
Figure 4.6. The firing pattern of MOR256-17 and SR1 OSNs	51
Figure 4.7. Strongest odorant response of MOR256-17 OSNs	53
Figure 4.8. Weakest odorant response of MOR256-17 OSNs	54
Figure 4.9. Non-activating odorants of MOR256-17 OSNs	54
Figure 4.10. Average peak current responses of MOR256-17 OSNs	56
Figure 4.11. Similar responses of MOR256-17 OSNs in the MOE and SO	58
Figure 4.12. Average peak current responses of SR1 OSNs	61
Figure 4.13. Traces of inward odorant current	62
Figure 4.14. SR1 and MOR256-17 OSNs respond to a variety of chemical compounds	63
Figure 4.15. Odorant-induced currents for the common ligands of SR1 OSNs and MOR256-17 OSNs	64
Figure 4.16. Dose-response curves for selected odorants	65
Figure 4.17. Dose-response curves analysis	67
Figure 4.18. Breeding strategy to generate M71 OSNs fNav1.7 knockout	68
Figure 4.19. Breeding strategy to generate control M71 OSNs	69
Figure 4.20. Breeding strategy to generate the final compound heterozygous	69
Figure 4.21. fNav1.7 -/- does not affect M71 glomeruli position	70
Figure 4.22. Dorsal glomerulus from 43 PD from fNav1.7xM71-IRES-CretdRFPxM71-IRES-tauGFP	70
Figure 4.23. Breeding strategy to generate Tm16b knockout M71-expressing 70OSNs mouse strain	71
Figure 4.24. Dorsal glomerulus from Tm16b x M71-IRES-Cre x tdRFP mouse	71
Figure 5.1. MOR256-17 neurons are more broadly tuned than SR1 OSNs	76

List of tables

Table 1. Mixture 1 (Mix1):	38
Table 2. List of chemical compounds:	39
Table 3. List of primers:	42

Table 4. X-gal staining buffers:	44
--	----

List of abbreviations:

AAB: Anterior accessory olfactory bulb
 ACIII: Adenylate cyclase
 Ano2: Anoctamin 2
 ATP: Adenosine triphosphate
 CaCCs: Calcium activated chloride channels
 CamKII: Ca^{2+} / calmodulin-dependent protein kinase II
 cGMP: cyclic guanosine monophosphate
 CNG: cyclic nucleotide gated-channel
 CNS: Central nervous system
 Cre: Causes recombination
 FPR: Formyl peptide receptor
 GBCs: Global basal cells
 GC-D: Guanylyl cyclase D
 GFP: Green fluorescent protein
 GG: Grueneberg ganglion
 GPCR: G-Protein coupled receptor
 GTP: Guanosine triphosphate
 H2-Mv: Histocompatibility complex genes
 HBCs: Horizontal basal cells
 IP3: Inositol triphosphate
 IRES: Internal ribosome entry site
 MOE: Main olfactory epithelium
 MVCs: Microvillar cells
 OB: Olfactory bulb
 OBP: Olfactory binding protein
 OR: Olfactory receptor
 OSN: Olfactory sensory neuron
 PAB: Posterior accessory olfactory bulb
 PDE1C: Phosphodiesterase 1C
 PDE4A: Phosphodiesterase 4A
 PFA: Paraformaldehyde

PIP2: Phosphatidyl inositol diphosphate
PLC: Phospholipase C
RGS: Regulator of G-protein signaling
RTP1: Receptor transporting protein
SO: Septal organ
SUS: Sustentacular/supporting cells
TAARs: Trace amine-associated receptors
tdRFP: Tandem dimer red fluorescent protein
TMEM16b: Transmembrane protein 16b
TRPC2: Transient receptor potential cation channel, subfamily C, member 2
TRPM5: Transient receptor potential channel subfamily M, member 5
TTX: Tetrodotoxin
V1R: Vomeronasal receptor 1
V2R: Vomeronasal receptor 2
VNO: Vomeronasal organ
 β 2AR: β 2 adrenergic receptor

Zusammenfassung

Charakteristisch für das olfaktorische System ist die hohe Komplexität in der Peripherie, durch die hohen Anzahl an exprimierten olfaktorischen Rezeptor-(OR) Gene und die kombinatorische Kodierungsstrategie zwischen verschiedenen ORs. Das olfaktorische System der Maus beruht auf etwa 1.100 OR Gene, die monogenisch und monoallelisch exprimiert werden. Es wird angenommen, dass jedes olfaktorische sensorische Neuron (OSN) nur eine Art von OR aus dem OR Repertoire exprimiert. Die OSNs, die die selben ORs exprimieren, laufen an der selben Stelle im olfaktorischen Bulbus (OB) zusammen, wo sie zwei oder mehr Glomeruli pro Bulbus formen. Dieser Prozess wird axonale Verschaltung genannt. Um die axonale Verschaltung zu verstehen, muss man verstehen was die OSNs dem Gehirn erzählen damit die olfaktorischen Information interpretiert werden.

Es wird angenommen, dass der exprimierte OR die Eigenschaften der Geruchsantwort bestimmt. Charakteristisch für einige ORs ist eine eng gefasste Empfindlichkeit für Geruchsstoffe. Andererseits haben andere OSNs eine breit gefächerte Empfindlichkeit für eine andere Reihe von Chemikalien. Die breitest gefächerte Empfindlichkeit, die bisher bei natürlichen OSNs der Maus beschrieben wurde, war bei OSNs, die das OR Gen für den septalen Rezeptor 1 (SR1) exprimieren, auch bekannt als MOR256-3 und Olfr124. In dieser Thesis wird gezeigt, dass die OSNs, die den OR MOR256-17, auch bekannt als OR3 und Olfr15, exprimieren, eine noch breiter gefächerte Empfindlichkeit als SR1 haben. Die Empfindlichkeit gegenüber Gerüche wurde mit Hilfe von Mausstämmen (SR1-IRES-tauGFP; MOR256-17-IRES-tauGFP), die mit dem grün fluoreszierendes Protein (GFP) markiert wurden, und perforierender patch clamp Aufzeichnungen, untersucht.

MOR256-17 OSNs reagierten auf 31 von 35 getesteten Chemikalien. Zudem waren alle 10 Chemikalien, auf die SR1 OSNs reagierten, ebenfalls in dem Geruchsfeld von MOR256-17 OSNs. Interessanterweise konnten MOR256-17 auf drei Amine (cyclohexylamine, isopenthyllamine and phenylethylamine) reagieren, die typische Liganden für OSNs sind, die Rezeptoren neurogene

Amine (TAARs) exprimieren. Es wurde kein Unterschied zwischen den Eigenschaften der Membran zwischen den zwei OSN Unterpopulationen festgestellt, was nahe legt, dass die Unterschiede in Geruchsreaktion auf den exprimierten ORs beruhen.

Zudem beschreibt diese Thesis den Einfluss von neuronaler Aktivität auf die axonale Verschaltung. Zwei Ionenkanäle wurden untersucht: ein von Kalziumchlorid aktivierter Kanal (CaCC), das Transmembranprotein 16B (Tm16b), auch bekannt als Anoctamin 2 (Ano 2), welcher eine wichtige Rolle im Transduktionsweg der OSNs spielen, indem sie das olfaktorische Signal verstärken; und ein Natriumkanal (Nav1.7), welcher eine kritische Rolle in der Weiterleitung von olfaktorischen Informationen zu den Mitralzellen im OB spielen. Die Rolle dieser zwei Kanäle wurde unabhängig untersucht, indem die axonale Verschaltung von den M71 (auch bekannt als Olfr151) exprimierenden OSNs mittels konditionalen Mutanten (-/- fNav1.7 und -/- Tm16b) in diesen Neuronen verglichen wurde. Die Idee war es, die monoallelische Expression der OSNs zu nutzen und in dem selben Mausstamm Kontroll-OSNs, die sowohl M71 als auch GFP exprimieren, und M71 OSNs denen die Expression von Nav1.7 oder Tm16b fehlt, welche das Reportergen tdRFP exprimieren, zu besitzen. Die Ergebnisse zeigten keinen Unterschied in der axonalen Verschaltung wenn Nav1.7 ausgeschaltet wurde und die Glomeruli erschienen in der normalen M71 glomerularen Position zu sein. Das gleiche gilt für den Tm16b Kanal.

Zusammengefasst hat diese Thesis ein extrem breites Reaktionsprofil von OSNs, die MOR256-17 exprimieren, mit anderen OSN Populationen mit spezifischen OR Genen der Maus verglichen, und eine redundante Funktion von Tm16b und Nav1.7 bei der axonalen Verschaltung gezeigt .

1 Abstract

The olfactory system is characterized by an extreme complexity at the periphery, due to the large number of olfactory receptor (OR) genes expressed, and the combinatorial coding strategy of ORs. The mouse olfactory system relies on approximately 1,110 OR genes expressed in a monogenic and monoallelic manner. It is believed that each olfactory sensory neuron (OSN) expresses only one type of OR from the OR gene repertoire. Axons of OSNs expressing the same OR converge to the same place in the olfactory bulb (OB), forming two or more glomeruli per OB. This process is known as OSN axonal guidance. Understanding olfactory coding and OSN axonal guidance is crucial to comprehend what OSNs are telling the brain to interpret olfactory information.

The OR expressed is thought to determine the odorant response properties of an OSN. Some ORs are characterized by a narrow tuning to odorants. However, others have a broad responsiveness to different chemical compounds. The broadest odorant response so far described in native mouse OSNs was for OSNs that express the OR gene septal receptor 1 (SR1), also known as MOR256-3 and Olfr124. This thesis demonstrated that the odorant responsiveness of OSNs expressing the OR (MOR256-17), also known as OR3 and Olfr15, was even broader than that of SR1-expressing OSNs. SR1 was so far the broadest OR described in native OSNs. The odorant responsiveness was studied using tagged green fluorescent protein (GFP) OSNs mouse strains (SR1-IRES-tauGFP; MOR256-17-IRES-tauGFP) and perforate patch clamp recordings. MOR256-17 OSNs responded to 31 chemicals from the 35 chemical compounds tested. Moreover, all the 10 compounds that activated SR1 OSNs, were included in the odorant space of MOR256-17 OSNs. Interestingly, MOR256-17 OSNs were able to detect three amines (cyclohexylamine, isopentylamine and phenylethylamine), which are typical ligands for OSNs expressing trace amine receptors (TAARs). No difference was observed in membrane properties between the two OSNs subpopulation, indicating that the odorant differences are related to the expressed OR.

This thesis also described the impact of neural activity on OSN axonal guidance. Two channels were investigated: a calcium activating chloride channel (CaCC), transmembrane protein 16b (TMEM16b), also known as anoctamin 2 (Ano2), which plays an important role in the transduction pathway in OSNs, by amplifying the olfactory signal; and a sodium channel Nav1.7, which has a non-redundant role in transferring the olfactory information to the mitral/tufted cells in the OB. The role of these two channels were investigated separately, by comparing within the same OB the axonal projections of conditional mutant $-/-$ fNav1.7 or $-/-$ Tm16b in a subpopulation of OSNs that express the OR M71, also known as Olfr151. The idea was to take the advantage of the OSN monoallelic expression feature, to generate in the same mouse strain, control OSNs expressing both M71 and GFP; versus M71 OSNs lacking the expression of Nav1.7 or Tm16b, and expressing a reporter gene tdRFP. The results showed no difference in axonal guidance when Nav1.7 was knocked out, and the glomeruli appear to be in the normal M71 glomeruli position. The same result was seen within the Tm16b channel.

Taken together, this thesis showed an extreme odorant responsiveness of OSNs expressing MOR256-17 among OSNs subpopulations expressing specific OR genes in the mouse, and a redundant role of Tm16b and Nav1.7 in axonal guidance.

2 Introduction

2.1 Evolutionary aspect of the olfactory system

Living organisms are in constant interaction with the external environment. This interaction allows them to move and react, with respect to their external surroundings and their own inner environment. For that, they require a constant flow of information between different body cell types. The nervous and endocrine systems are the two major networks of intracellular communication. Certain nervous system cells have differentiated into sensory receptors, which are able to encode physicochemical stimuli, which serve to inform the organism about changes in their environment. The information arising from the sensory systems causes a sensation, which is interpreted and perceived by the central nervous system (CNS). Species according to their phylogenetic position have developed very different and sophisticated ways of sensory perception, in order to sense the external environment; among them, the ability to encode and perceive chemical cues. From bacteria to mammals, chemosensation is an essential process. Coding the identity and the intensity of external chemical signals is crucial for the survival and continuity of species. In most vertebrates, chemoreception has evolved into four modalities: The main olfactory system, the accessory olfactory system, the trigeminal system, and the gustatory system (Lledo et al., 2005). Olfaction is the principal chemosensory modality in animals. Notably, the sense of smell allows animals to detect food in order to survive, to identify mates allowing reproduction, and to avoid predators averting death (Su et al., 2009).

The detection of odorants is different according to the living environment. The solubility of stimuli in water is critical for aquatic animals, while volatility is an essential feature for terrestrials (Zippel and Lüthje, 2003). In mammals and specifically in rodents, the capacity to detect odorant stimuli relies on distinct peripheral anatomical structures, and is organized in different olfactory subsystems. The main olfactory epithelium (MOE) with the vomeronasal organ (VNO) represents the main and the accessory olfactory

system, respectively. Two other subsystems have been also discovered; the septal organ (SO) and the Grueneberg ganglion (GG).

2.2 Organization of the mouse olfactory system

2.2.1 Main olfactory epithelium

Located inside the nasal cavity, the MOE contains several million OSNs. OSNs are bipolar neurons with a single dendrite that ends in the apical surface of the epithelium with a knob-like structure (Menco and Morrison, 2003). The knob diameter is $\sim 1\text{-}2\text{ }\mu\text{m}$ and $\sim 2\text{-}3.5\text{ }\mu\text{m}$ in mouse and rat, respectively (Ma et al., 1999). Emanating from the dendritic knob are the cilia, which contain the OR proteins and the transduction machinery (Brunet et al., 1996; Buck and Axel, 1991; Wong et al., 2000). The cilia length is different depending on the localization of the OSNs (Challis et al., 2015). For example, OSNs located in the dorsal anterior region of the MOE have longer cilia in contrast to the cilia of OSNs located in the posterior or ventral regions (Challis et al., 2015). Mucosal secretions from the Bowman's glands protect the tissue that is in direct contact with the external environment (Solbu and Holen, 2012). The mucus contains some components implicated in perireceptor events, like odorant-degrading enzymes and olfactory binding proteins (OBPs) (Getchell et al., 1984; Pelosi, 2001).

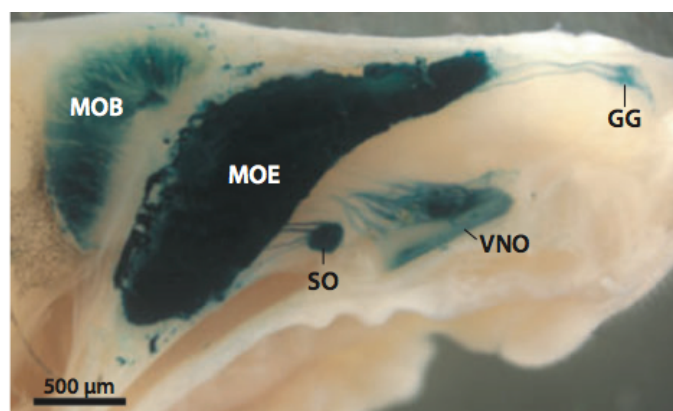


Figure 2.1 Mouse olfactory subsystems. Sagittal whole-mount dissection of the nasal cavity, and the forebrain of an OMP-IRES-tauLacZ mouse, with X-gal staining in blue. MOE, main olfactory epithelium; MOB, main olfactory bulb; VNO, vomeronasal organ; SO, septal organ; GG, Grueneberg ganglion. (From Munger et., al 2009)¹¹

OSN axons cross the cribriform plate and project to the OB. It is believed that one OSN expresses only one type of an estimated 1100 OR genes (Chess et al., 1994). OSNs expressing the same OR project to the same glomeruli in the OB; usually two glomeruli per OB (Mombaerts, 2006).

OSNs are surrounded by glia-like cells named sustentacular/supporting cells (SUS) (Getchell, 1977). SUS cells are the second most abundant cell population in the MOE after OSNs. SUS cells are involved in ion and water regulation (Menco and Morrison, 2003), endocytosis (Bannister and Dodson, 1992), phagocytosis, and metabolism of xenobiotics (Carr, 2005). They are also implicated in calcium flux between the basal cells and OSNs, suggesting that SUS cells communicate with OSNs, basal cells, and SUS cells themselves (Hegg et al., 2009). Patch clamp recordings from murine SUS cells revealed that they are electrically excitable. SUS cells are able to generate action potentials and they are electrically coupled by gap junctions (Vogalis, 2005; Vogalis et al., 2005).

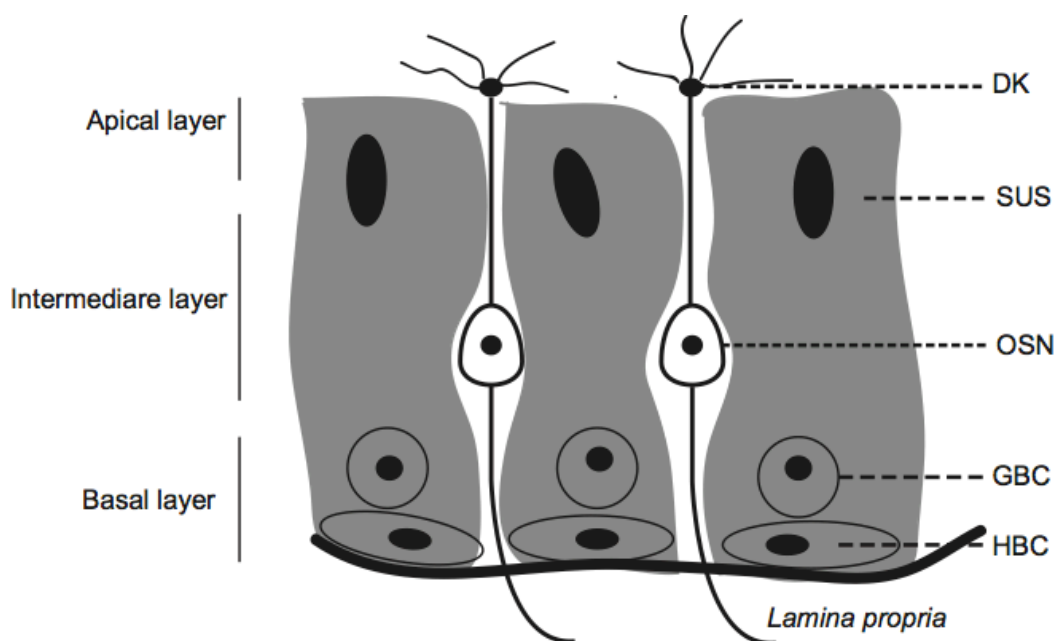


Figure 2.2 Olfactory epithelium. Abbreviations used: DK, dendritic knob; SUS, sustentacular/supporting cell; OSN, olfactory sensory neuron; GBC, global basal cell; HBC, horizontal basal cell.

OSNs are characterized by a constant turnover, and renewal throughout postnatal life (Graziadei and Graziadei, 1979). This feature is due to basal cells located in the basal compartment of the MOE (Beites et al., 2005). According to their morphology, basal cells are divided in two types: horizontal basal cells (HBCs) and globose basal cells (GBCs). These two types of stem cells can give rise to all cell types in the MOE (Brann and Firestein, 2014).

Besides the ciliated OSNs, SUS cells, and basal cells, the MOE also contains other cell types equipped with microvilli, which are located in the apical part of the MOE. Morphologies of microvillous cells are variable, and less abundant than SUS cells and OSNs (Menco and Morrison, 2003). Microvillous cells are thought to be of heterogeneous function; for instance, some cells express the transient receptor potential cation channel M5 (TRPM5), a key receptor in gustation (Hansen and Finger, 2008). Furthermore, they do not have axonal projections to the OB, they do not express neural markers, and they are not in contact with trigeminal fibers (Hansen and Finger, 2008). However, a recent study reported that these cells are cholinergic and also sensitive to chemicals such as adenosine triphosphate (ATP), volatile odorants, and thermal stimulations (Ogura et al., 2011).

Taken together, the MOE contains five cell types: OSNs, SUS cells, basal cells and microvillous cells. Of these populations, SUS and microvillous cells need more investigation to characterize their specific role in olfaction.

2.2.2 Vomeronasal organ

First described in 1813 by the physician and anatomist Ludvig Jacobson, the vomeronasal organ (VNO) is present in a large number of animals, including rodents. The morphology and the location of the VNO are different across vertebrates (Trotier and Døving, 1998). In rodents, the VNO is located in the two sides in the ventral part of the nasal septum, enclosed in a cartilaginous capsule (Trotier and Døving, 1998). The vomeronasal sensory epithelium consists of basal cells, SUS, and vomeronasal sensory neurons (VSNs) (Keverne, 1999). VSNs are located in two different layers in the

neuroepithelium of the VNO; an apical and a basal layer. VSNs express two receptors derived from the G-protein coupled receptor multigene family (Dulac

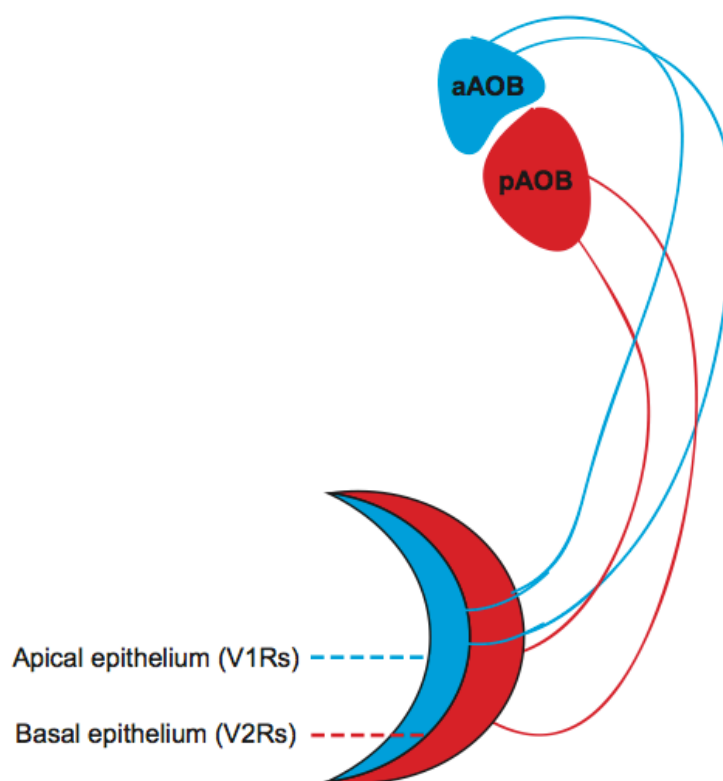


Figure 2.3 Axonal wiring of vomerosensory neurons (VSNs). Abbreviations used: V1Rs, vomeronasal receptors 1; V2Rs, vomeronasal receptors 2; aAOB, anterior accessory olfactory bulb; pAOB, posterior accessory olfactory bulb.

and Axel, 1995). Specifically, VSNs expressing the vomeronasal type 1 receptor (V1R) are found in the apical layer, and those expressing vomeronasal type 2 receptor (V2R) are found in the basal layer (Dulac and Axel, 1995; Herrada and Dulac, 1997). By detecting pheromones, VSNs are crucial in communication and social behavior between species (Munger and Leinders-Zufall, 2009). VSNs expressing V1R and V2R project their axons to the anterior accessory olfactory bulb (aAOB) and posterior accessory olfactory bulb, respectively (pAOB) (Jia and Halpern, 1996) (Ishii and Mombaerts, 2011).

In addition to the different locations of V1R and V2R, components of their signaling transduction cascades also differ. While V1R-VSNs express $G\alpha_{i2}$, the transient receptor potential cation channel C2 (TRPC2), and

phosphodiesterase 4A (PDE4A); V2R-VSNs express $G\alpha_o$, TRPC2, and H2-Mv (Ishii et al., 2003). Furthermore, the V1R mouse genes exhibit a monogenic, monoallelic pattern of expression (Rodriguez et al., 1999). In contrast, it appears that V2R-VSNs co-express multiple genes (Silvotti et al., 2007).

Phospholipase C (PLC) and TrpC2 are key elements in the transduction pathway that facilitates the conversion of a chemical signal into an electrical one (Holy et al., 2000; Liman et al., 1999). Once a stimulus is bound to a VSN receptor, the specified G protein activates PLC, which converts phosphatidylinositol diphosphate (PIP_2) to inositol triphosphate (IP_3). IP_3 activates diacylglycerol (DAG), which leads to the opening of TrpC2, the entry of Ca^{2+} and Na^{+} cations, thus leading to cell depolarisation (Munger, 2009).

The VNO contains two other subpopulations of neurons. The first one is defined by the expression of some OR genes, which are thought to be responsible for odorant detection. These neurons project their axons to the AOB (Lévai et al., 2006). The second population is a new chemosensory family, defined by the expression of formyl peptide receptor (FPR), which are implicated in the identification of pathogens (Rivière et al., 2009). This finding demonstrates that the olfactory system is involved in functions others than that of odorant and pheromone detection.

2.2.3 The septal organ of Masera

The septal organ (SO) is a small patch of cells located in the two sides of the ventral part in the nasal septum. It is situated near to the choana, an orifice leading to the nasopharynx, and separated from the MOE by the respiratory epithelium. The cellular components of the SO are similar to the MOE; however, the density of OSNs in this area is lower. Furthermore, epithelial thickness in the MOE is greater than in the SO; $\sim 20 \mu m$ and $60-80 \mu m$, respectively. Thus, OSNs in the SO are characterized by a short dendrite, flattened somata, and a slightly larger olfactory knob than those in the MOE (Ma et al., 2003). Approximately 93% of OSNs in the SO express only eight

ORs genes, the most abundant one being MOR256-3 (septal receptor1; SR1) gene which is expressed in ~50% of the cells (Tian and Ma, 2004).

The majority of OSNs in the SO exhibit $G\alpha_{olf}$, ACIII, and cAMP pathway signaling, with a small subset of cells signaling via cyclic guanosine monophosphate (cGMP) and guanylyl cyclase D (GC-D) (Ma et al., 2003). Patch clamp recordings from dendritic knobs of single SO OSNs indicate that these cells are responsive not only to odorants but also mechanical stimuli (Grosmaître et al., 2009; 2007).

Despite several investigations in the SO, the exact role of this olfactory subsystem remains elusive. It has been postulated that this system is involved in sensing compounds of low volatility (Wysocki et al., 1980), and participating in sensing general odor environment owing to the broad range of molecules that the SO is capable of detecting (Grosmaître et al., 2009; Tian and Ma, 2004).

2.2.4 Grueneberg ganglion

The Grueneberg ganglion (GG) was discovered in 1971 by Hans Grueneberg (Grüneberg, 1973). The mouse has two GGs, which are anteriorly, close to the naris opening. The structure of the GG is different among species (Brechtbühl et al., 2014). In mouse, gene targeting experiments directed against olfactory marker protein has shown that these cells are organized in a grape-like structure (Fuss et al., 2005). Furthermore, their axons project to the MOB near the AOB, and do not exhibit dendrites or ciliated structure (Fuss et al., 2005).

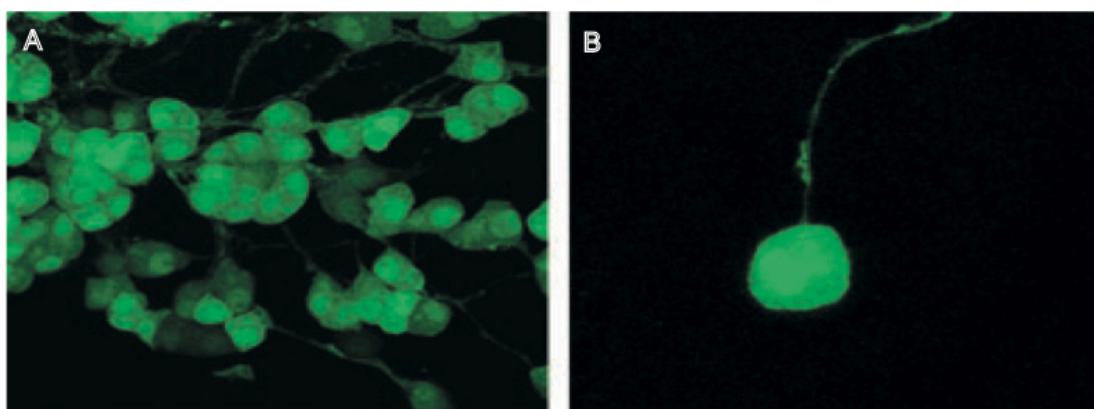


Figure 2.4 Morphology of Grueneberg ganglion (GG) neurons. A, a cluster of GG neurons in an OMP-GFP mouse. B, view of a single GG neuron. (from Fuss et al., 2005).

GG neurons express cGMP as primary second messenger (Fleischer et al., 2009). Patch clamp recordings revealed that GG neurons have a voltage gated current, voltage dependent ionic currents, and display different patterns of spontaneous firing (Liu et al., 2012).

The GG appears very early during the development (E14.5), suggesting a chemosensory role during the neonatal period (Fuss et al., 2005). It has also been implicated in thermoregulation (Schmid et al., 2010) and the detection of alarm pheromones (Brechtbühl et al., 2008).

2.3 Physiological properties of OSNs

2.3.1 Membrane properties of OSNs

The resting membrane potential of OSNs varies amongst species, ranging from -30 mV to -90 mV (Schild and Restrepo, 1998). On average, resting potentials are -58 mV and -55 mV in rat and mouse, respectively (Ma et al., 1999).

Whole-cell recordings have shown an intrinsic voltage-gated current characterized by two major currents; a faster transient inward current followed by a slower outward current (Firestein and Werblin, 1987; Ma et al., 1999). Pharmacological perturbation of the inward-outward currents revealed different components. The inward phase is composed of two components; the first carried by Na^+ and sensitive to tetrodotoxin (TTX), followed by a second sustained inward current carried by Ca^{+2} and sensitive to nifedipine (Trombley and Westbrook, 1991). Action potential repolarization is terminated by the activation of three mainly outward K^+ currents; one that is voltage-dependent, one that is Ca^{+2} dependent, and a delayed rectifier K^+ current (Ma et al., 1999) (Trombley and Westbrook, 1991) (Lynch and Barry, 1991) (Maue, 1987).

2.3.2 Odorant-induced currents

The electric activity in the olfactory mucosa was first studied by Hosoya and Yoshida in dogs (1937), and separately in rabbits and frogs by Ottoson (1956) who introduced and described the electro-olfactogram (EOG) (Scott and Scott-Johnson, 2002). The EOG detects potential changes when the olfactory mucosa is stimulated by odorant-saturated air. While it is still an important tool to understand the electrophysiological properties of OSNs by giving an overview of the electrical ensemble of OSNs, it does not allow to study a single neuron. However, much of our knowledge regarding OSN physiology and odorant-induced currents has been derived from patch clamp recordings.

There are several methods of measuring odorant-induced current and voltage-gated conductance including whole cell patch clamp recordings, (under voltage clamp) and current clamp mode configuration. This configuration allows measurement of odorant-induced current and voltage-gated conductance (Lowe and Gold, 1991). However, the direct contact of the recording pipette with the cell inner milieu can wash out some intracellular cell components. A cell-attached configuration allows the measurement of currents through a single or a few channels of the patch (Lynch and Barry, 1989). The perforated patch technique uses antibiotics (nystatin or amphotericin for example) to perforate the cell membrane, allowing the recording pipette to come in contact with the inner cell milieu (Ma et al., 1999). Like whole cell recordings, this configuration allows the measurement of voltage gated ionic current, and odorant-induced current under voltage clamp and current clamp mode, whilst preventing the diffusion of large cytoplasm components to the recording pipette. However, this technique is not without its limitations; for instance, the rupture of the patch can lead to the contamination of the cytosol.

The first studies of odorant-induced current were carried out using dissociated OSNs and occasionally in explant slices, derived mainly from amphibians. The response to odorant stimuli diluted in solutions has been well described. Often, odorant responsiveness is measured in voltage clamp mode after a

brief pulse of odorants. One of the earliest studies done in this manner was by Firestein and Werblin in 1989. Using a mixture of odorants, they stimulated the phase salamander OSNs in a slice preparation; OSNs that responded generated an inward receptor current. The response latency was approximately 140-570 ms (Firestein and Werblin, 1989). Patch clamp recordings from a mouse intact MOE preparation also revealed a shorter latency of approximately 160 ms (Grosmaître et al., 2006; Ma et al., 1999). Furthermore, the peak current varied in a dose-response manner, depending on the stimulus concentration. In addition, OSNs expressing the same OR have shown response heterogeneity in terms of sensitivity and response kinetics from one cell to another (Grosmaître et al., 2006).

Prolonged stimulation of OSNs leads to adaptation and desensitization, as demonstrated by a decrease with the time of the odorant-induced current (Zufall et al., 1991) (Reisert and Matthews, 1999). In rodents, a short-term adaptation is also observed when the OSN is subjected to a brief paired repeated stimuli; in this scenario, the odorant-induced current is smaller in the second stimulus than the first one, and 10 to 20 s is required for full recovery (Ma et al., 1999). This adaptation was thought to be mediated primarily via cAMP signaling (Ma et al., 1999).

2.4 Transduction pathway signaling

2.4.1 cAMP signaling

By separately stimulating and recording OSN odorant-induced currents in the axons, soma, and dendrites, it was clear that the transduction occurred in the cilia (Lowe and Gold, 1991). The major elements in OSNs transduction pathway are well known. The conversion of the chemical signal to an electric one occurs once a stimulus binds to an OR (Buck and Axel, 1991). ORs belong to the G-protein coupled receptor (GPCR) superfamily, and a specific subtype of G protein (G_{olf}) is expressed in canonical OSNs. G_{olf} is activated by binding a guanosine tri-phosphate (GTP) (Jones and Reed, 1989), which in turns activates adenylyl cyclase 3 (ACIII) (Bakalyar and Reed, 1990). ACIII converts adenosine triphosphate (ATP) to cyclic adenosine monophosphate

(cAMP), a molecule used in cell signaling as a second messenger. An increase in intracellular cAMP leads to the activation of a cyclic nucleotide gated channel (CNG) (Firestein et al., 1991; Nakamura and Gold, 1987), which conducts an inward current of monovalent and divalent cations such Na^+ and Ca^{2+} . Consequently, this cationic influx increases the charge inside the cell, and once the threshold is reached an action potential is generated (Firestein, 2001). Moreover, the signal is amplified by the opening of another Ca^{2+} gated chloride channel, the opening of which is triggered by the initial influx of Ca^{2+} ions. Opening this channel, leads to an efflux of Cl^- , ultimately depolarizing the neuron further (Lowe and Gold, 1993).

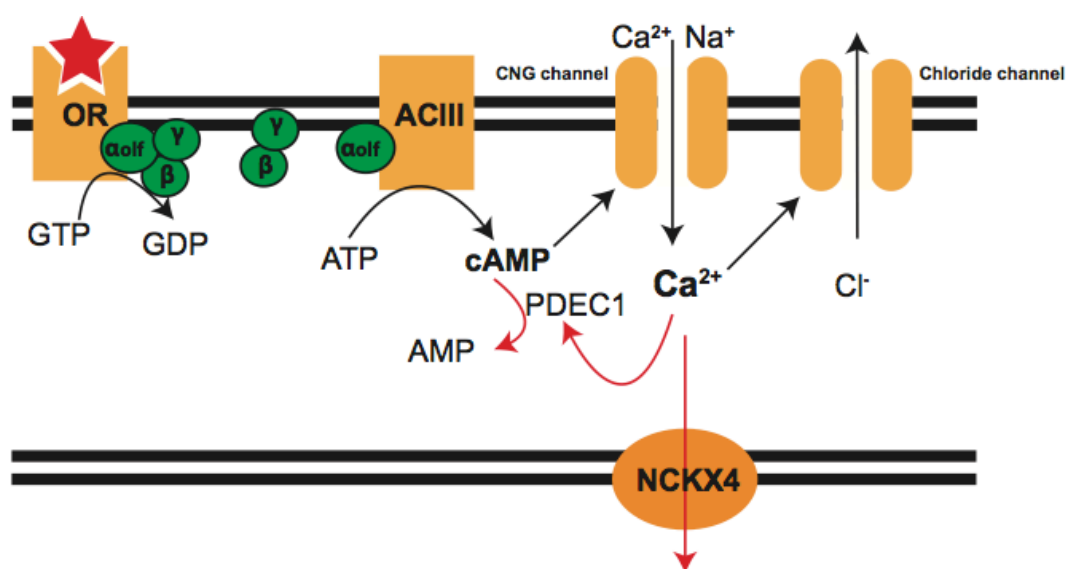


Figure 2.5 cAMP transduction pathway in OSNs. The binding of odorants to ORs leads to an increase of intracellular cAMP mediated by ACIII activation. cAMP gates CNG channel that depolarize the neuron via an influx of Na^+ and Ca^{2+} . The opening of a calcium chloride channel further depolarizes the cell.

A number of mechanisms may contribute to the termination of the odorant-induced current. This includes the hydrolysis of cAMP to AMP by phosphodiesterase C (PDE1C) (Cygnar and Zhao, 2009), the closing of CNG channel and Ca^{2+} activated Cl^- channel by removal of Ca^{2+} using the $\text{Na}^+/\text{Ca}^{2+}$ exchanger (Reisert and Matthews, 2001), or by the regulator of G-protein signaling (RGS) which also attenuates odorant signaling by reducing ACIII activity (Sinnarajah et al., 2001).

2.4.2 Additional signaling pathways

Studies have shown that genetic disruption of one of the transduction signaling components described above (G_{olf} , ACIII, CNG), causes general anosmia in mice, showing the importance of cAMP signaling in olfactory coding (Belluscio et al., 1998; Brunet et al., 1996; Wong et al., 2000). However, there is responsiveness to certain odorant in CNGA2 (a subunit of the CNG channel) knockout mice, suggesting that independent cAMP pathways exist in the MOE (Lin et al., 2004). It is obvious that some OSN subpopulations express different signaling pathways other than cAMP. For instance, OSNs expressing guanylyl cyclase GC-D receptor use the cGMP cascade to convert chemosensory signals (Munger, 2009).

Recently, Omura and Mombaerts (2014) have shown two new OSN subpopulations expressing signaling components for different pathways other than those described previously. The first OSN subpopulation expresses OR genes and relies for chemosensory transduction on ACIII, CNGA2, and TRPC2, a channel known to be expressed and implicated specifically in VSNs (Omura and Mombaerts, 2014). The second OSN subpopulation expresses a guanylate cyclase (*Gucy1b2*) receptor, co-expresses CNGA2, and TRPC2, but lacks ACIII expression (Omura and Mombaerts, 2014; Omura and Mombaerts, 2015). The physiological roles of these two populations are unknown.

2.5 Trace amine-associated receptors

Some OSNs express trace amine-associated receptors (TAARs). TAARs are GPCR receptor encoded by 15 genes in mouse, 17 genes in rat, and 6 in humans (hTAARs) (Liberles, 2015). TAARs use the same signaling pathway as canonical OSNs; for example, TAAR4 is associated with the expression of G_{olf} , ACIII, CNGA2, TMEM16b, and PDE4A (Zhang et al., 2004). OSNs expressing TAARs can be activated by some amine-based odorants (Pacifco et al., 2012). Patch clamp recordings have shown a broad and exquisite sensitivity detection to amines; for example, OSNs expressing TAAR3 and TAAR4 can detect amines at nanomolar concentrations (Zhang et al., 2013).

In mouse, the repertoire of TAAR genes is clustered on chromosome 10; genetic ablation of the TAAR gene cluster abolished innate aversion to amines (Dewan et al., 2013). Moreover, the deletion of TAAR4 resulted in the lack of avoidance towards predators urine (Dewan et al., 2013). This study revealed the essential contribution of TAARs in the detection of amines and thus, predators.

2.6 OSNs spontaneous activity

Spontaneous activity (also called basal activity or noise) occurs in central and peripheral neural systems. This activity is crucial for maintaining the development of neural circuits (Blankenship and Feller, 2010). In the olfactory system, OSNs fire action potentials in the absence of odorant stimulation. This neural activity is crucial for the establishment and maintenance of the wiring in the OB (Yu et al., 2004).

Patch clamp recordings from dissociated and intact OSNs expressing different GFP tagged ORs have shown different frequencies of spontaneous activity (Connelly et al., 2013; Reisert, 2010), suggesting that the type of OR influences spontaneous firing. The mean firing frequency in intact OSNs was higher than in dissociated OSNs, and is attributed to the loss of cilia during OSN dissociation (Connelly et al., 2013). Moreover, the spontaneous activity varied even in OSNs expressing the same OR (Connelly et al., 2013).

It would appear that spontaneous activity is driven by ciliary transduction components. The application of niflumic acid (a Ca^{+2} activated Cl^- channel blocker) abolished the spontaneous activity (Reisert, 2010). Patch clamp recordings from OSNs expressing a mutant OR incapable of G-protein activation also indicated that basal activity was abolished (Connelly et al., 2013). Hence, it is apparent that basal activity is derived from ORs themselves.

2.7 OSNs mechanical response

Odorant detection aside, OSNs are responsive to mechanical stimuli. Mechanosensitivity in OSNs was investigated by patch clamp recordings from

the SO and the MOE (Grosmaître et al., 2007). OSNs were able to detect a pressure derived from Ringer puff stimulation and generated an inward current (Grosmaître et al., 2007). OSNs displayed a latency of hundreds of ms after stimulation (Grosmaître et al., 2007). Furthermore, the peak amplitude generated increased in a dose-dependent manner (Grosmaître et al., 2007). Remarkably, mechanosensitivity enhanced neural activity. The stimulation of an OSN invoked by the same odorant concentration, with different pressures generated different odorant-induced currents. The increased pressure led to stronger inward currents, which could be important for the system to detect stimuli at weaker concentrations (Grosmaître et al., 2007).

Mechanosensitivity is derived from ORs themselves; different OSNs expressing different ORs types have demonstrated variable mechanosensitivity (Connelly et al., 2015). Moreover, the response to mechanical stimuli shares the same classical transduction pathway components implicated in OSN chemosensitivity. The disruption of any of these components (OR, G_{olf} , ACIII, or CNGA2) by genetic or pharmacological manipulation, led to the drastic reduction or complete abolishment of OSN mechanosensitivity (Connelly et al., 2015) (Grosmaître et al., 2007).

2.8 Ca^{+2} activated Cl^{-} channel (TMEM16b, Ano2)

The CaCCs were described in the early 1980s by using voltage clamp recordings from *Xenopus* oocytes (Barish, 1983). CaCCs act by depolarizing the cell membrane after being activated by an increase in the cytosolic Ca^{+2} concentrations. They are physiologically important across a variety of cell types and functions, like the membrane excitability of neurons and cardiac myocytes, phototransduction, gustation (Hartzell et al., 2005), and olfaction as aforementioned.

The molecular identity of the exact CaCC channel implicated in olfactory transduction was unknown. TMEM16B (transmembrane protein 16B) also known as (Ano2 for anoctamin 2) belong to the recently identified gene family TMEM16 (A-K), described by Katoh and Katoh using a bioinformatics approach (Katoh and Katoh, 2003). All TMEM16 proteins consist of eight

transmembrane segments and intracellular NH₂ and COOH termini. In 2008 three independent groups demonstrated that the first two genes TMEM16A and TMEM16B are CaCCs (Yang et al., 2008) (Caputo et al., 2008) (Schroeder et al., 2008), which is why the anoctamin nomenclature was proposed (anion + octa). Thus, TMEM16A was designated as Ano1, and TMEM16B as Ano2 (Yang et al., 2008).

TMEM16B has been detected utilizing a variety of different techniques, ranging from proteomic screening of cilia membrane (Stephan et al., 2009), in situ hybridization (Hengl et al., 2010), and by immunohistochemistry (Dauner et al., 2012). All these studies revealed that TMEM16B expression is restricted only to the cilia of OSNs. Moreover, TMEM16B is only expressed in chemosensory neurons in all of the olfactory subsystems of the mouse, except for the GG (Dauner et al., 2012).

In addition, patch clamp recordings from HEK-293 cells expressing the olfactory form of TMEM16b and CNGA2 channel generated Ca⁺² dependent chloride currents suggesting that TMEM16B is the major component of the olfactory CaCC (Stephan et al., 2009). Indeed, the generation of the Ano2^{-/-} knockout mice confirmed this (Billig et al., 2011). Whole-cell patch clamp analysis of Ano2^{-/-} OSNs indicated that all Ca⁺² activated Cl⁻ currents were completely abolished (Billig et al., 2011). Surprisingly, EOG recordings have shown a moderate decrease of global OSN neural activity in Ano2^{-/-} mice (Billig et al., 2011). Moreover, olfaction was not altered in newborn Ano2^{-/-} mice, which exhibited normal growth and survival patterns. Importantly, Ano2^{-/-} OSNs coalesce and form regular glomeruli without any disruption in the OB (Billig et al., 2011).

2.9 The voltage-gated sodium channel Nav1.7

Voltage-gated sodium channel genes have been identified in a variety of species from bacteria to mammals; they play an indispensable role in the initiation and propagation of action potentials in excitable cells. Nine genes (Nav1.1–Nav1.9) have been identified in mammals (Catterall et al., 2005). The

structure of the sodium channel proteins is well characterized in mammals; they are composed of a long polypeptide containing around 2000 amino acids, consisting of a complex of a single α subunit and one or more β subunits. The α subunit contains 24 transmembrane segments with an intracellular amino and carboxy termini and organized on four domains (I-IV). Within each domain are four transmembrane segments (S1-S4) that are involved in voltage sensing and two transmembrane segments (S5-S6), which are the part of the channel that form the pore (Catterall, 2000).

The sodium current has been described from the classical work of Hodgkin and Huxley using voltage clamp technique in the giant axon of the squid. They described three features related to sodium: a voltage dependent activation, rapid inactivation, and a selective ion conductance (Hodgkin and Huxley, 1952a) (Hodgkin and Huxley, 1952b).

The Nav1.7 channel, also known as PN1 (peripheral nerve 1 sodium channel) is encoded by the Scn9a gene and located on chromosome 3. Nav1.7 is highly expressed in peripheral neurons (Dib-Hajj et al., 2012). It was first detected in somatosensory and sympathetic ganglion neurons (Toledo-Aral et al., 1997). Nav1.7 exhibits a rapid activating and inactivating current. The channel is TTX sensitive and can be blocked by nanomolar concentrations (1.1 nM) (N Klugbauer, 1995). Nav1.7 is implicated in nociception; the deletion of Nav1.7 from the dorsal root ganglion neurons causes a reduction or complete knockdown of inflammatory pain (Nassar et al., 2004). Nav1.7 is a predominant transcript in OSNs with a high level of expression in OSN axons bundles (Weiss et al., 2011; Ahn et al., 2011). In humans and mice, the loss of function of Scn9a gene causes general anosmia (Weiss et al., 2011). The genetic ablation of Nav1.7 from OSNs in mice causes a loss of synaptic transfer to the OB (Weiss et al., 2011). Nav1.7 $-/-$ OSNs were able to generate odorant-induced currents, but the mitral cells with which OSNs synapse remained completely silent. This study provided evidence that Nav1.7 is crucial for the signal propagation to the OB (Weiss et al., 2011).

2.10 Progress in OR-ligand identification

Discovered by Buck and Axel in 1991, OR genes represent the largest gene family in mammals (Buck and Axel, 1991). The mouse genome contains around ~1100 OR genes expressed in monogenic and monoallelic manner (Chess et al., 1994). ORs are composed of seven transmembrane domains typical of GPCRs, containing ~300-500 amino acids (Gaillard et al., 2004). Based on phylogenetic analysis, OR genes were classified in two classes: a fish-like class I and a mammalian-like class II (Freitag et al., 1995).

One of the intriguing questions in the field was: how can ~1100 ORs detect the enormous repertoire of odors? A combinatorial strategy has been described, using calcium imaging to measure Ca^{+2} flux after odorant stimulation in a single OSN and single-cell RT-PCR to recognize the specific OR expressed in this cell. This approach revealed that a single OR is able to recognize multiple odorants, that a single odorants can activate different OR types, but also that different odorants are detected by different combinations of ORs (Malnic et al., 1999). The same strategy was utilized for human ORs, and similar results observed (Gonzalez-Kristeller, 2015). Moreover, some ORs show sensitivity to a wide variety of compounds, whilst others had only a narrow window of sensitivity.

Deorphaning ORs (identifying ligand-receptor combination) is crucial to our understanding of olfactory coding at the peripheral and central level. Substantial progress have been made since the discovery of the first OR-ligand pair (octanal and I7 in rat) (Zhao et al., 1998). Other OR-ligand pairs have been identified either by calcium imaging experiments from dissociated OSNs, eugenol and MOR-EG (Kajiya et al., 2001), Lyr1 and MOR23 (Touhara et al., 1999), acetophenone/benzaldehyde and M71 (Bozza et al., 2002), or by patch clamping in ex vivo preparation, of single OSNs expressing an OR tagged with GFP, Lyr1 and MOR23 (Grosmaître et al., 2006), acetophenone analogues and M71/M72 receptors, 2-phenylethyl alcohol and the S1 receptor (Lam and Mombaerts, 2013).

Moreover, in vivo calcium imaging has been carried out in the OB, followed by dye injections in the activated glomerulus which facilitated the tracing and the identification of the specific OR expressed, by RT-PCR (Oka et al., 2006).

More recently, two in vivo assays have been described. The first one is based on GFP targeting of the S100a5 gene, which encodes a Ca^{2+} and zinc binding protein, located in both OSN cilia and axons (Kuhlmann et al., 2014; Schäfer et al., 2000). S100a5 expression is correlated with odor stimulation (Bennett et al., 2010). After odorant exposure, RNA from activated GFP positive neurons were measured, this assay permitted the re-identification of ORs that respond to eugenol and muscone (McClintock et al., 2014). The second one is an assay called DREAM, which rise for deorphanization of receptors based on expression alterations of mRNA levels (von der Weid et al., 2015). This technique is based on measuring the decrease of OR mRNA level after odorant exposure. The DREAM approach allowed the identification olfactory receptor-ligand pairs in vertebrates and invertebrates. It has made possible, to screen a response profile of thousand of ORs to specific molecule. Until recently, DREAM is the most rapid in vivo assay used to deorphan ORs.

Others rapid assays used are the forced expression of ORs in heterologous cells, such as human embryonic kidney (HEK293T) (Saito et al., 2004). Progress was slow due to the lack of OR expression at the cell surface (Gimelbrant et al., 1999). However, the discovery of receptor transporting protein (RTP), a 20 N-terminal amino-acid rhodopsin derivative, resolved the problem of inadequate cell surface and many ORs have since been deorphanized (Saito et al., 2004). The assay is based on the co-expression of a specific OR, $G_{\alpha_{\text{olf}}}$, RTP, and the measurement of cAMP or the cAMP response element (CRE) levels, using a CRE-luciferase reporter assay system. Similarly, measuring the increase of Ca^{2+} levels following odorant stimulation has also been used in heterologous systems (Krautwurst et al., 1998; Kajiya et al., 2001). Furthermore, the use of biosensors in an attempt to mimic the nose have been employed; in a such an approach a biosensor is built and a combination of optical, resonant, and electrochemical technologies

are used to mimic OR signaling, ultimately creating a bioelectronics nose (Glatz and Bailey-Hill, 2011).

Taken together, we can sum up the different approaches developed to deorphan mammalian ORs into four groups. (i) In vivo assays; (ii) physiological assays based on the combination of calcium imaging and single cell RT-PCR, calcium imaging or electrophysiological recordings from transgenic mice expressing tagged ORs; (iii) ORs expressed in heterologous systems with measurement of cAMP, increases in intracellular Ca^{2+} , or by electrophysiological recordings from heterologous systems (i.e. ORs expressed in *Xenopus leavis* oocytes), and (iiii) biosensor technology.

2.11 Olfactory receptor responsiveness

A given OR and the population of OSNs that express this OR reside on a wide spectrum of odorant response profiles, from having a narrow response window to that of a broad one. Narrow responsiveness means that a specific OR can detect only few chemical compounds from different chemical groups, or many chemical analogous compounds from the same chemical group. However, a broadly responsive OR can detect a wide range of chemical compounds, from different chemical groups, for example aliphatic, cyclic, or aromatic. This broad responsivity is poorly understood at the molecular and the physiological level.

In humans, olfaction is based on approximately 400 OR genes (Malnic et al., 2004), and to date only a small percentage (~10%) of these receptors have a known agonists (Gonzalez-Kristeller, 2015). Some human ORs are very narrowly tuned to odorants, like OR7D4 which is only activated by androstenone, and androstadienone (Keller et al., 2007). However, other ORs can have a broad responsiveness range to odorants (Gonzalez-Kristeller, 2015), like the OR1G1 receptor (Sanz et al., 2005).

In insects, specifically in *D. melanogaster* and *A. gambiae*, a wide range of OR specificities, from narrow to broad tuning was screened (Hallem and Carlson, 2006; Wang et al., 2010). The combinatorial coding is consistent in

insects, since ORs were activated by multiple odorants, and most ligands activated multiple ORs (Andersson et al., 2015). For example in Hallem and Carlson, 2006, a large panel of 110 odorants from different chemical groups was tested, the broad tuned ORs were characterized by a strong excitatory response and sensitivity to similar odorant structure. Or67a was able to respond to 31 different odorants, including lactone, organic acids, aldehydes, ketones, aromatics, alcohols and esters (Hallem and Carlson, 2006).

In mice, OSNs that express OR gene SR1 (also known as Olfr124 and MOR256-3) have thus far demonstrated the broadest odorant responsiveness in a homologous ex vivo system (i.e. in native OSNs that express an unmodified OR protein from the endogenous locus in the genome) (Grosmaître et al., 2009). OSNs expressing SR1 were able to detect camphor, amyl acetate, octanoic acid, heptanoic acid, and benzaldehyde (Grosmaître et al., 2009). The response profile MOR256-17 (also known as Olfr15 and OR3), have been investigated only in heterologous expression systems; in HEK293T cells (Saito et al., 2009; Dahoun et al., 2011), in micelle and nanodisc biomimetic chemical sensors (Goldsmith et al., 2011), and in *Xenopus laevis* oocytes (Liu et al., 2012). A third member of the MOR256 family, MOR256-31 (formally known as Olfr42 and now designated Olfr263), also conveys a broad odorant response profile when expressed in heterologous HEK293T cells, following recovery of the transcript by RT-PCR from a single native OSN that responded broadly to odorants (Nara et al., 2011; Yu et al., 2015). Recently, Yu et.al showed essential residues in the SR1 protein structure which are critical for its broad response; disruption of just a few residues substantially narrowed the response profile for this receptor (Yu et al., 2015). Conversely, an OR with a narrow response profile, could be converted to a broad one by manipulating a small number of amino-acid residues (Yu et al., 2015).

2.12 OSN axons guidance

In the mouse olfactory system, OSNs expressing the same OR are unique that their axons navigate from the MOE, cross the cribriform plate to reach the OB, and coalesce in the same position making two or a few glomeruli (Bozza et al., 2002). Depending on the OR expressed, glomeruli for a specific OSN

population can exhibit variable positions in the OB (Zapiec and Mombaerts, 2015). The glomerulus is an organized neuropil in the OB; the result of connections made by the OSN axons, and the dendrites of mitral and tufted cells (Pinching and Powell, 1971). Glomeruli are completely formed after birth; however, axon terminals reach the OB early on during development and maybe synaptically active (Lam and Mombaerts, 2013). At the time of birth, there are thought to be around 1600-1800 glomeruli (Mombaerts, 2006).

The mechanisms controlling axonal wiring are not completely understood. Early studies using knock-in, knockout mice greatly clarified our understanding of axonal guidance. Using a gene-targeting strategy Mombaerts et al. found that the ORs themselves are essential for guidance of axons to the correct position in the OB (Mombaerts et al., 1996). In particular, replacing the P2 sequence with that of the M12 receptor led to the formation of a glomerulus, but in a completely different position to that of the regular P2 and M12 glomerular position in the OB (Mombaerts et al., 1996). Glomerular shifting as a consequence of OR substitution is in accordance with other such studies (Wang et al., 1998; Bozza et al., 2002; Feinstein and Mombaerts, 2004; Bozza et al., 2009).

However, the replacement of M71 receptor sequence with another non-olfactory $\beta 2$ adrenergic receptor ($\beta 2AR$) also led to glomerular formation (Feinstein et al., 2004), suggesting that the OR itself is not the only element required for axonal guidance. Thus, components of the transduction pathway have also been investigated for their role in axonal guidance. In $-/-$ ACIII mice OSN wiring was dramatically affected (Zou et al., 2007). The deletion of ACIII gene affected the cells in different ways. In some populations of OSNs, the cell number decreased and the axons were able to navigate to the OB, but were unable to form a glomerulus (Zou et al., 2007). The decrease in cell number suggests that a threshold must be attained in order for glomerular formation to occur. This was not the case for MOR23 neurons, where the cell number remained constant but also failed to form glomeruli (Zou et al., 2007). In other instances, axons were able to form glomeruli but the position was shifted in contrast to wild-type counterparts (Zou et al., 2007). These results

suggest a different role for ACIII in OSNs expressing different ORs. The perturbation of G-protein signaling or CNGA2 also led to disordered axonal wiring (Imai et al., 2006; Zheng et al., 2000).

Further, other mechanisms independent from OR activity have been implicated in axonal wiring. For instance, the adhesion molecule neuropilin-1 (Pasterkamp et al., 1998). The interaction between plexin-1/neuropilin-1 complexes enables the detection of the chemo-repulsive protein semaphoring 3A (Takahashi et al., 1999). Semaphorin 3A repels growing olfactory axons expressing neuropilin-1 which is critical for spatial arrangement of glomeruli (Taniguchi et al., 2003). P2 OSNs specifically lacking semaphorin 3A expression form multiple smaller glomeruli (Schwartz and Raitcheva, 2004; Schwarzenbacher et al., 2004), indicating the perturbation of the regular wiring organization. Furthermore, other cell adhesion molecules such as Kirrel2 and Kirrel3 have been reported to influence axonal sorting and organization, as well as the repulsive molecules ephrins (Serizawa et al., 2006).

2.13 Aims of the thesis

Identifying OR-ligand pairs is challenging due the high OR genes number expressed in mice, but critical for our understanding of the olfactory coding at the peripheral, and the central levels. Moreover, less interest was given to broad responsiveness ORs, the mechanisms, and the role of these ORs in the olfactory system remains elusive.

The glomeruli in the OB are remarkably organized. Despite the progress done in our understanding of OSN axons navigation, the whole process is not yet achieved. Specifically, the implication of neural activity in axonal guidance is not well understood and remains controversial.

The objectives of this thesis were to:

1. Study the physiology, and the odorant responsiveness of MOR256-17 OSNs, and SR1 OSNs.
2. Explore the implication of neural activity in axonal guidance, by investigating the role of the sodium ion channel Nav1.7, and the calcium gated chloride channel TMEM16B, in M71 OSNs.

3 Materials and methods

3.1 Animals

All animals were generated in-house, unless otherwise specified. A gene targeting strategy has been developed based on the integration of marker genes such as green or red fluorescent protein (GFP and RFP, respectively) and LacZ, for example (Mombaerts, 1996). Integration of these markers at OR loci is achieved by homologous recombination in mouse embryonic stem cells (Mombaerts, 1996). The gene targeting cassette also contains an internal ribosome entry site (IRES); derived from the encephalomyocarditis virus (Kim et al., 1992), it is recognized by ribosomes that facilitates an initiation of translation in the middle of a messenger RNA (mRNA).

In order to study the physiology of odorant responsivity, the MOR256-17-IRES-tauGFP (Tazir et al., 2015), and SR1-IRES-tauGFP (Grosmaître et al., 2009) strains were used.

For studies of axonal guidance, the MOR256-17-IRES-tauLacZ (generated in-house), M71-IRES-tauGFP (Bozza et al., 2002), M71-IRES-Cre (Lin et al., 2004), tdRFP (Luche et al., 2007), Nav1.7-lox (Weiss et al., 2011), and Tm16b-lox (Billig et al., 2011) strains were used.

Mouse experiments were carried out in accordance with the guidelines of the National Institute of Health regarding the care and use of animals for experimental procedures, and in accordance with the German Animal Welfare Act, the European Communities Council Directive 2010/63/EU, and the institutional ethical and animal welfare guidelines of The Rockefeller University, the Max Planck Institute of Biophysics, the Max Planck Research Unit for Neurogenetics, and the Université de Bourgogne. Approvals came from the Institutional Animal Care and Use Committee of The Rockefeller University, the Regierungspräsidium Darmstadt, and the Veterinäramt of the City of Frankfurt. In Frankfurt, mice were maintained in specified pathogen-free conditions in individually ventilated cages (Techniplast, Italy). Mice received ad libitum water and gamma-irradiated ssniff V1124-727 (ssniff,

Soest, Germany). Nesting, bedding, and enrichment were provided as nestpak, Datesand Grade 6 (Datesand, Manchester, United Kingdom). In Dijon, mice were housed in cages with Lignocel select fine bedding (SORAC, Spain), and given A03 feed (SAFE, Augy, France) and water ad libitum.

3.2 Electrophysiology experiments

3.2.1 Dissecting the olfactory epithelium

The mice were deeply anesthetized via intraperitoneal injection of ketamine/xylazine (150 mg/kg and 10 mg/kg, respectively), and then decapitated using a rodent guillotine (World Precision Instruments, Sarasota, FL, USA). The head was immediately put in a petri dish and immersed in ice-cold oxygenated Ringers solution containing 124 mM NaCl, 3 mM KCl, 1.3 mM MgSO₄, 2 mM CaCl₂, 26 mM NAHCO₃, 1.25 mM NaH₂PO₄, 15 mM glucose, at pH 7.5 and 305 mOsm, oxygenated with 95% O₂ and 5% CO₂ (All from Sigma Sigma-Aldrich, Saint-Quentin-Fallavier, France).

A longitudinal medial incision was made in the dorsal part of the head to

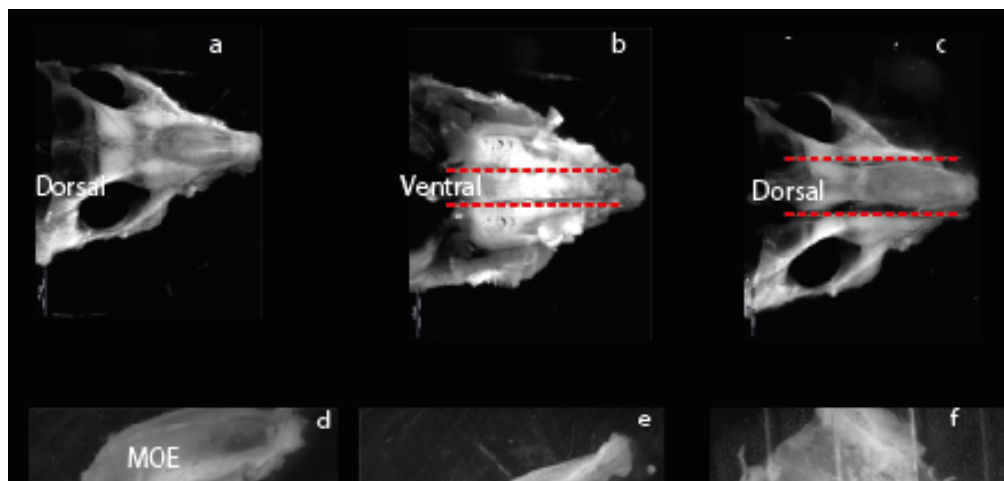


Figure 3.1 Dissection of the MOE. a, Dorsal head view after removing the skin and the lower jaws; b, two sagittal cuts are made in the ventral part to remove the teeth; c, two sagittal cuts are made in the dorsal part to remove the; d, MOE after removing the anterior dorsal bones of the scale; e, upper view of the MOE; f, MOE transferred to recording chamber.

remove the skin. The lower jaws with the upper teeth were removed, and then a coronal cut was made behind the eyes. The preparation was transferred to another petri dish, with a clean cold oxygenated Ringer solution for dissection under the scope (SZX16 Olympus), as seen in the figure 3.1. The olfactory

mucosa attached to the nasal septum was removed and kept in oxygenated Ringer solution. Before use, the mucosa was gently peeled away from the underlying bone and transferred to a recording chamber. During recording, the preparation was continuously perfused at a rate of approximately 1 mL/min at room temperature. In this intact epithelial preparation neither mechanical nor enzymatic treatments were used. The OSNs cilia were intact with long axons and the neurons were not isolated from their natural milieu in contrast to dissociated cells. This approach is advantageous as it approximates in vivo conditions (Grosmaître et al., 2006; Ma et al., 1999). The quality of the dissection is important; in order to obtain intact neurons, the dissection should be fast (<10 minutes) and precise to avoid tissue damage. The preparation was kept for around two hours for patch clamp recordings.

3.2.2 Visualizing fluorescent dendritic knob

The dendritic knobs of OSNs were visualized through an upright microscope (Olympus BX51WI), equipped with an Olympus DP72 camera, and a 40X water-immersion objective. An accessory lens in the light path achieved an extra 4X magnification. The GFP-labeled cells were visualized under fluorescence illumination. Superimposition of the fluorescent and bright-field images allowed identification of the GFP positive cells under bright field (figure 3.3).

2.2.3 Patch clamp recordings

Recordings were controlled with an EPC-10 amplifier combined with Patchmaster Software (HEKA Electronic, Germany). Perforated patch clamping was performed on the dendritic knobs with 260 μ M nystatin. Nystatin was prepared in dimethyl sulfoxide (DMSO), vortexed and sonicated for approximately five minutes and kept in the dark.

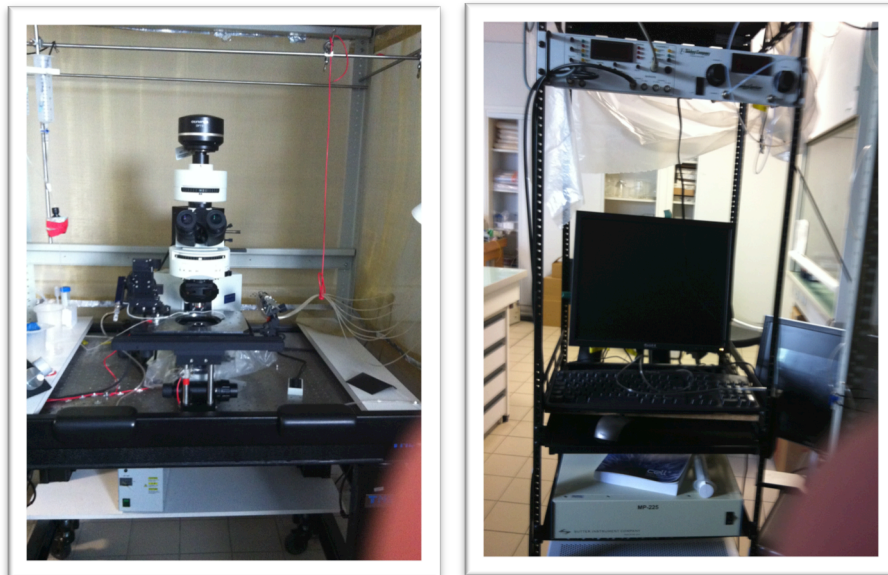


Figure 3.2 Experimental setup used for patch clamping

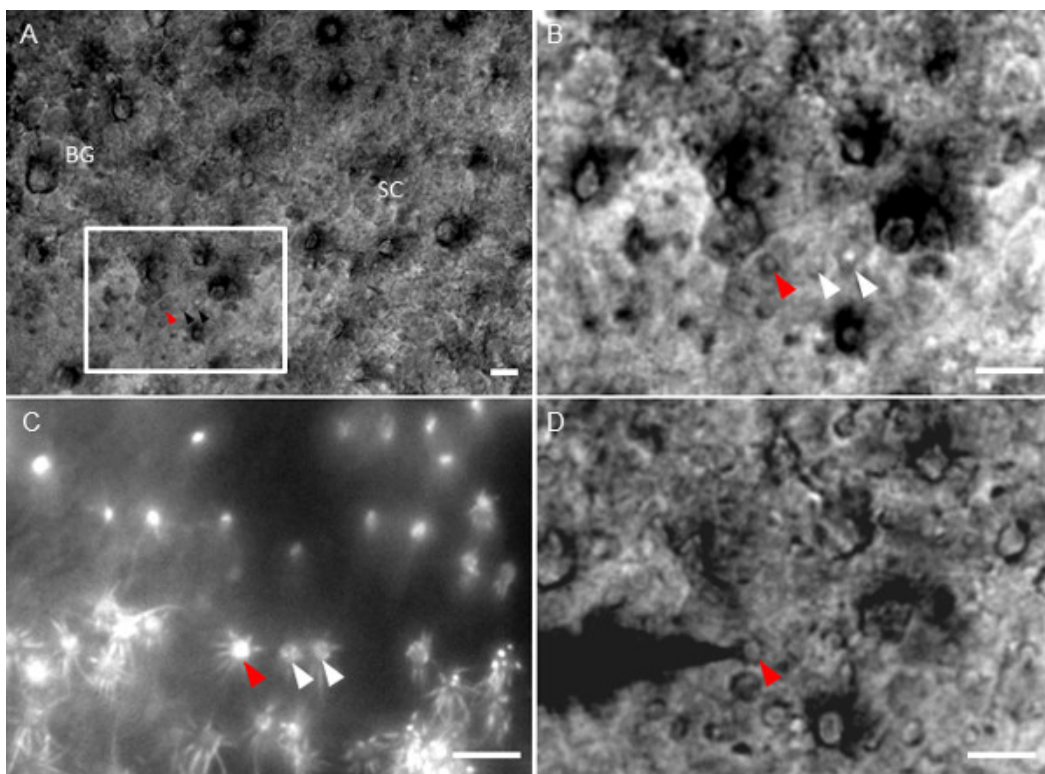


Figure 3.3 Detection of GFP OSNs. A, Intact MOE taken from SR1-IRES-tauGFP mouse, observed under bright-field condition at the 40X magnification. Arrows show OSN dendritic knob in a mesh of supporting cells (SC) and Bowman glands (BG). B, dendritic knobs of SR1 OSNs. C, the same field as in B showing SR1 OSNs under fluorescent light. D, Recording pipette approaching SR1 neurons under bright field, the red arrow represent the same SR1 dendritic knob. Scale bar, 5 μ M. (From Jarriault et al. 2015). 1

Borosilicate-recording pipettes (Sutter Instrument, Novaco, CA, USA) were pulled with a Flaming/Brown micropipette puller model (P-97, Sutter

instruments CO, USA). The pipette was filled with the following solution: 70 mM KCl, 53 mM KOH, 30 mM methanesulfonic acid, 5.0 mM EGTA, 10 mM HEPES, 70 mM sucrose; this was adjusted to pH 7.2 with KOH and to 310 mOsm with sucrose. The resistance of the pipette in the bath solution was approximately 20 M Ω . The junction potential was approximately 9 mV and was corrected in all experiments off-line. For odorant-induced transduction currents, signals were sampled at 20 kHz. Under voltage-clamp mode, the signals were initially filtered at 10 kHz and then at 2.9 kHz.

2.2.4 Odorant stimulation

A seven-barrel pipette was used to deliver stimuli by pressure ejection through a picospritzer (Pressure System IIe, Toohey). The seven-barrel pre-pulled pipette was manually prepared. Six-glass pipette (Glass THINW W/FIL 1.0MM, World Precision Instruments, Sarasota, FL, USA) were curved at 45

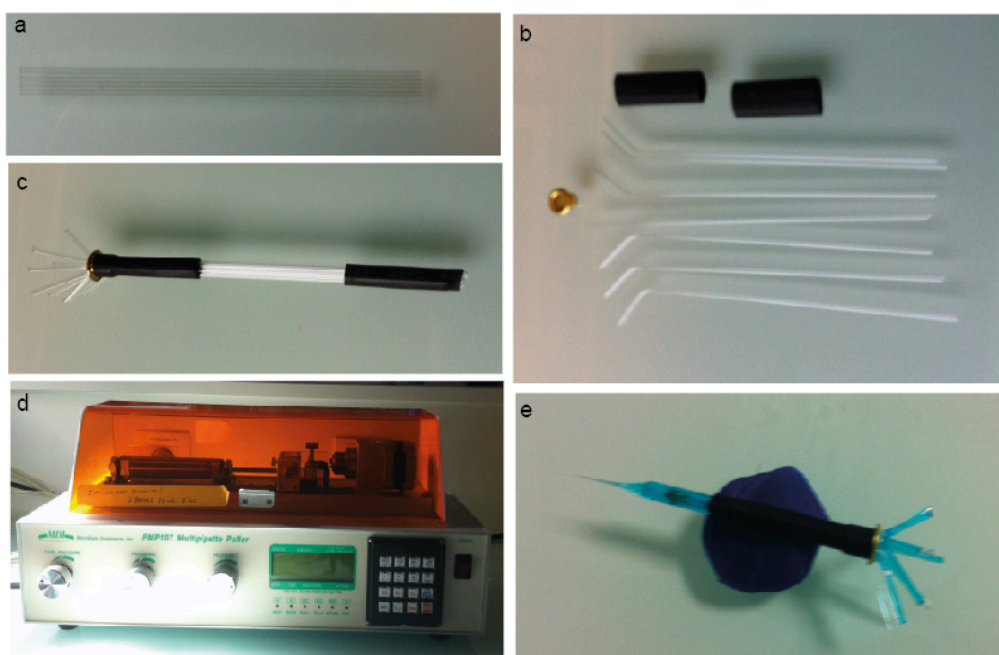


Figure 3.4 Preparation of the stimulation pipette. a, Seven glass pipettes; b, six glass pipettes are curved, resembled together using eyelet and heat-shrink tube; c, pre-pulled pipette; d, a multibarrel-pipette puller; e, a multibarrel-pipette pulled and filled up with odorants.

degrees, about 1 cm from the tip using a flame. The six bent glasses were inserted in an eyelet with another straight pipette in the middle. The eyelet and the seven glass pipettes are maintained together using a heat-shrink

tube. White glue was applied around the eyelet and stored to dry overnight. The pre-pulled pipette was pulled before the beginning of each experiment, using a multi-pipette puller (PMP-107, MicroData Instrument, Inc., S. Plainfield, NJ, USA).

Odorant stocks were prepared at 0.5 M solution in DMSO and stored at 20°C. The list of odorant is described in table 2. Mixture 1 (Mix1) contains 19 compounds in equal molar concentration (table 1). Mix1 was prepared as at 0.1 M in DMSO, and stored at -20°C.

Table 1. Mixture 1 (Mix1):

Chemical compound	Chemical group
heptanol	Alcohol
octanol	Alcohol
hexanal	Aldehyde
heptanal	Aldehyde
octanal	Aldehyde
heptanoic acid	carboxylic acid
octanoic acid	carboxylic acid
cineole	Terpenoid
amyl acetate	Ester
(+) limonene	Terpene
(-) limonene	Terpene
(+) carvone	Terpene
(-) carvone	Terpene
2-heptanone	Ketone
3-heptanone	Ketone
ethyl vanilline	aromatic aldehyde
benzaldehyde	aromatic aldehyde
anisaldehyde	aromatic aldehyde
acetophenone	aromatic ketone

Final solutions of odorants were prepared before each experiment by adding Ringers solution, and 1 µg/mL erioglaucine, a blue dye used to visualize successful delivery of the odorant to the dendritic knob.

Table 2. List of chemical compounds:

Chemical compound	Chemical group
menthol	aromatic alcohol
phenethyl alcohol	aromatic alcohol
ethyl maltol	aromatic alcohol
trans-2-hexanal	Aldehyde
heptanal	Aldehyde
Octanal	Aldehyde
Lylal	aromatic aldehyde
ethyl vanillin	aromatic aldehyde
benzaldehyde	aromatic aldehyde
dihydrocarvone	Terpene
(+/-) carvone	Terpene
(+) limonene	Terpene
(-) limonene	Terpene
1-heptanethiol	Thiol
1-hexanethiol	Thiol
1-octanethiol	Thiol
heptanoic acid	carboxylic acid
octanoic acid	carboxylic acid
decanoic acid	carboxylic acid
3,4-hexanedione	Ketone
2,3-hexanedione	Ketone
4-tert-butylcyclohexanone	Ketone
cyclohexanone	Ketone
2-heptanone	Ketone
acetophenone	Ketone
musk Ketone	Ketone
amyl acetate	Ester
amyl hexanoate	Ester
ethyl isobutyrate	Ester
whiskey lactone	Lactone
2-coumaranone	Benzofuran
eugenol	Phenylpropanoid
3-nitrotoluene	Toluene
Mix1	Mixture of 19 chemical compounds

*Note: All chemical were purchased from Sigma-Aldrich (Saint-Quentin-Fallavier, France) except for Lylal, which was provided as a generous gift from International Flavors & Fragrances (Dijon, France).

3.3 Genotyping

3.3.1 Genomic DNA extraction

Approximately 5 mm of mouse-tail was cut, placed in 1.5 mL sterile screw-cap tubes, and stored at -20°C. Before genotyping, the tails were incubated overnight at 55°C in 200 µL of Proteinase K (Biolone, Luckewald) diluted at 1:100 in digestion buffer (Peglab, Erlangen) on a rocking platform. The following day, the lysed tails were incubated at 85°C for 45 min to deactivate enzymatic digestion, and subsequently stored at 4°C.

3.3.2 Polymerase chain reaction

Polymerase chain reaction (PCR) was used for DNA amplification to confirm and determine the mouse strain of interest using a SimpliAMP/Thermocycler (Applied Biosystems, Darmstadt). A standard reaction mix was prepared with MilliQ water (Millipore, Billerica MA, USA), 10X reaction buffer, deoxyribose nucleotide tri-phosphates (dNTPs) and Taq polymerase (Taq Hot Start). 10X buffer, dNTPs, and Taq polymerase were provided by Takara Bio Inc, Shiga, Japan. PCR steps are described in figure 3.5.

PCR primers were provided by Sigma-Aldrich, St. Louis MO, USA. For all the mouse strains a primer pair for the wild type allele (WT) and the mutant allele (MUT) was tested, except for the fNa1.7 and TMEM16B genes, where only the mutant allele was tested due to its unknown locus in the genome. Each genotyping experiment contained two positive controls, containing MUT DNA of the mouse strain and WT B6 DNA mouse strain, and a negative control containing only distilled water.

3.3.3 Agarose gel electrophoresis

The amplified DNA was separated using gel electrophoresis. The gel was made using 1.2% agarose (Carl Roth + Co. KG, Karlsruhe) in TBE buffer (Tris/borate/EDTA; Carl Roth + Co. KG, Karlsruhe) mixed, and heated in a microwave. After heating, 3 µL of ethidium bromide (EtBR) was added. The intercalation of the EtBR with the DNA permits its visualization under ultraviolet (UV) light, at a wavelength of 302nm. A blue dye was added to the

samples to show DNA migration in the gel. A voltage of 120 V was applied for 30 min. Electrophoresis separates DNA fragments by size; while larger fragments migrate slower and remain near the top of the gel, shorter fragments migrate faster and are found near the end.

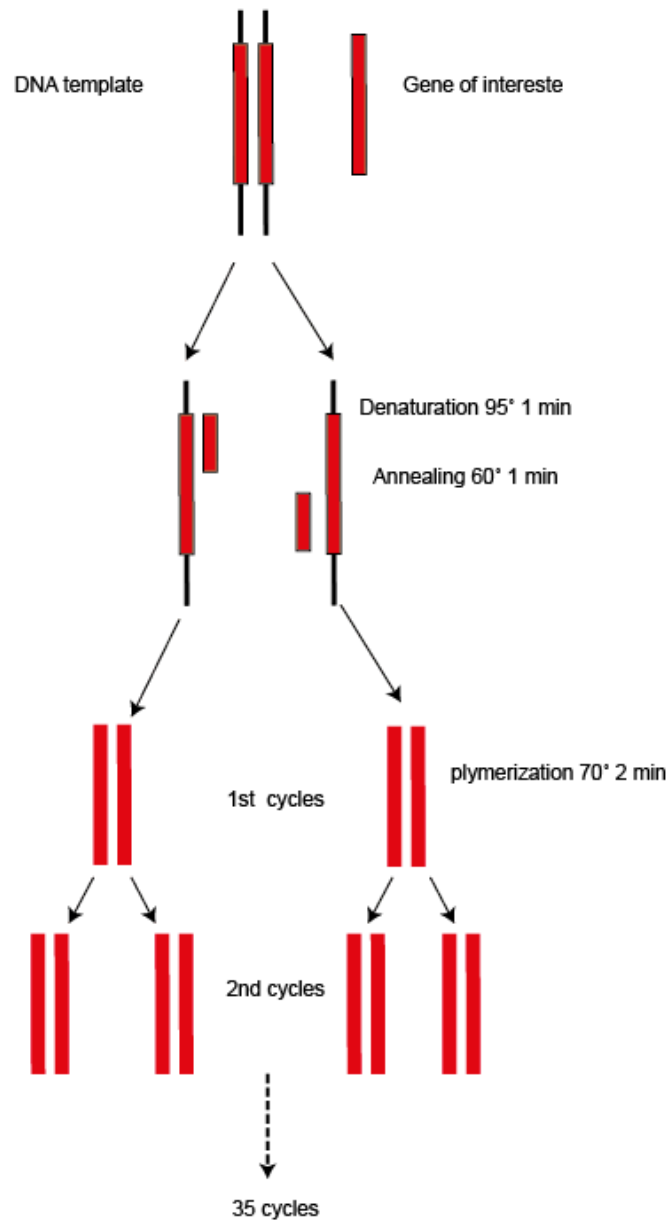


Figure 3.5 PCR protocol for genotyping. The denaturation consists of heating the reaction, which causes DNA melting by disrupting the hydrogen bonds between the DNA bases. The annealing steps occurred at 60° for 1 min permitting the annealing of the primers to the stranded DNA. In the polymerization step the taq polymerase synthesize a new DNA strand complementary to the DNA template.

Table 3. List of primers:

Mutant name	Oligo wildtype	WT band size	Oligo MUT	MUT band size
M71-IRES-tauGFP	1121B/A114A	309 bp	819/A114A	~250 bp
M71-IRES-Cre	1121B/A114A	309 bp	900A/901A	~450 bp
tdRFP (ROSA-tdRFP)	HL54/ HL152	210 bp	HL152/ HL15	301bp
Tm16b		177 bp	778/7781	211 bp
fNav1.7		317 bp	16s / 17a	461bp
MOR256-17-IRES-tauGFP	MK162/ MK163	455 bp	MK99/ MK163	401bp
MOR256-17-IRES-tauLacZ	MK162/ MK163	455 bp	MK100/ MK163	415 bp
SR1-IRES-tauGFP	SF1/SF2	562 bp	SF3/ SF2	439 bp

3.4 Immunohistochemistry

Mice were deeply anaesthetized by intraperitoneal injection of 0.01 mL/g anesthetic (0.25 mL 2% xylazine, 1.2 mL 10% ketamine and 8.55 mL 0.9% NaCl). To perform an intracardial perfusion, the skin from the abdomen was sterilized by alcohol and removed. To reach the heart the ribcage was removed, a needle was inserted in the left ventricle, and then a small incision was made in the right atrium. The blood was washed away by 10 mL cold PBS. Tissue fixation was achieved by perfusing 20 mL 4% paraformaldehyde (PFA) (Sigma-Aldrich, St. Louis, MO, USA & Merck, Darmstadt).

The mouse was decapitated and dissected for post fixation; specifically, the skin, eyes, lower jaw, and palatine bones were removed. The head was immersed in 4% PFA and incubated for 2 H at 4 ° C with agitation, followed by decalcification with 0.5 M EDTA (Carl Roth + Co. KG, Karlsruhe) overnight

and cryoprotected with ascending grades (10%, 15%, and 30%) over the period of three nights at 4° C with gentle agitation. Mouse heads were then frozen in optimal cutting temperature (O.C.T) compound (Tissue-Tek, Torrance, CA, USA), and sectioned at 12 µm on a cryostat Leica CM3050 S.

MOR256-17 sections were collected on Superfrost™ slides (ThermoScientific, Germany) and blocked in 10% normal donkey serum (NSD) in PBS for one hour at room temperature, followed by incubation with primary antibodies MOR256-17 (1:800; Strotmann et al., 2004, a gift from Prof. Dr. Jörg Strotmann), GFP 1:500 (chicken polyclonal, Abcam, Cambridge, MA, USA), OMP 1:5,000 (goat antiserum, Wako Chemicals USA, Richmond, VA, USA), all in 2% normal donkey serum overnight at 4°C. Sections were washed in 0.1% Triton in PBS (PBS-T), and incubated with secondary antibody fluorescein conjugated donkey anti-chicken 1:800 (Jackson ImmunoResearch Lab, West Grove, PA, USA), rhodamine-red-X-conjugated donkey- anti-rabbit 1:800 (Jackson ImmunoResearch), and Cy5-conjugated donkey-anti-goat 1:1000 (Jackson ImmunoResearch). Immunostained sections were examined and imaged with a Zeiss LSM 510 confocal microscope (Jena, Germany).

For Nav1.7 immunostaining, sections of 12 µm were performed using a cryostat (Leica Biosystems, Wetzlar), collected on Superfrost™ slides (ThermoScientific, Germany), and stored at -80°C until required for immunostaining.

The slides were taken from -80°C, dried with cold wind dryer, covered with aluminum and stored overnight at room temperature to dry further. Before applying the primary antibody the slides are washed 3 x 5 min in PBS, and blocked on 10 % NDS in PBS-T at room temperature for one hour. Excess of blocking solution was removed, and followed by an overnight incubation in primary antibody anti-Nav1.7 (1:500, rabbit polyclonal; Millipore) at 4°C. Sections were washed 3 x 10 min with 0.1 Triton in PBS at room temperature, followed by 1.5 H incubation in secondary antibody (1:100, Alexa fluor 555 donkey anti rabbit, Invitrogen), at room temperature. Following secondary antibody incubation, the slides were washed 3 x 10 min in PBS-T, stained with DAPI for 10 min at room temperature, mounted and coverslipped with Moviol,

and left overnight to dry at room temperature.

3.5 X-gal staining

X-gal staining (also called lacZ staining) is a powerful technique to visualize the OSNs axon guidance and their projections in the OB. This staining is rapid and simple to perform. The technique is based on the expression of the bacterial (E-coli) gene LacZ, which encodes the β -galactosidase enzyme. This enzyme catalyzes the hydrolysis of X-gal (5-bromo-4-chloro-3-indolyl-beta-D-galactopyranoside) into galactose and 5-bromo-4-chloro-3-hydroxyindole; this latter is oxidized into 5,5'-dibromo-4, 4'-dichloro-indigo, an intensely blue product allowing visualization of LacZ activity.

Table 4. X-gal staining buffers:

Buffer A	Buffer B	Buffer C
100 mM PBS (pH 7.4)	100 mM PBS (pH 7.4)	5 mM hexacyanoferrate (II)
2 mM MgCl ₂	2 mM MgCl ₂	5 mM hexacyanoferrate (III)
5 mM EGTA	0.01% Na deoxycholate	1 mg/mL X-gal in DMF in Buffer B
	0.02% IGEPAL CA-630	

X-gal staining was performed in sagittal or dorsal whole mount preparation. Dorsal dissection allows the visualization of dorsal glomeruli, whilst dissection in the sagittal aspect allowed visualization of medial glomeruli. The mice were anesthetized as aforementioned in chapter (2.4) and decapitated, followed by removal of the skin, lower jaw, and skull to expose the OB. The head was fixed with 4 % PFA on ice for 30 min, and then washed with Buffer A 3x for 5 min, at room temperature. The head was washed with Buffer B 2x for 5 min, at room temperature and incubated in dark with Buffer C for 15 min at 37°C. Once the color change to blue was deemed sufficient, the head was stored in 4 % PFA at 4°C.

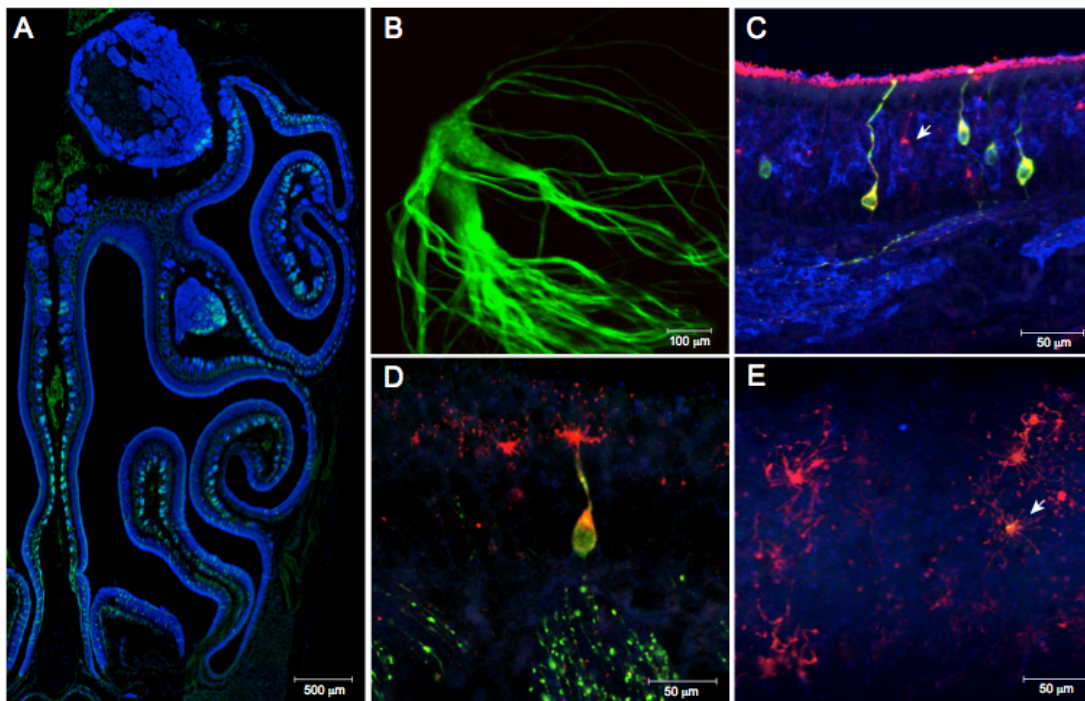
3.6 Data analysis and statistics

Unpaired t tests were performed with GraphPad Prism software (La Jolla, CA, USA), to indicate statistical differences between the two populations of OSNs, P values <0.05 were considered significant. Dose-response curves were fitted with Origin 9.1 (OriginLab, Northampton, MA) using the Hill equation, $I = I_{\max} / (1 + (K_{1/2}/C)^n)$, where I represents the peak of odor-induced response, I_{\max} the maximum response at saturating concentrations, $K_{1/2}$ the concentration when half of the maximum response was reached (EC_{50}), C the concentration of odorant, and n the Hill coefficient. Electrophysiology data analysis was performed using PatchMaster (Heka electronics, Germany) and Igor pro software (Wavemetrics, Lake Oswego, OR, USA). Averaged data are shown as mean \pm SEM.

4 Results

4.1 The MOR256-17 mouse strain tagged with GFP

The mouse OR gene MOR256-17 is also referred to as OR3 (Nef and Hermans-Borgmeyer, 1992) and Olfr15. The mouse strain MOR256-17-IRES-tauGFP was generated in-house, by gene targeting in embryonic stem cells (Tazir et al., 2015) along the same design as in (Luxenhofer et al., 2008). In heterozygous or homozygous mice, OSNs coexpress tauGFP and MOR256-17. This is due to a bicistronic strategy that is afforded by the internal ribosome entry site (IRES). Expression of tauGFP can be visualized by using the intrinsic fluorescence of GFP or with anti-GFP antibodies (Tazir et al., 2016).



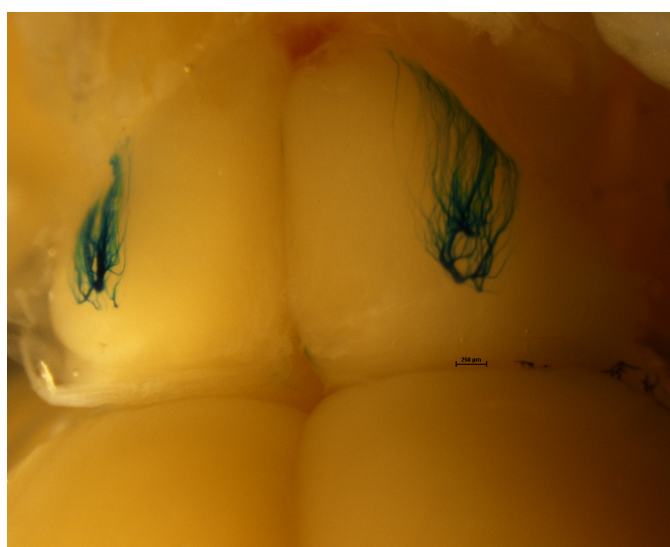
4.1 The olfactory system of the MOR256-17-IRES-tauGFP mouse strain. A, coronal section of a heterozygous post-natal day (PD) 35 mouse, immunostained for OMP (blue) and intrinsic GFP fluorescence (green). B, confocal z-stack image of GFP fluorescence of the lateral glomerulus in a whole mount of a homozygous PD45 mouse. C, immunostaining with MOR256-17 antibody (red), GFP antibody (green) and OMP (blue) in a heterozygous PD35 mouse. Arrow shows MOR256-17 antigen in a GFP-negative OSN, consistent with monoallelic expression. D, MOR256-17 immunostaining (red) reveals the arborization of OSN cilia in a heterozygous PD35 mouse. E, confocal en face image of dendritic knobs, with colocalization of MOR256-17 immunostaining and GFP (arrow) in a heterozygous. (From Tazir et al. 2016).

In a coronal cryosection of the nasal cavity of a 35-day old mouse heterozygous for MOR256-17-IRES-tauGFP, green-fluorescent cells are

observed scattered across a broad zone in the middle of the main olfactory epithelium (MOE) (Figure 4.1A). In a whole-mount of a 45-day old mouse homozygous for MOR256-17-IRES-tauGFP, green-fluorescent axons coalesced into a complex and large glomerulus within a ventral domain of the lateral face of the olfactory bulb (Figure 4.1B). An antibody against MOR256-17 (Strotmann et al., 2004; Schwarzenbacher et al., 2004; Schwarzenbacher et al., 2006; Fuss et al., 2007) colabelled GFP immunoreactive cells in heterozygous mice (Figure 4.1C-E). Approximately half of the MOR256-17 immunoreactive cells were GFP immunoreactive in heterozygous mice, consistent with the well-established principle of monoallelic expression of OR genes.

The intrinsic fluorescence of tauGFP expressed from an OR locus was sufficiently high to visualize these OSNs including their dendritic knobs and cilia in intact epithelial preparations, thus allowing single-cell electrophysiological recordings according to a well-established method (Ma et al., 1999; Grosmaître et al., 2006; Grosmaître et al., 2009; Lam and Mombaerts, 2013; Omura et al., 2014).

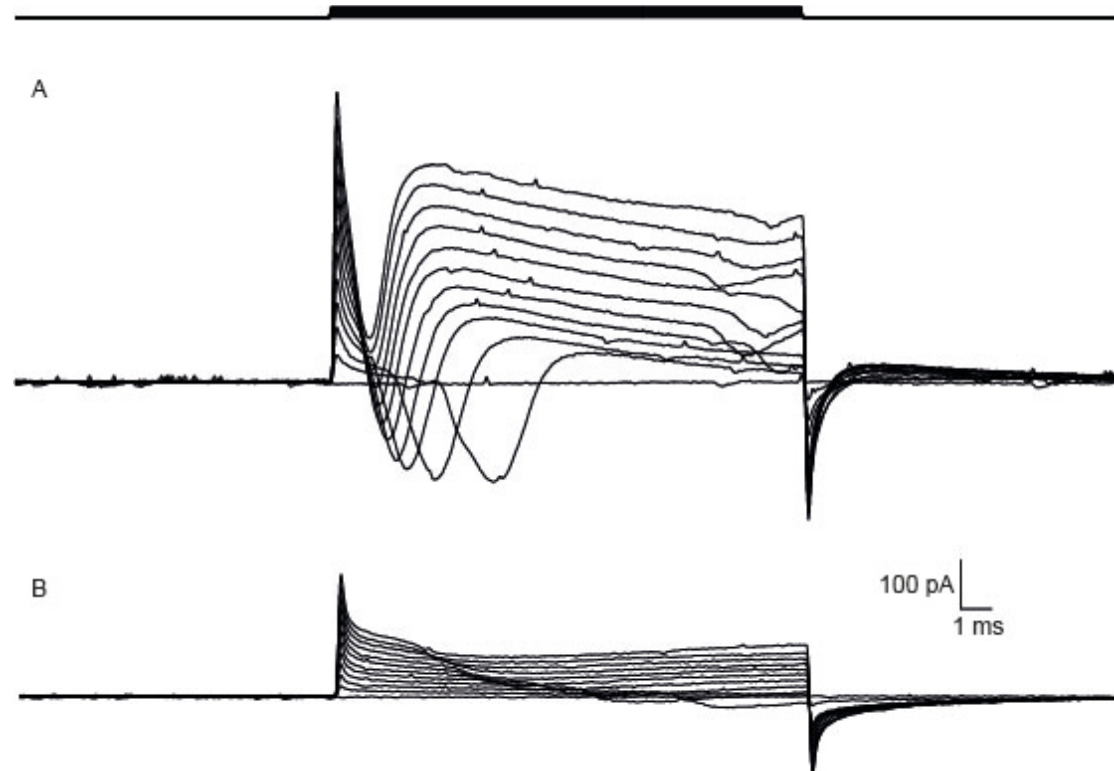
The MOR256-17-IRES-tauLacZ strain was generated in-house (at Rockefeller University, NY, USA). This mouse was used to visualize MOR256-17 OSNs wiring and their glomeruli in the OB.



4.2 Axonal wiring of MOR256-17-IRES-tauLacZ. Two lateral dorsal glomeruli of MOR256-17-IRES-tauLacZ.

4.2 Electrophysiology study of MOR256-17-IRES-tauGFP and SR1-IRES-tauGFP OSNs

4.2.1 Monitoring the state of the cells during recordings



4.3 Membrane properties of OSN under voltage clamp recording. A, Voltage gated current elicited by increasing depolarizing steps, from a healthy cell. B, voltage gated current recorded from unhealthy cell.

Once a gigaohm seal was made, nystatin perforated the cell membrane, permitting the contact of the recordings pipette with the cell cytosol, a voltage-gated ionic current was observed under voltage clamp mode by eliciting increasing depolarization steps from the membrane potential -67 mV to 40 mV from a holding potential of -70 mV. As described in chapter (2.3.2) three currents were observed, one sodium current and two potassium currents (transient current and delayed rectifier current). The voltage-gated ionic current was used to examine cell health, and the quality of the recordings during the experiments. A healthy cell has a current pattern as seen in figure 4.3A, whilst in an unhealthy or a dying cell, the currents are dramatically

decreased or completely absent (Figure 4.3B). Recordings were only taken from healthy cells.

4.2.2 Spontaneous activity analysis

The spontaneous activity of the MOR256-17-IRES-tauGFP, and SR1-IRES-tauGFP OSNs was analyzed using the perforated whole-cell patch clamp configuration. The total recording time for each cell was between 20-30 s. Examples of spontaneous firing are given in Figure 4.4.

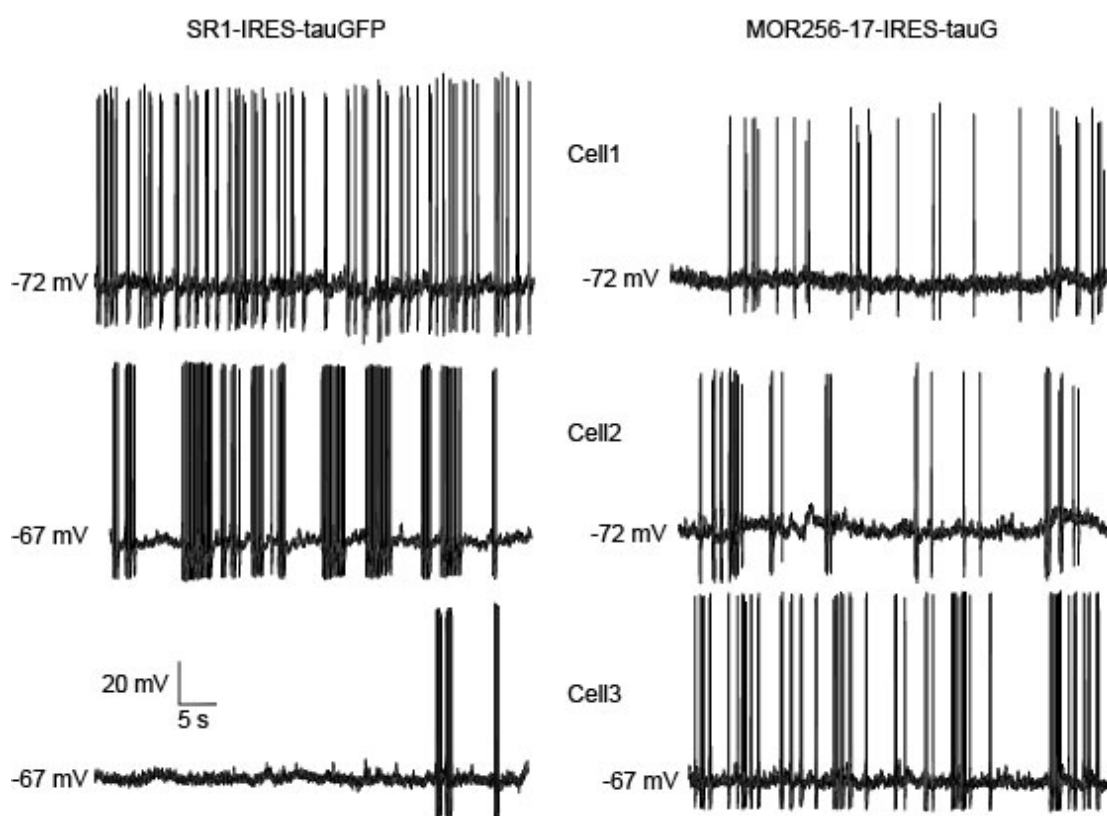


Figure 4.4 Spontaneous activity of SR1 and MOR256-17 OSNs. Spontaneous activity recordings from three different MOR256-17 cells and three different SR1 cells.

The spontaneous firing pattern was varied from cell to another. Some cells fire repetitive bursts whilst other cells fired single action potentials followed by bursts of action potentials, while other cells were silent for 10 to 15 s before firing action potentials.

The spontaneous activity of 9 cells from each cell population (SR1, n=9; MOR256-17, n=9) was analyzed. The average resting potential was -69.97 ± 0.76 mV for SR1-GFP OSNs and -70.36 ± 0.79 mV for MOR256-17-GFP OSNs.

Four parameters were analyzed; the mean firing frequency, the instantaneous firing frequency (a time segment during which bursts of action potentials occur), the inter-spike interval defined as the time between each spike during the whole recordings and the spike number. These different parameters were compared between SR-1 and MOR256-17 cell populations.

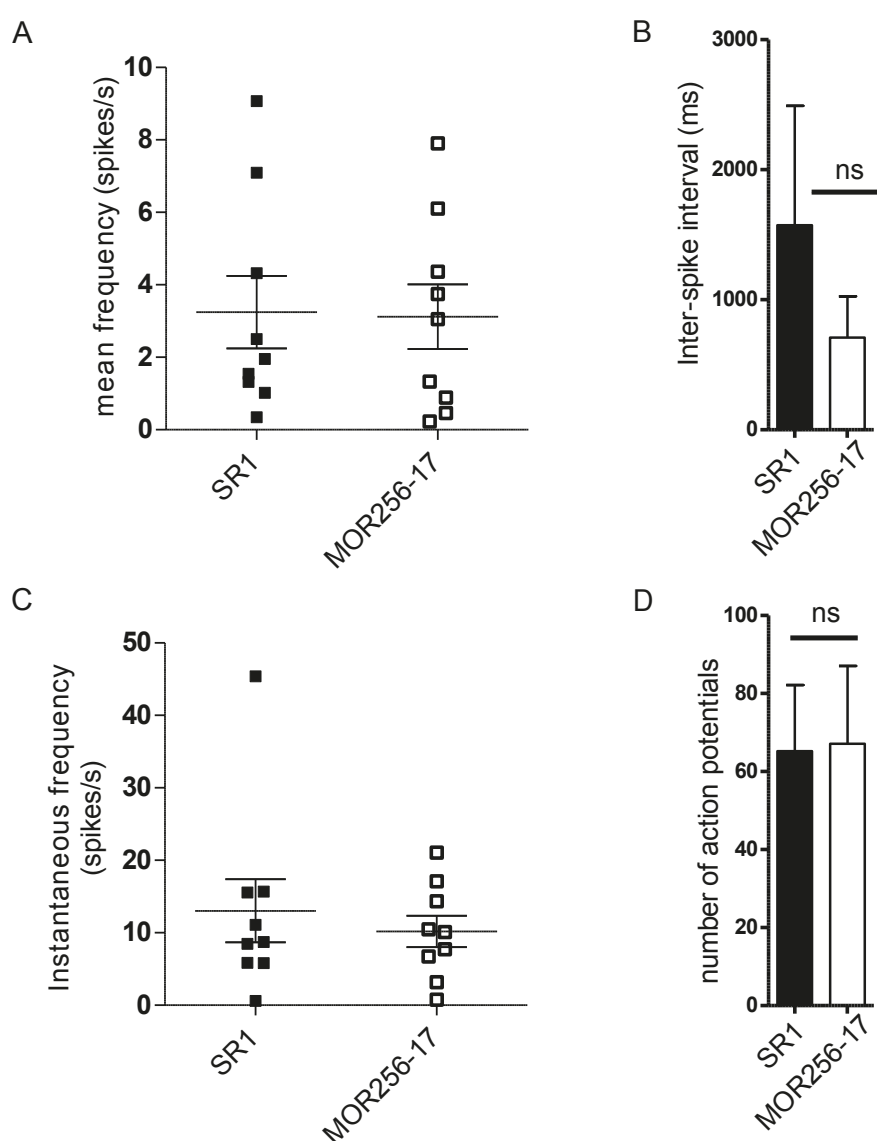


Figure 4.5 Spontaneous activity analysis of SR1 and MOR256-17 OSNs. B, mean firing frequency. Data are shown for nine individual OSNs of each population. C, Instantaneous firing frequency. Data are shown for nine individual OSNs for each population. D, Inter-spike interval. E, number of action potentials. Data are presented as mean \pm SEM. (Tazir et al. 2016).

There was no significant difference in the mean frequencies: 3.12 ± 0.89 Hz for SR1 vs. 3.24 ± 1 Hz for MOR256-17 (Figure 4.5A). Similarly, there was no difference in the instantaneous frequencies: 13.03 ± 4.34 Hz for SR1 vs. 10.17 ± 2.17 Hz for MOR256-17 (Figure 4.5C). There was no significant difference in the inter-spike interval either: $1,573.08 \pm 917.25$ ms for SR1 vs. 708.65 ± 318.23 ms for MOR256-17 (Figure 4.5B). Finally, there is also no significant difference in the number of action potentials: 65.22 ± 16.95 for SR1 vs. 67.11 ± 19.96 for MOR256-17 (Figure 4.5D). Within a single OSN population, the spontaneous activity varied considerably from cell to cell.

4.2.3 Current-induced activity analysis

To study the membrane excitability of SR1 cells and MOR256-17 cells, firing patterns were analyzed by eliciting action potentials, via injection of a depolarizing current of 7 pA into SR1 neurons ($n = 6$ cells) or MOR256-17 neurons ($n = 6$ cells)

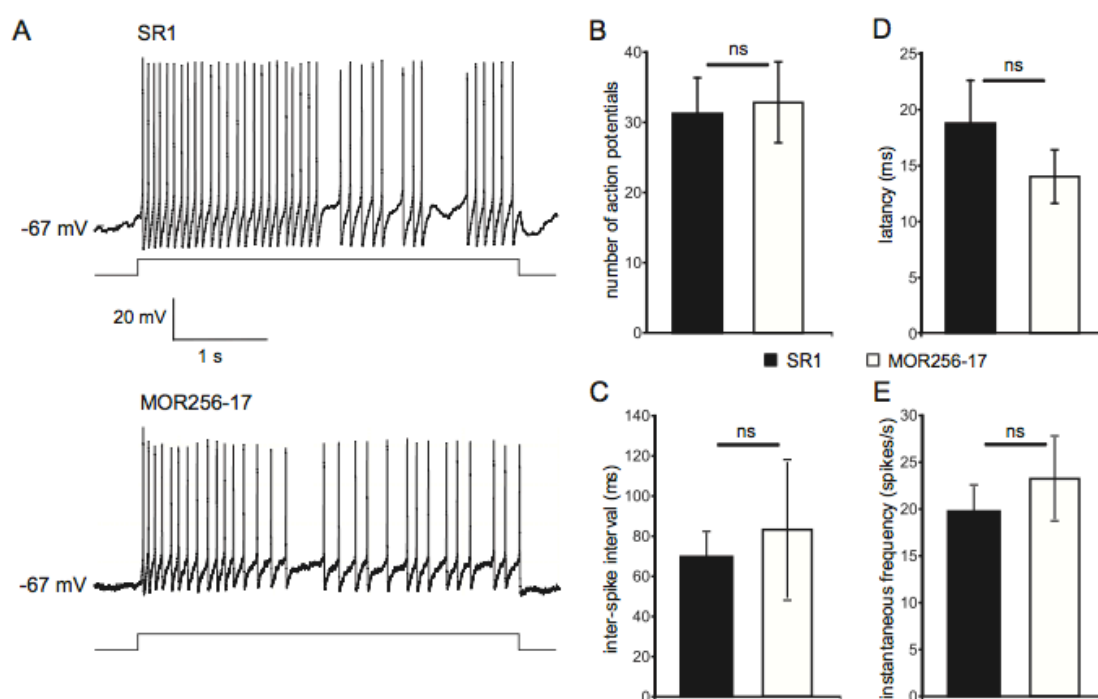


Figure 4.6 The firing pattern of SR1 OSNs and MOR256-17 OSNs current-clamp mode. A, traces representing action potentials elicited by injecting a current of 7 pA to the cells. B, number of action potentials. Data are shown for six OSNs of each population. C, inter-spike interval. D, latency is defined as the time that the cell takes to fire the first action potential after the current is injected. E, instantaneous firing frequency. Data are presented as mean \pm SEM. (from Tazir et al. 2016).

(Figure 4.6A). As with analysis of spontaneous activity, the same four parameters (the mean firing frequency, instantaneous firing frequency, inter-spike interval, and the spike number) were analyzed, and compared between the two cell populations. There is no significant difference in the number of action potentials, 31 ± 4.9 for SR1 vs. 32.5 ± 5.95 for MOR256-17 (Figure 4.6B); in the inter-spike interval, 69.48 ± 12.3 ms for SR1 vs. 83.3 ± 34.87 ms for MOR256-17 (Figure 4.6C); in the latency, 18.84 ± 3.89 ms for SR1 vs. 14 ± 2.36 ms for MOR256-17 (Figure 4.6D); and in the instantaneous firing frequency, 19.55 ± 3 Hz for SR1 vs. 23.16 ± 4 Hz for MOR256-17 (Figure 4.6E).

4.2.4 Extremely broad responsiveness of MOR256-17 OSNs

The odorant response of MOR256-17 OSNs was characterized using a mixture of odorant (Mix1) containing 19 chemical compounds (Grosmaître et al., 2009), and 35 single chemical compounds at 10 μ M, belonging to more than 9 chemical groups including alcohols, aldehydes, amines, carboxylic acids, esters, ketones, terpenes, and thiols. Some chemicals were chosen from previous heterologous systems studies, from previous broad OSNs reports, or randomly. The closely related chemicals within each functional group family, were taken in consideration, in order to examine the ability of these neurons to respond to similar odorants (same functional group but different carbon chain length), or odorants with different functional groups. At least five cells were tested for each odorant and Mix1. The response rate to a given odorant was either 0% or 100% within a given OSN population.

MOR256-17 OSNs have shown an extremely broad responsiveness to different chemical compounds from different chemical groups. In fact, MOR256-17 OSNs were able to respond to Mix 1 and 31 out of 35 single chemical compounds tested.

At 10 μ M, MOR256-17 cells respond the strongest to acetophenone ($\text{CH}_3\text{COC}_6\text{H}_5$) 145.26 ± 37.34 pA, $n = 9$ cells; 4-tert-butylcyclohexanone ($((\text{CH}_3)_3\text{CC}_6\text{H}_9(=\text{O}))$) 119.82 ± 32.35 pA, $n = 16$ cells; (+/-) carvone ($\text{C}_{10}\text{H}_{14}\text{O}$) 111.5 ± 14.44 pA, $n = 8$ cells; 3-nitrotoluene ($\text{CH}_3\text{C}_6\text{H}_4\text{NO}_2$) 105.13 ± 16.29

pA, $n = 15$ cells; and to Mix 1 118.3 ± 30.1 pA, $n = 22$ cells. Examples of recordings traces in both voltage-clamp, and current-clamp mode are shown in Figure 4.7. Bumps of action potentials can be seen in voltage clamp mode, due to imperfections in clamp space.

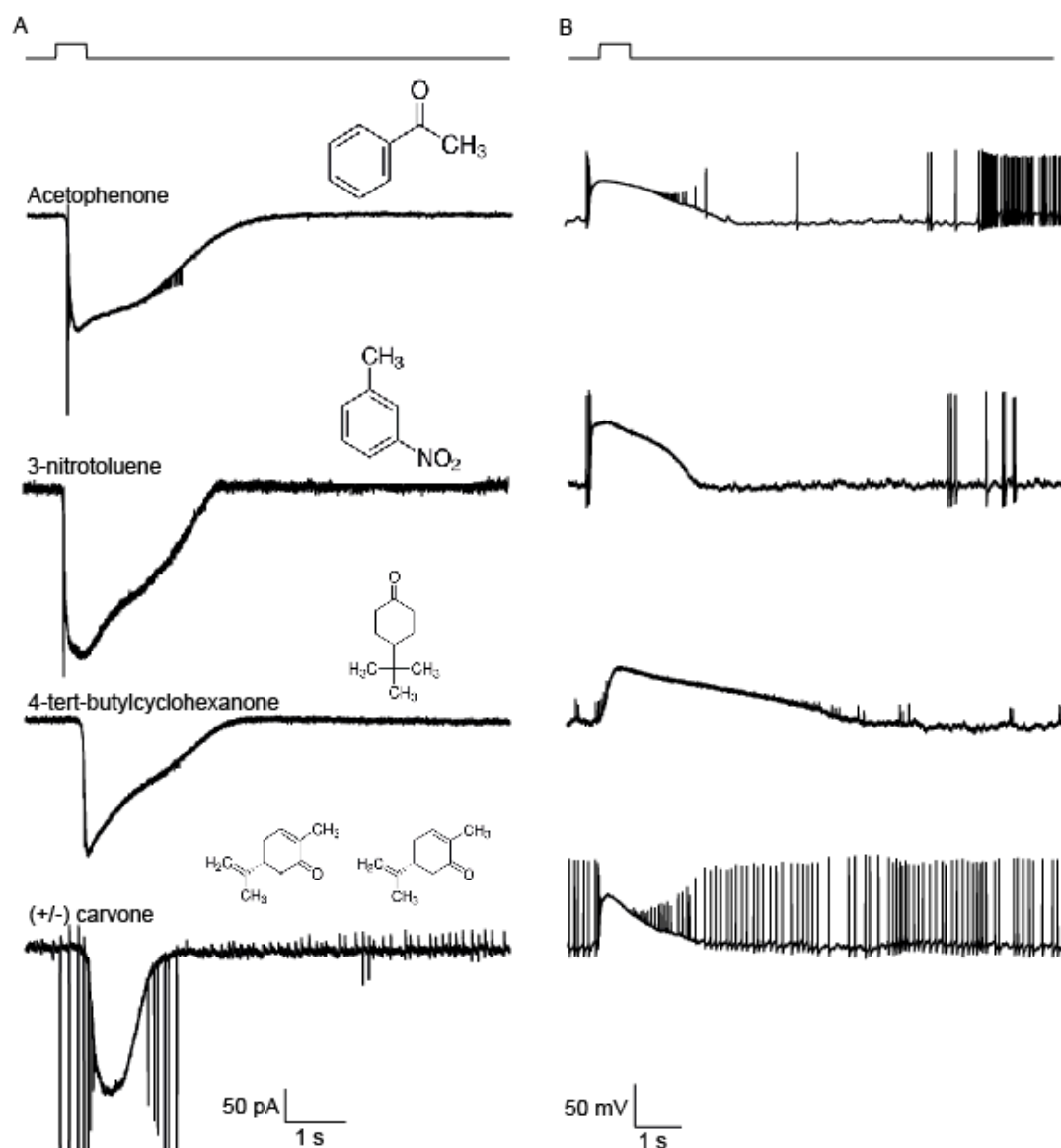


Figure 4.7 MOR256-17 OSNs respond to divers odorant compounds. A, single neuron responded to four odorant at $1 \mu\text{M}$ under voltage clamp holding potential -70 mV, B response of the same neuron under current clamp mode.

At $10 \mu\text{L}$, MOR256-17 cells responded the weakest to eugenol ($\text{C}_{10}\text{H}_{12}\text{O}_2$) 41 ± 9.88 pA, $n = 7$; 2-coumaranone ($\text{C}_8\text{H}_6\text{O}_2$) 41.85 ± 15.28 pA, $n = 7$; and ethyl

maltol ($C_7H_8O_3$) 43 ± 6.32 pA. Examples of odorant response in voltage clamp and current clamp mode are given in Figure 4.8.

MOR256-17 OSNs were also able to detect other chemical group compounds; the responses amplitudes recorded in voltage clamp mode are resumed in table 4.1.

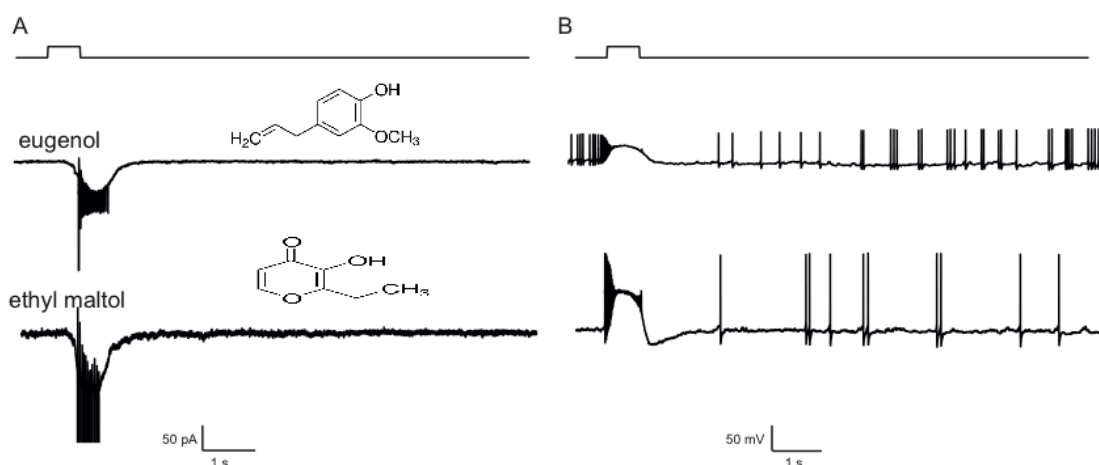


Figure 4.8 weakest odorant response of MOR256-17. A,B single neuron responding to eugenol and ethyl maltol in voltage clamp mode (left) holding potential -70 mV and current clamp mode (right).

However, MOR256-17 neurons failed to respond to (+) limonene ($C_{10}H_{16}$), $n = 6$ cells; (-) limonene ($C_{10}H_{16}$), $n = 10$ cells; cyclohexanone ($C_6H_{10}(=O)$), $n = 6$ cells; and heptanoic acid ($CH_3(CH_2)_5COOH$) $n = 7$ cells (fig 3.9).

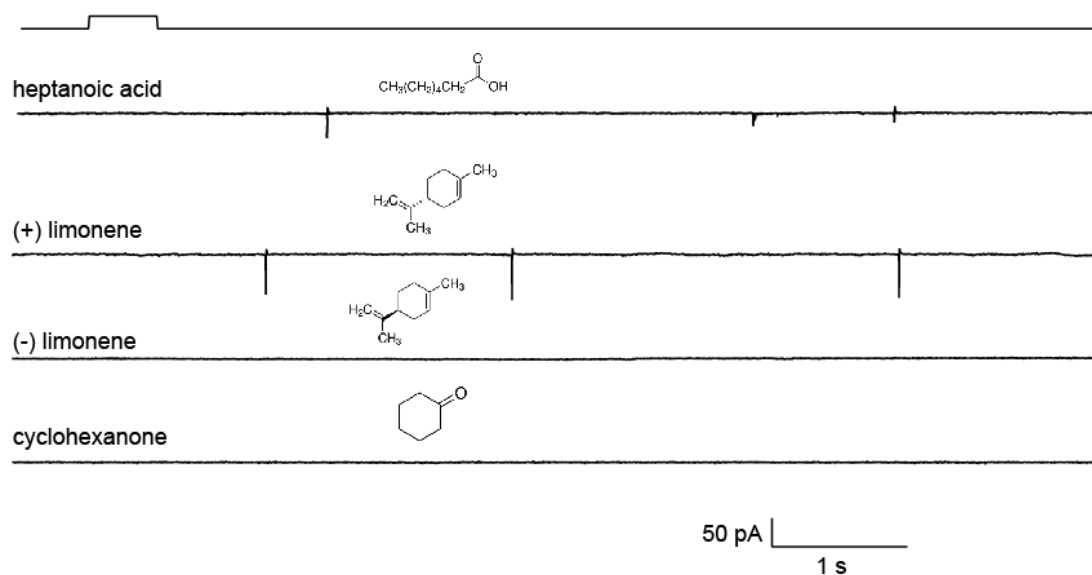


Figure 4.9 Voltage clamp recording from single MOR256-17 neurons. The flat traces represented negative response to heptanoic, (+) limonene, (-) limonene and cyclohexanone

Table 4.1 Average peak current response under voltage clamp of MOR256-17 OSNs

Chemical compound	Peak current (pA)	Cell number
(-) limonene	0	n = 10
(+) limonene	0	n = 6
(+/-) carvone	111.5 ± 14.44	n = 8
1-heptane thiol	41.75 ± 11.24	n = 8
1-hexane thiol	38.5 ± 11.64	n = 8
1-octane thiol	80.16 ± 23.87	n = 6
2-coumaranone	41.85 ± 15.28	n = 7
2-heptanone	96.63 ± 25.10	n = 10
2,3-hexandione	0	n = 9
3-nitrotoluene	105.13 ± 16.29	n = 15
3,4-hexanedione	30.26 ± 9.09	n = 9
4,tert-butylcyclohexanone	119.82 ± 32.35	n = 16
acetophenone	145.26 ± 37.34	n = 9
amyl acetate	54.12 ± 19.06	n = 8
amyl hexanoate	67 ± 18.73	n = 5
cyclohexanone	0	n = 6
cyclohexylamine	79.51 ± 33.45	n = 7
decanoic acid	50 ± 17.79	n = 5
dihydrocarvone	36.65 ± 5.97	n = 7
ethyl isobutyrate	62 ± 14.28	n = 6
ethyl maltol	43 ± 6.32	n = 5
ethyl vanillin	58.71 ± 17.32	n = 7
eugenol	41 ± 9.88	n = 7
heptanal	82.25 ± 21.98	n = 8
heptanoic acid	0	n = 7
isopentylamine	66.62 ± 28.84	n = 5
Lylal	41 ± 9.88	n = 7
menthol	50.28 ± 8.47	n = 8
Mix1	118.29 ± 30.14	n = 22
musc ketone	35.38 ± 4.35	n = 7
octanal	551.6 ± 10.78	n = 5
octanoic acid	28.66 ± 6.05	n = 9
phenethyl alcohol	55.33 ± 9.79	n = 9
phenethylamine	87.54 ± 40.58	n = 7
trans-2-hexanal	66.62 ± 14.64	n = 9
whiskey lactone	55 ± 21.69	n = 5

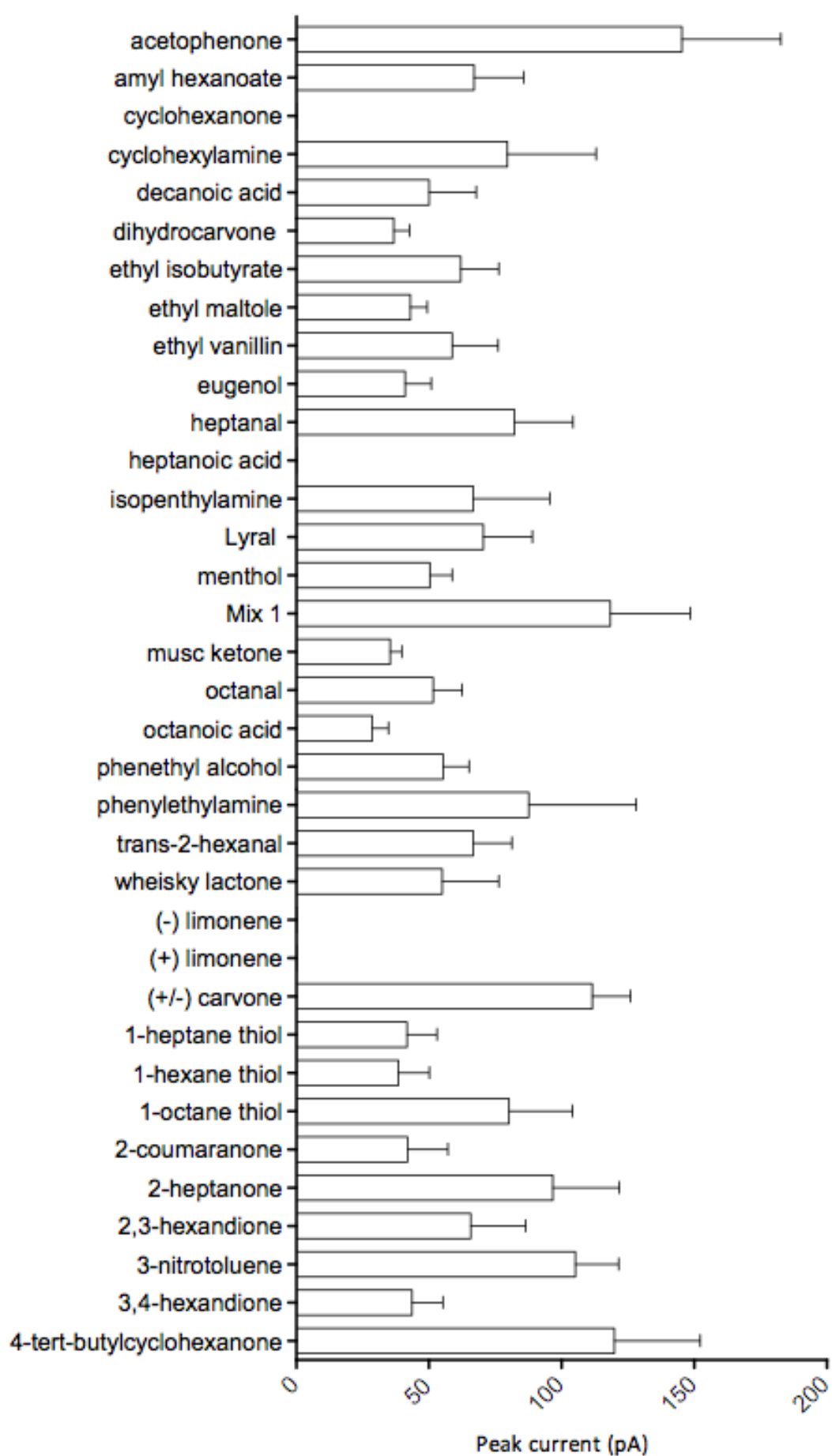


Figure 4.10 Average peak current responses of MOR256-17 OSNs

However, MOR256-17 neurons failed to respond to (+) limonene ($C_{10}H_{16}$), $n = 6$ cells; (-) limonene ($C_{10}H_{16}$), $n = 10$ cells; cyclohexanone ($C_6H_{10}(=O)$), $n = 6$ cells; and heptanoic acid ($CH_3(CH_2)_5COOH$) $n = 7$ cells (Figure 4.9).

Interestingly, MOR256-17-GFP OSNs were activated by three amines at 10 μ L, cyclohexylamine, 79.51 ± 33.45 pA, $n = 7$ cells; isopentylamine 66.62 ± 28.84 pA, $n = 5$ cells; and phenylethylamine 87.54 ± 40.52 pA, $n = 7$ cells. These are typically viewed as ligands for chemosensory neurons in the main olfactory epithelium that express TAAR genes, a family of 15 genes encoding G-protein coupled receptors unrelated in sequence to ORs.

4.2.5 Similar odorant responses of MOR256-17 neurons in the MOE and the SO

SR1 cells showed similar response in two different olfactory subsystems (MOE and, SO), to amyl acetate, (+) camphor, benzaldehyde, octanoic acid, and heptanal (Grosmaître et al., 2009).

MOR256-17 neurons are also expressed in the MOE, and the SO. Thus, an odorant responsiveness comparison of MOR256-17 cells was conducted in the SO and the MOE. Like SR1 neurons, MOR256-17 neurons could also detect the same odorants in the SO and the MOE. Some, but not all the odorant compounds were tested in the SO; the most of the recordings experiments were conducted in the MOE. In contrast with SR1-GFP neurons, there were more MOR256-GFP neurons in the MOE than the SO. MOR256-17 neurons in the SO were able to respond to 4-tert-butylcyclohexanone ($n = 6$ cells), dihydrocarvone ($n = 1$ cell), trans-2-hexanal ($n = 2$ cells), 3,4-hexandione ($n = 1$ cell), and menthol ($n = 2$ cells).

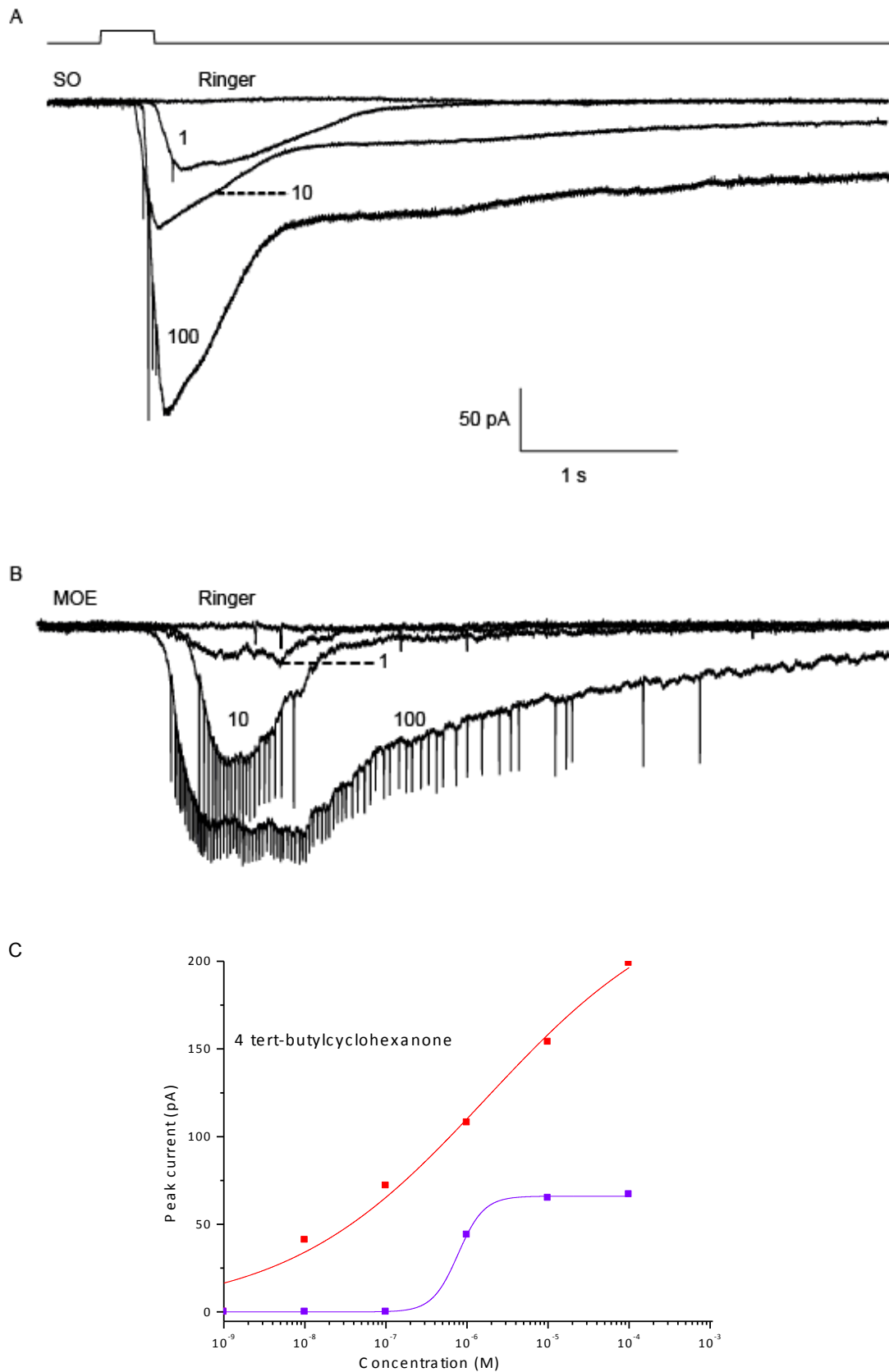


Figure 4.11 Similar response of MOR256-17 in the MOE and SO. A, single MOR256-17 neuron responding to different concentration (1 μ M, 10 μ M, and 100 μ M) of 4-tert-butylcyclohexanone at voltage clamp in the SO, holding potential -70 mV. B, response to MOR256-17 to different concentration of 4-tert-butylcyclohexanone in the MOE. C, dose response curve of two MOR256-17 neurons in the SO.

4.2.6 Odorant responsiveness comparison of MOR256-17 OSNs and SR1 OSNs

After confirmation of the broad responsiveness of MOR256-17 neurons, the same range of odorants was also tested in SR1 neurons. MOR256-17 neurons responded to Mix1 and 31 out of 35 single compounds, whereas SR1 responded to Mix1 and only 10 single chemical compounds. The average response amplitude recorded in voltage-clamp mode is shown in Table 4.2. Moreover, the odorant response profile of SR1 OSNs is fully included within that of MOR256-17 (Figure 5.1). SR1 neurons were not able to respond to the three amines tested cyclohexylamine (n=9 cells), isopentylamine (n=9 cells), and phenethylamine (n=11 cells) (Figure 4.12). SR1 OSNs were not responsive to the three thiols: 1-heptanethiol (n=6 cells), 1-hexanethiol (n=8 cells), and 1-octanethiol (n=5 cells) (Figure 4.13).

At 10 μ M, SR1 OSNs showed a strong response to whiskey lactone 133.07 ± 17.94 pA, n = 8 cells; (+/-) carvone 95.75 ± 23.11 pA, n = 10 cells; 2-heptanone 95.64 ± 22.52 pA, n = 13 cells; and octanal 91.44 ± 25.33 pA, n = 5 cells. At the same concentration SR1 OSNs responded the weakest to 2-coumaranone 44.54 ± 9.41 pA, n = 7 cells; heptanal 52.91 ± 18.92 pA, n = 6 cells; and acetophenone 57.94 ± 30.17 , n = 5 cells.

Moreover, the response profile reported for SR1 OSNs was five odorants: camphor, amyl acetate, benzaldehyde, octanoic acid, and heptanal (Grosmaître et al., 2009). In this study six more odorants activating SR1 OSNs, were identified: (+/-) carvone (95.75 ± 23.11 pA, n=10 cells), 2-heptanone (95.64 ± 22.52 pA, n=13 cells), acetophenone (57.94 ± 30.17 pA, n=5 cells), 2-coumaranone (44.51 ± 9.41 pA, n=7 cells), phenylethyl alcohol (69.75 ± 17.10 pA, n=6 cells) and whiskey lactone (133.07 ± 17.94 pA, n=9 cells).

Table 4.2 Average peak current responses under voltage clamp of SR1 OSNs

Chemical compound	Peak current (pA)	Cell number
(-) limonene	0	n = 8
(+) limonene	0	n = 8
(+/-) carvone	95.75 ± 23.11	n = 10
1-heptane thiol	0	n = 8
1-hexane thiol	0	n = 6
1-octane thiol	0	n = 8
2-coumaranone	44.54 ± 9.41	n = 7
2-heptanone	95.64 ± 22.52	n = 13
2,3-hexandione	0	n = 6
3-nitrotoluene	0	n = 7
3,4-hexanedione	0	n = 5
4,tert-butylcyclohexanone	0	n = 9
acetophenone	57.94 ± 30.17	n = 5
amyl acetate	88.92 ± 35.9	n = 7
amyl hexanoate	0	n = 7
cyclohexanone	0	n = 7
cyclohexylamine	0	n = 9
decanoic acid	0	n = 7
dihydrocarvone	0	n = 7
ethyl isobutyrate	0	n = 7
ethyl maltol	0	n = 7
ethyl vanillin	0	n = 6
eugenol	0	n = 7
heptanal	52.91 ± 18.92	n = 6
heptanoic acid	0	n = 5
isopentylamine	0	n = 9
Lyril	0	n = 6
menthol	0	n = 6
Mix1	145.61 ± 38.08	n = 20
musc ketone	0	n = 8
octanal	91.44 ± 25.33	n = 5
octanoic acid	98.67 ± 26.74	n = 11
phenethyl alcohol	69.75 ± 17.10	n = 6
phenethylamine	0	n = 11
trans-2-hexanal	0	n = 10
whiskey lactone	133.07 ± 17.94	n = 8

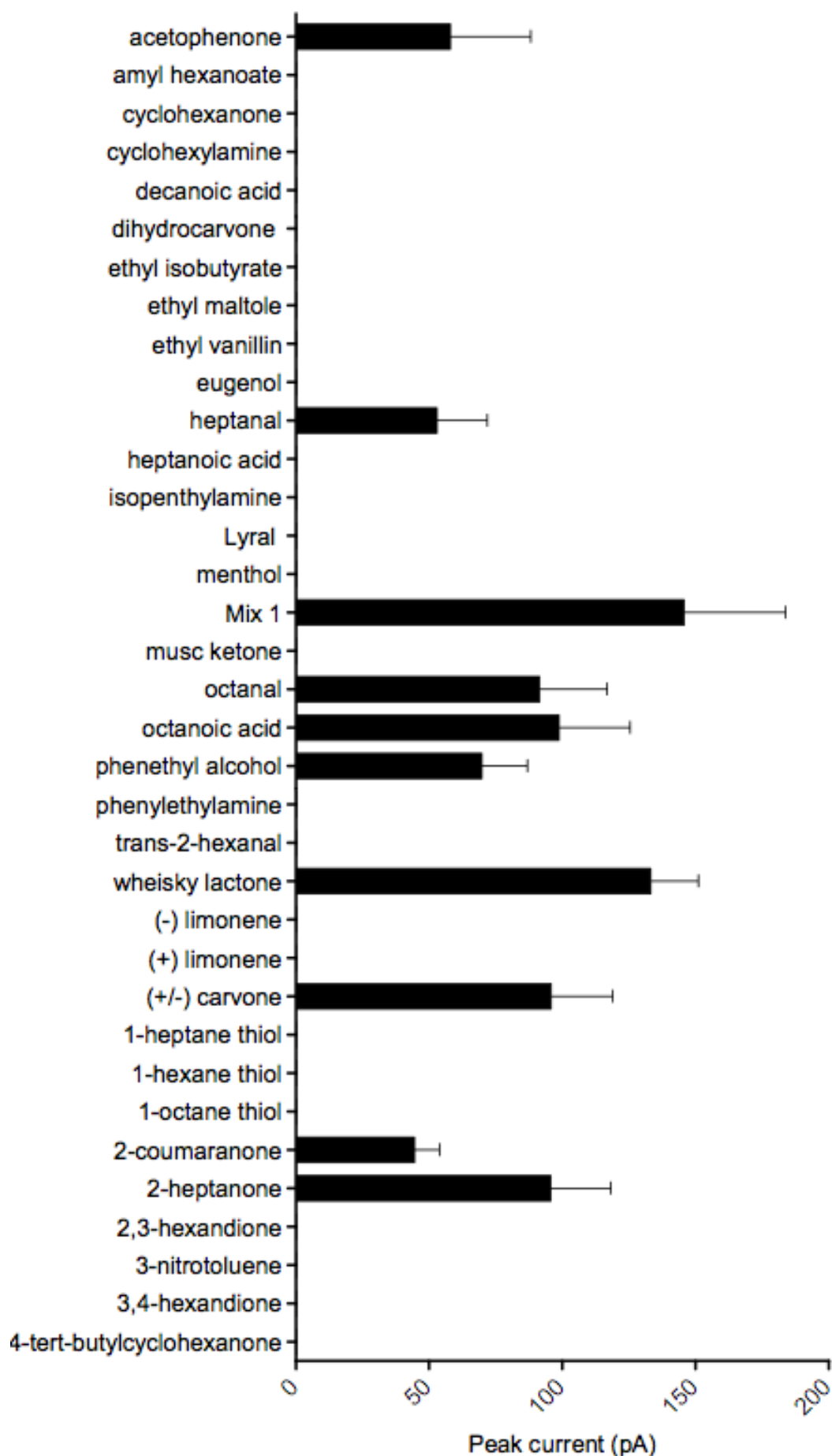


Figure 4.12 Average peak current responses of SR1 OSNs to the 35 odorants tested

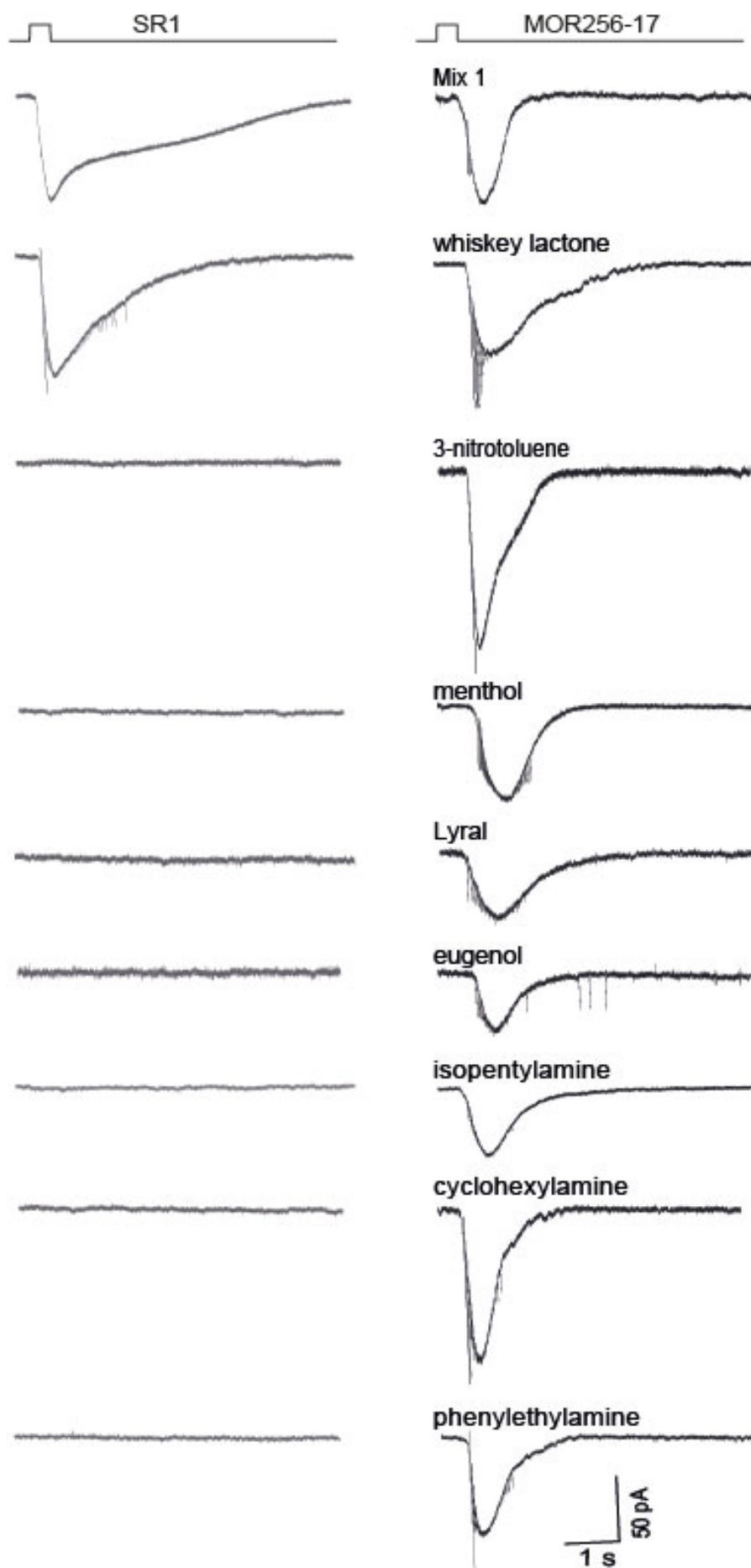


Figure 4.13 Traces of inward odorant current for Mix 1 and chemical compounds in SR1 OSNs and MOR256-17 OSNs, under voltage clamp. Flat traces indicate no response to odorant stimulus. (From Tazir et al.2015).

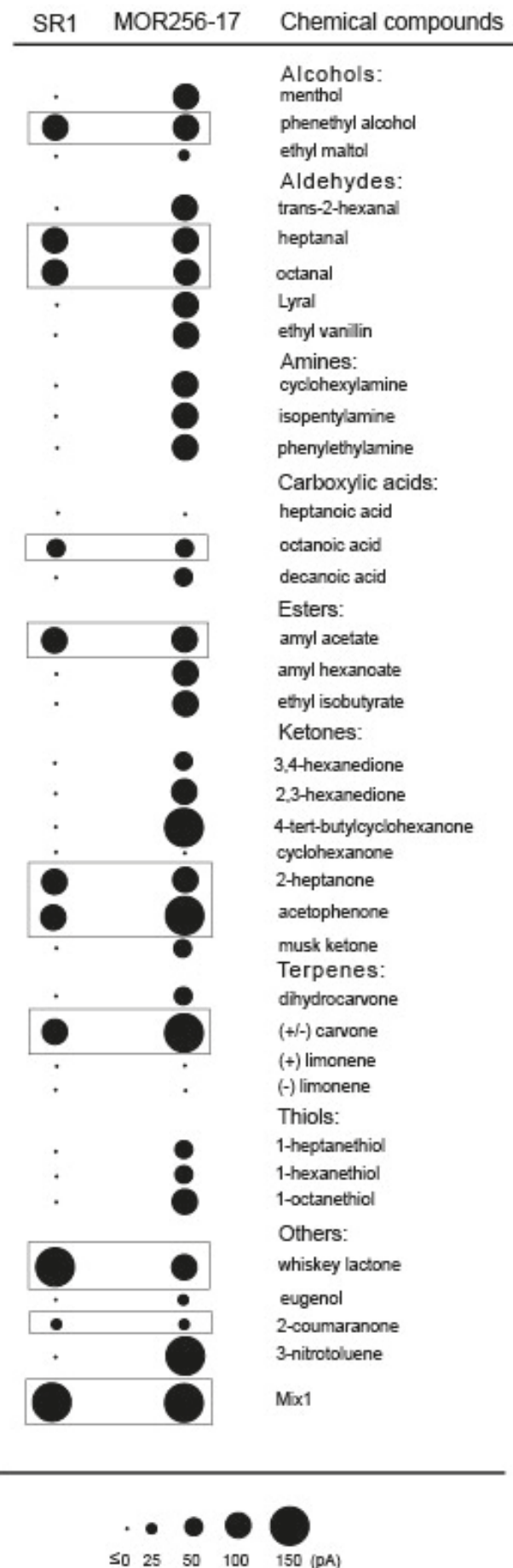


Figure 4.14 SR1 OSNs and MOR256-17 OSNs respond to a variety of chemical compounds. Voltage clamp recordings in SR1 and MOR256-17 OSNs to 35 chemical compounds at 10 μ M and Mix1, which consists of 19 odorants each at 10 mM. Each dot represents the average response of at least five OSNs. (From Tazir et al., 2016)

4.2.7 Differences in odorant response properties between SR1 and MOR256-17 OSNs

To compare the responses to the 10 ligands and Mix1 that are shared between SR1 and MOR256-17 OSNs, five parameters of the odorant-induced current were analyzed: latency, rise time, peak current, half-width, and total charge area (Figure 4.15 A).

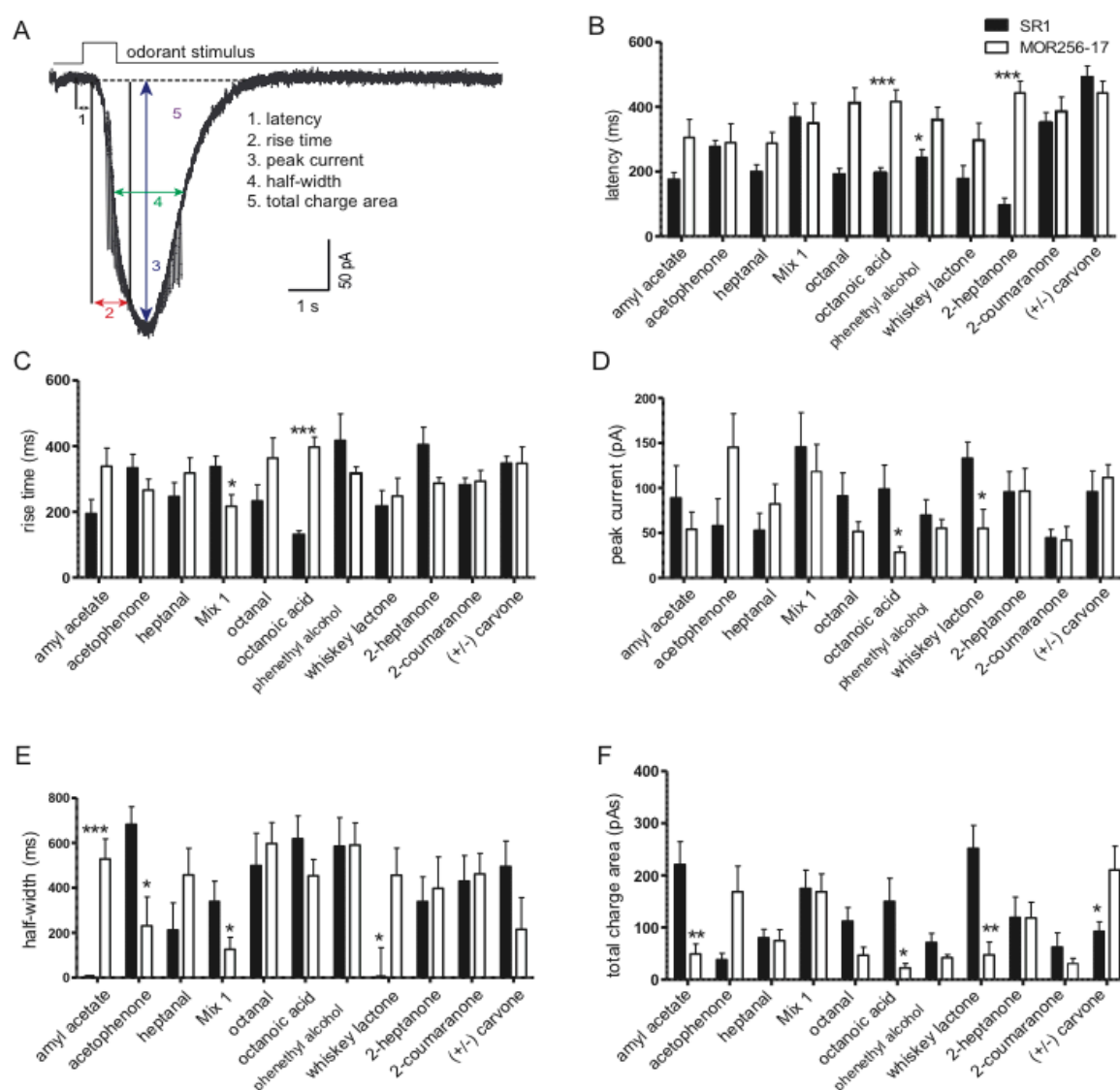


Figure 4.15 Odorant-induced currents for the common ligands of SR1 OSNs and MOR256-17 OSNs. (A) Analysis of five parameters of odorant-induced current under voltage-clamp mode. Latency is the time between the onset of the stimulus and the starting point of the response; the rise time is the time that it takes the current to reach 90% of the peak from the starting point of the response; the half-width of the current is the time between the rising and falling phase at 50% of the peak; and the total charge area is the area of the entire response. (B–F) Analysis of voltage-clamp kinetics for common ligands of SR1+ OSNs and MOR256-17+ OSNs. Data are presented as mean + SEM. (From Tazir et al., 2015)

As populations, SR1 OSNs and MOR256-17 OSN populations differ in certain parameters for various chemicals. But a consistent pattern is seen only with

octanoic acid; SR1+ OSNs respond with a shorter latency (Figure 4.15B), a shorter rise time (Figure 4.15C), and a higher peak current (Figure 4.15D), and overall have a higher total charge area (Figure 4.15F). The half-width (Figure 4.15E) is the only parameter in which SR1 OSNs and MOR256-17 OSNs do not differ in their responses to octanoic acid. Thus, the response to octanoic acid is faster and stronger in SR1 OSNs than in MOR256-17 OSNs. But neither population has a faster and stronger response than the other

4.2.8 Dose-response curves

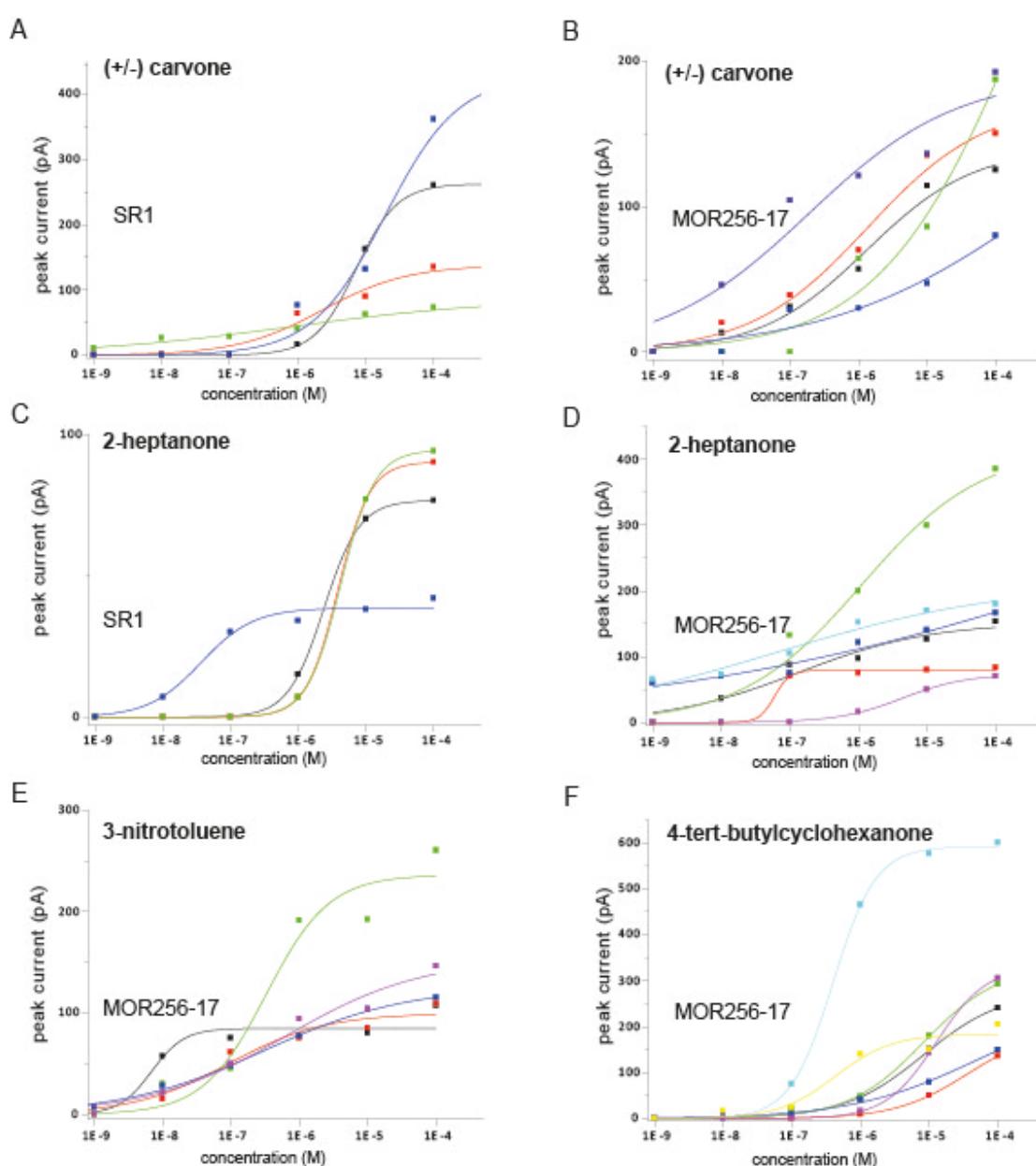


Figure 4.16 Dose-response curves of the peak current for selected odorants. Different colours in A–F correspond to individual cells. (A) Responses of SR1+ OSNs to (+/-) carvone. (B) Responses of MOR256-17+ OSNs to (+/-) carvone. (C) Responses of SR1+ OSNs to 2-heptanone. (D) Responses of MOR256-17+ OSNs to 2-heptanone. (E) Responses of MOR256-17+ OSNs to 3-nitrotoluene. (F) Responses of MOR256-17+ OSNs responding to 4-tert-butylcyclohexanone. (Tazir et al., 2016)

Dose-response curves of SR1 OSNs and MOR256-17 OSNs for (+/-) carvone and 2-heptanone was measured (Figure 4.16A-D). Moreover, dose-response curves of MOR256-17 OSNs for 3-nitrotoluene and 4-tert-butylcyclohexanone (Figure 4.16E-F) was also measured. The relation between odorant dose and peak odorant-induced current was fitted using the Hill equation. Several dose-response curves of MOR256-17 OSNs did not show a sigmoidal shape, presumably because the highest concentration tested was not saturated.

Three parameters of the kinetics of the dose-response curves were compared: the $K_{1/2}$ (EC50), the maximum amplitude (V_{max}), and the Hill coefficient (H_n). No significant difference was observed between the two cell populations. Figure 4.17 shows the EC50 values and the V_{max} values as scatter plots.

Table 4.3 Dose-response curves kinetics of SR1 OSNs:

	2-heptanone	(+/-) carvone
Vmax (pA)	74.95 ± 12.70	229.20 ± 76.19
EC50 (μM)	2.62 ± 0.95	7.37 ± 4.20
H_n	1.58 ± 0.16	0.80 ± 0.23

Table 4.4 Dose-response curves kinetics of MOR256-17 OSNs:

	3-nitrotoluene	2-heptanone	(+/-) carvone	4-tert-butylcyclohexanone
Vmax (pA)	143.32 ± 28.92	179.49 ± 47.79	152.81 ± 20.87	278.11 ± 58.40
EC50 (μM)	0.25 ± 0.09	0.83 ± 0.62	2.43 ± 1.31	6.31 ± 1.88
H_n	0.61 ± 0.15	1.02 ± 0.54	0.53 ± 0.05	1.11 ± 0.14

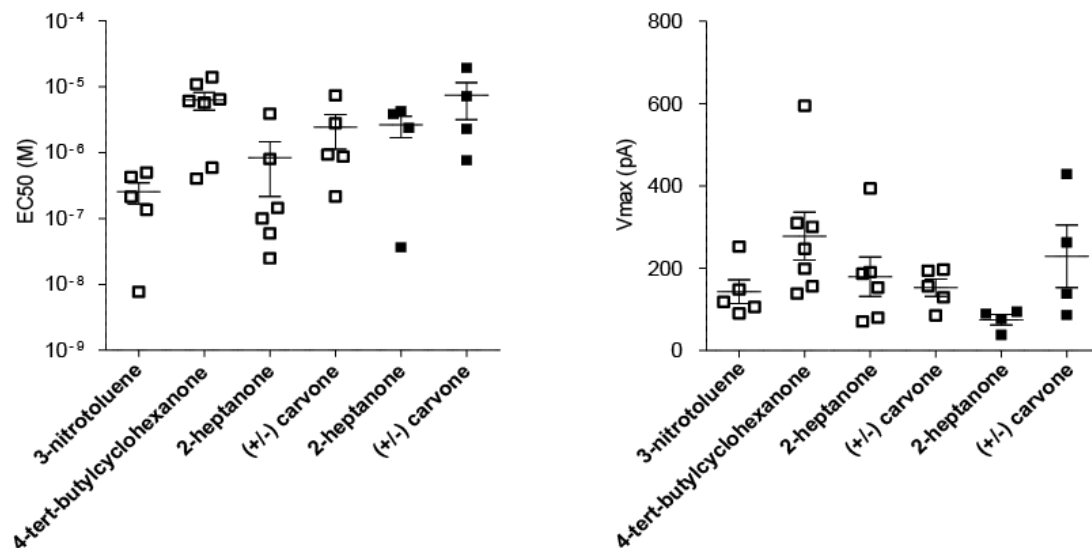


Figure 4.17 Dose-response curves analysis. EC₅₀ values (in log₁₀) of dose–response curves to odorants for MOR256-17+ OSNs (open symbols) and SR1+ OSNs (filled symbols). V_{max} values of dose–response curves to odorants for MOR256-17+ OSNs (open symbols) and SR1+ OSNs (filled symbols). Data are presented as mean ± SEM. From Tazir et al.2016

4.3 Nav1.7 Knockout in specific subpopulation M71 OSNs

As mentioned in Chapter 1.9, Weiss et al. showed the importance of Nav1.7 in the transmission of the olfactory signal to the second order neurons (Mitral/tufted cells) in the OB: *-/-* Nav1.7 OSNs were able to generate an odorant-induced current, however, the mouse was completely anosmic due to silencing of the mitral cells (Weiss et al., 2011).

In this chapter, the role of Nav1.7 in axonal guidance was investigated by generating a Nav1.7 conditional knockout mouse in one subtype of OSN. The Nav1.7 channel was knocked out in some OSNs, and expressed in other OSNs belonging to the neuron subpopulations M71, in the same mice. This approach allowed in vivo competition between OSNs expressing a specific OR gene, and the comparison within the same OB axonal projections of *-/-* Nav1.7, and *+/-* Nav1.7, M71-expressing OSNs. This was possible due the monogenic and the monoallelic features of OR genes (Chess et al., 1994).

A breeding strategy was performed by crossing different gene-targeted mouse strains expressing M71 gene. M71 is a suitable OR gene to study axonal guidance, due to the dorsal axonal projections in the OB, which allowed glomeruli imaging. Moreover, M71 gene is an OR gene that is very well studied and characterized (Bozza et al., 2002; Feinstein and Mombaerts, 2004) .

In the first strain, the fNav1.7 conditional null mouse (Weiss et al., 2011) was crossed to M71-IRES-Cre x tdRFP mouse strain already available in-house. This strain was the result of a cross between M71-IRES-Cre, with the tdRFP mouse strain; tdRFP was used as a reporter gene for the Cre recombinase. The fNav1.7 x M71-IRES-Cre x tdRFP offspring were intercrossed till the acquisition of mice homozygous for the three mutations fNav1.7, M71-IRES-Cre and tdRFP. In this strain, the Cre recombinase recognized the two loxP sites and flank the Nav1.7 channel, resulting in conditional knockout in M71 OSNs with expression of tdRFP (Figure 4.18).

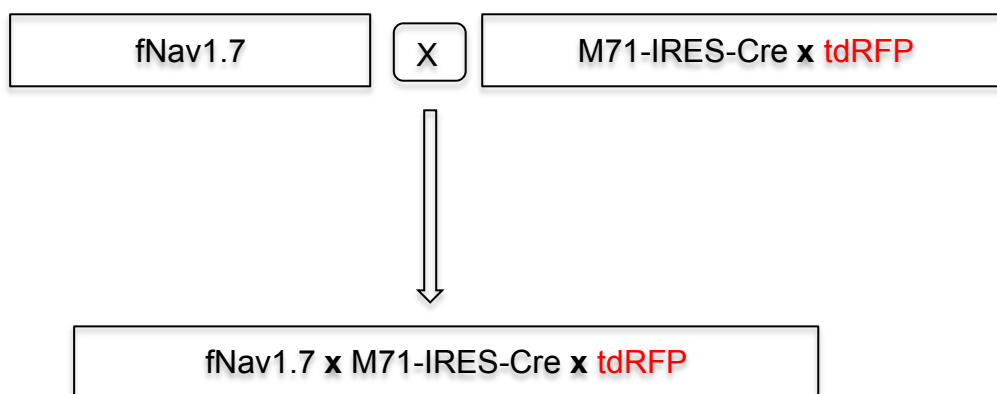


Figure 4.18 Breeding strategy to generate M71 OSNs with a fNav1.7 knockout

In the second strain, the fNav1.7 conditional null mice were crossed to the M71-IRES-tauGFP strain, and once mice homozygous for M71-IRES-tauGFP and fNav1.7 genes were obtained, fNav1.7 x M71-IRES-tauGFP was crossed to the tdRFP mouse strain (Figure 4.18). In this strain the fNav1.7 is intact, because the Cre recombinase is absent, resulting in M71 OSNs with expression of GFP and fNav1.7 channel, which were the control OSNs.

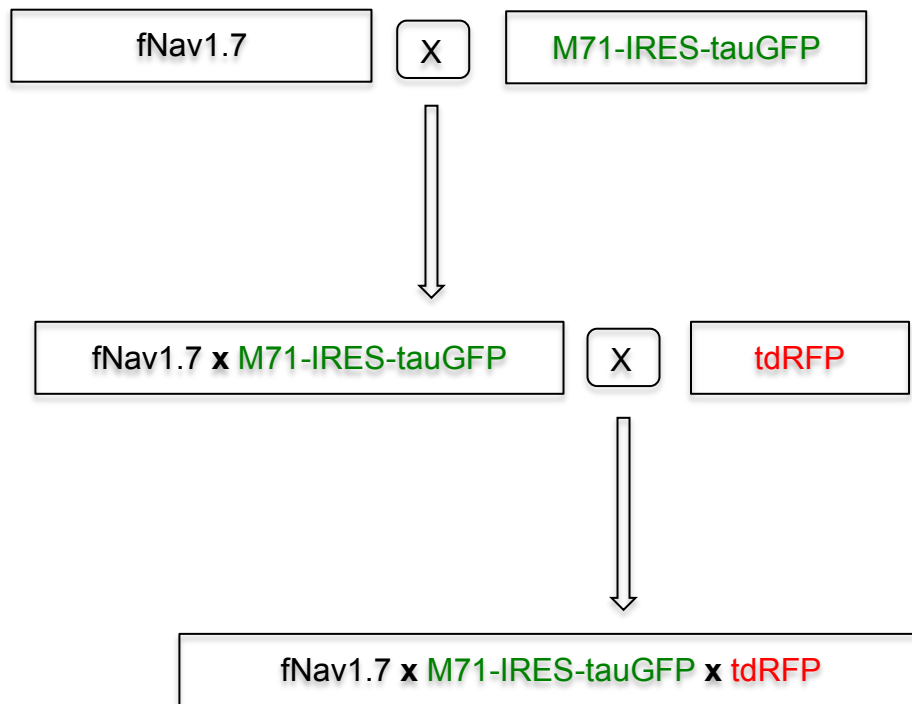


Figure 4.19 Breeding strategy to generate control M71 OSNs

In the final strain, the two triple crossed homozygous strains fNav1.7 x M71-IRES-Cre x tdRFP and fNav1.7 x M71-IRES-tauGFP x tdRFP were crossed.

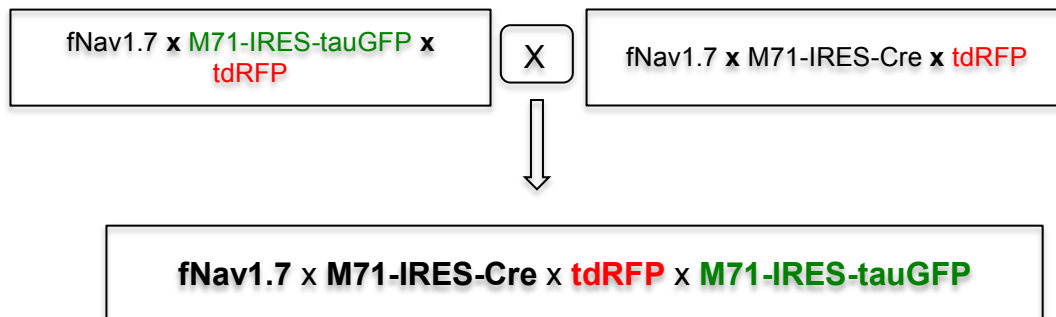


Figure 4.20 Breeding strategy to generate the final compound heterozygous mice. In this strain M71 OSNs expressing fNav1.7 (green) coexist with M71 OSNs lacking expression of fNav1.7 (red).

The offspring were intercrossed till the acquisition of quadruple homozygous mice for the mutations fNav1.7, M71-IRES-tauGFP, M71-IRES-Cre and tdRFP. In this final mouse strain the M71 expressing tauGFP OSNs are healthy neurons, however, M71 OSNs expressing tdRFP are lacking fNav1.7 expression. This allowed the comparison of the impact of fNav1.7 channel on axonal guidance within the same OB.

The axonal guidance was normal in the triple cross strain lacking the expression of fNav1.7, in the triple cross strain expressing the fNav1.7 channel, and in the final compound heterozygous quadruple mutant strain (Figure 4.21). At 21 postnatal days, the axons from both fNav1.7 ^{-/-} and fNav1.7 ^{+/-} M71 OSNs colocalized, in the normal dorsal lateral position of the M71 glomerulus (Figure 4.21B).

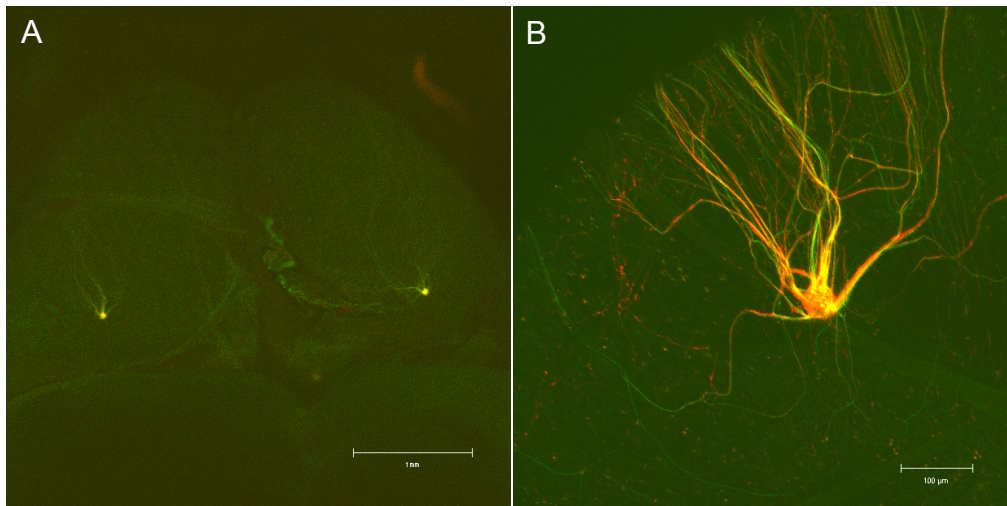


Figure 4.21 fNav1.7 does not affect M71 glomerular position. A, Dorsal view of the left and right OBs from a PD21 fNav1.7 x M71-IRES-Cre x tdRFP x M71-IRES-tauGFP mouse. The dorsal glomeruli appear normal, the red M71 OSNs axons lacking fNav1.7 expression coalesce with the green M71 OSNs axons expressing fNav1.7. B, High magnification of the left dorsal glomerulus.

The axonal wiring was also verified at PD42.

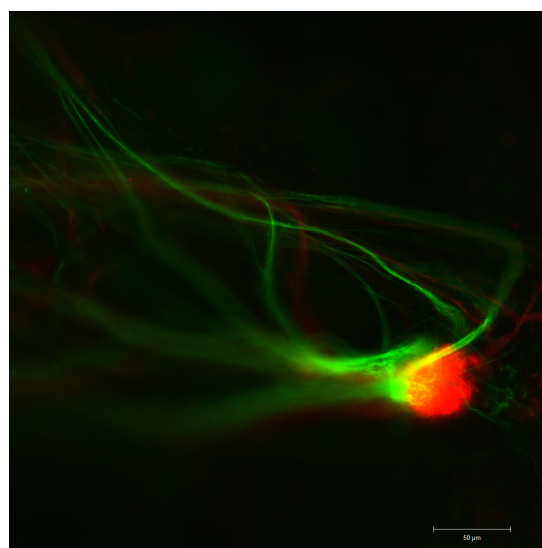


Figure 4.22 Dorsal glomerulus a PD43 mouse from the fNav1.7 x M71-IRES-Cre x tdRFP x M71-IRES-tauGFP strain.

heterozygous quadruple mutant mouse, no difference in the wiring was seen between *fnav1.7* ^{-/-} and *fnav1.7* ^{+/+} M71 OSNs (Figure 4.22).

4.4 Tm16b Knockout in specific subpopulation M71 OSNs

The same breeding strategy performed for *fnav1.7* was used to investigate the role of the CaCC Tm16b in OSNs axonal wiring (Figure 4.23).

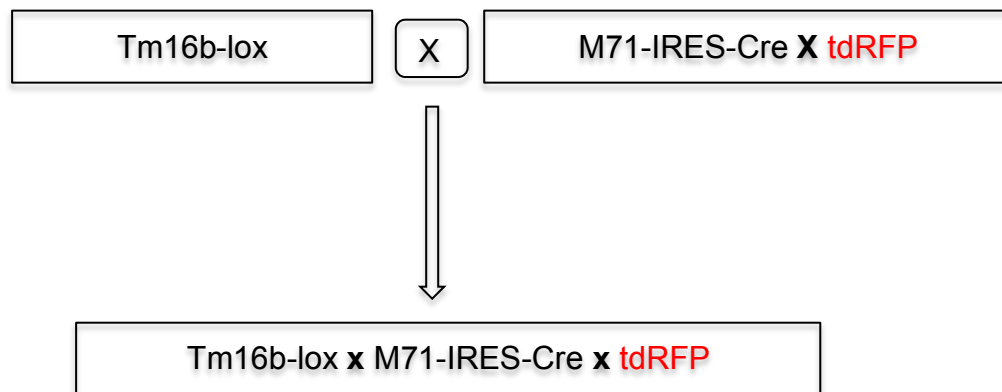


Figure 4.23 Breeding strategy to generate Tm16b knockout M71-expressing OSNs mouse strain.

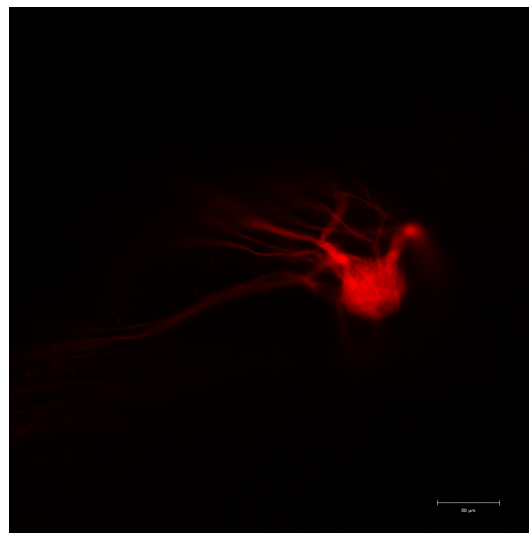


Figure 4.24 Dorsal glomerulus from a PD56 Tm16b x M71-IRES-Cre x tdRFP mouse.

The final triple homozygous mutant strain Tm16b x M71-IRES-Cre x tdRFP was analyzed, using whole-mount dissection, and no effect in the axonal guidance of M71 neurons was observed. The glomerulus looked normal and located in the normal position of M71 glomerulus.

In Chapters 3.3 and 3.4, the impact of neural activity on OSNs axonal guidance was investigated by studying two channels Nav1.7 and Tm16b. The results revealed no obvious changes in wiring of OSN axons or in the glomerular formation in conditional mutant M71-expressing OSNs.

5 Discussion

25 years ago after the discovery of the OR genes (Buck and Axel, 1991), it is apparent that the olfactory system relies on the combination of different ORs (Buck, 2004), in order to detect the enormous number and variety of chemical compounds present in the environment. Olfactory coding at the periphery of the olfactory system is not completely understood. Thus, investigating odorant-OR pairs is crucial to provide further insight. The mouse genome contains approximately 1100 intact OR genes (Godfrey et al., 2004). Despite technical progress to identify OR ligands, most of these ORs still orphans and only a few odorant-pairs are known.

In this thesis, a detailed and comparative electrophysiological study was performed in two mouse strains, each expressing a specific OR tagged with GFP, SR1-IRES-tauGFP and MOR256-17-IRES-tauGFP, respectively. This targeting strategy allowed their identification in intact epithelial preparation *ex vivo*. Thus, the activity of native OSNs expressing defined ORs from their endogenous locus in an environment mimics an *in vivo* scenario was investigated.

This well-established method (Ma et al., 1999) (Jarriault and Grosmaitre, 2015) has been previously used to characterize responses of OSNs expressing an OR with a narrow response profile such as MOR23 (Grosmaitre et al., 2006) or S1 (Lam and Mombaerts, 2013), an OR with a broad response profile such as SR1 (Grosmaitre et al., 2009), and the β 2-adrenergic receptor expressed in OSNs from an OR locus (Omura et al., 2014)). This preparation has been informative in a variety of experimental contexts such as aging (Lee et al., 2009), the effect of variations in OR sequence to odorant responses (Zhang et al., 2012), prenatal development (Lam and Mombaerts, 2013), spontaneous activity (Connelly et al., 2013) odorant-induced plasticity (Cadiou et al., 2014), and the correlation of OSN ciliary length with sensitivity in the septum and dorsal recess (Challis et al., 2015).

This study provided quantitative and qualitative results concerning the olfactory coding of broad tuned ORs, by recording odorant-induced current from defined OSNs populations, 130 OSNs expressing MOR256-17 and 88 OSNs expressing SR1 have been analyzed.

5.1 Intrinsic membrane properties of SR1 and MOR256-17 neurons

In order to characterize the membrane properties of SR1 and MOR256-17 OSNs the firing patterns were studied. The two populations fired spontaneous, and repetitive action potentials when a current of 7 pA was injected to the cells (Chapters 4.2.2 and 4.2.3; Figures 4.5 and 4.6), as showed before in rat and mouse OSNs (Ma et al., 1999).

The spontaneous firing rates and the instantaneous activity of SR1 OSNs (3.12 ± 0.89 Hz, $n = 9$ cells), (13.3 ± 4.34 Hz, $n = 9$ cells) were similar to those reported by Connelly et al (3.79 ± 0.57 Hz, $n = 11$ cells), (10.73 ± 1.7 Hz, $n = 11$ cells), which used cell attached patch clamp configuration, with the same intact olfactory epithelium preparation and the same SR1 mouse strain, used in this study (Connelly et al., 2013).

The firing frequency between the SR1 and MOR256-17 OSNs (figure 4.5A), was not statistically significant (Figure 4.5A, $p > 0.9$), which is in disagreement with other studies that reported a variety of spontaneous activity between different OSNs populations (Reisert, 2010) (Connelly et al., 2013). This may be attributed to other OSN populations expressing different ORs, like broadly responsive ORs, which do not exhibit variation in spontaneous activity. Reisert has compared only three OSN populations (mOR-EG, M71, and I7) (Reisert, 2010), and Connelly et al. investigated just five OSN populations (M71, I7, SR1, mOR-EG, and MOR23) (Connelly et al., 2013).

Moreover, SR1 and MOR256-17 OSNs revealed a spontaneous spiking heterogeneity pattern among the same population (Figure 4.4). These results extend previous findings in OR-IRES-tauGFP mouse strains, it has been

shown that spontaneous activity varies among OSNs expressing the same OR (Connelly et al., 2013).

Variations in a homogenous population of OSNs are not well understood, and difficult to examine. It is evident that ORs themselves drive the spontaneous activity (Connelly et al., 2013), thus, the number of receptors expressed could influence the spiking rate of the cell. Recently, OSNs have shown variation in cilia length and odorant sensitivity, depending on where the neurons are located in the neuroepithelium (Challis et al., 2015). It would be informative to compare the spontaneous activity of a defined OSN population in these different zones, to determine if cilia length influences the spontaneous firing of OSNs.

Comprised of thousands of OSN axons (Bressel et al., 2016), spontaneous firing is necessary for establishing and maintaining the organization of glomeruli in the bulb (Yu et al., 2004). Therefore, differences in spontaneous activity between OSNs belonging to the same neuron subpopulation may play a role in this process.

5.2 Extremely broad odorant responsiveness of MOR256-17 OSNs

Earlier work investigating the OR responsiveness in amphibians suggested the existence of broad ligand specificity of OSNs (Sicard and Holley, 1984) (Firestein et al., 1993). However, the only characterized broadly tuned OSNs in mouse were SR1 neurons (Grosmaître et al., 2009) and MOR256-31 (Nara et al., 2011), owing to the slow progress in this aspect of olfaction.

In this study, MOR256-17 OSNs responded to 31 out of 35 single chemical compounds tested (Figures 4.10 and 4.14). The odorant responsiveness of

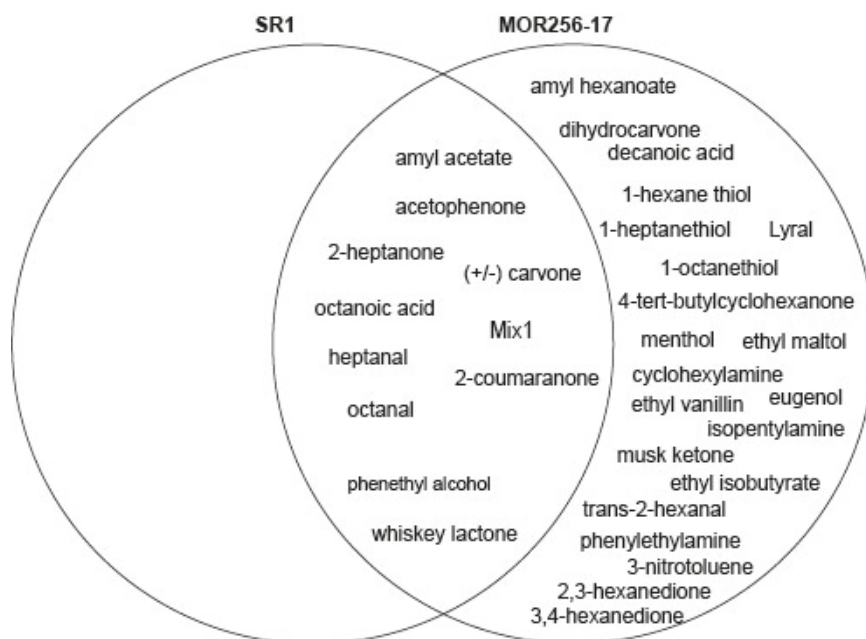


Figure 5.1 MOR256-17 neurons are more broadly tuned than SR1 OSNs. Venn diagram showing that SR1 odorant panel is included in the MOR256-17 one.

these neurons was broader than that of SR1 neurons: all 10 ligands for SR1 OSNs also activated MOR256-17 OSNs (Figure 5.1). It is possible that a different scenario would result with a larger ligand set; however, the low throughput nature of patch clamping does not make this a feasible option.

Interestingly, MOR256-17 OSNs were able to detect cyclohexylamine, isopentylamine, and phenylethylamine, while SR1 OSNs were not able to detect them (Figure 4.14). These amines are classical ligands for TAARs and TAAR-expressing OSNs (Liberles and Buck, 2006); (Pacifico et al., 2012); (Dewan et al., 2013); (Zhang et al., 2013). However, the concentration required to elicit a response in MOR256-17 OSNs was high 10 μ M compared to the extremely high sensitivity of TAAR-expressing chemosensory neurons in the MOE, for instance TAAR4-expressing OSNs were able to detect phenylethylamine at the picomolar level (0.1 pM) (Zhang et al., 2013). Amine detection by canonical OSNs expressing an OR such as MOR256-17 may modify the behavioral response to amines at higher concentrations or in mixtures.

In ORs with a narrow response window, it is clear that the physicochemical characteristics of odorants are critical. Some ORs have a particular preference to some specific structural features, and tolerance for others, which enable the exquisite discrimination of hundreds of odorants. For instance, the I7 receptor is activated by saturated aliphatic aldehydes with a length of 7-10 carbon atoms (Zhao et al., 1998). The aldehyde group and the molecule length were critical; replacing the aldehyde group with other functional groups reduced the odorant evoked amplitude in EOG recordings (Araneda et al., 2000). In addition, M71 and M72 also showed affinity to acetophenone and its analogues like propiophenone, 4-methylacetophenone, 4-methoxyacetophenone and 2-hydroxyacetophenone (Zhang et al., 2012). However, in broadly responsive ORs the odorant response was more complex due to the large odorant panel detected. MOR256-17 OSNs were responsive to a broad range of odorants, all five aldehydes, three amines, three esters, three thiols, three alcohols, all the ketones tested (except cyclohexanone), and toluene activated MOR256-17. There is some subtle selectivity: in each functional group, MOR256-17 OSNs showed tail length tuning for homologous n-compounds. These cells responded to some carbon chain lengths, but not others. For example, responses were observed more frequently and with higher amplitudes for 8-carbon chains (octanoic acid, 1-octanethiol) compared to 7-carbon chains (no response to heptanoic acid and an even weaker response to 1-heptanethiol). This was not specific to all 7-carbon chains however; amyl acetate, heptanal, and 2-heptanone responded with high amplitude (Figure 4.10).

MOR256-17 showed a preference to some six-carbon cyclic molecules in which the response was the highest, such as acetophenone, 3-nitrotoluene, (+/-) carvone, and 4-tert-butylcyclohexanone (Figure 4.7). This was not the case for the cyclic compound cyclohexanone, which has the same ring structure as 4-tert-butylcyclohexanone but lacks the tert functional group. Thus, trying to find a link between the chemical structure and the activation of broadly tuned ORs is extremely complex.

Furthermore, limonene and carvone are monoterpenes that differ only in one carbonyl group (Clarín et al., 2010), limonene failed to elicit a response from MOR-256-17, while (+/-) carvone did (Figures 4.7 and 4.9).

Taken together, these results showed discriminating features of MOR256-17 neurons in detecting different chemical compounds, and demonstrated that odorant detection depends not only on the chemical structure or the presence of a specific functional group but on the interaction of the odorant with the OR.

In other species like *Drosophila Melanogaster*, Or67a too was broadly tuned, and responded to 31 odorants unrelated in chemical structure. However, the broad tuning was related to stimulus intensity; at low concentrations Or67a was not sensitive to odorants and the broad response profile was strongly affected (Hallem and Carlson, 2006). The animals in their natural environment encounter a wide range of odorant concentrations. The intensity of the odorant stimulus also depends on the distance; it is possible the intensity code may play a role in the fly navigation, or for emerging different odorant perception in the brain. In this study only 4 from the 35 odorants tested did not activate MOR256-17 OSNs at 10 μ M. However, 25 odorants were not able to activate SR1 OSNs at the same concentration (Figure 4.12). Previous studies have reported that higher odorant concentrations activated more neurons than lower concentrations (Ma and Shepherd, 2000) (Hallem and Carlson, 2006). Thus, increasing the concentration of the non-activating odorants of SR1 OSNs could change their response.

To characterize the sensitivity of the two OSN subpopulations SR1 and MOR256-17, dose-response curves for certain odorants were performed and analyzed. The dose-response curves of MOR256-17 OSNs exhibit a broad dynamic range and high sensitivity, and were similar to dose-response curves of SR1 OSNs (Figure 4.16).

Sensitivity to odorants varied within the same sub-population of OSNs. Some neurons were able to detect the same odorant (for instance 4-tert-butylcyclohexanone) at concentrations as low as 0.01 μ M, whereas others did

not respond until concentrations of 0.1 μ M or 1 μ M were attained (Figures 4.16F and 4.11C). This result is consistent with previous studies, where MOR23 showed differences in sensitivity to Lyr al (Gros maitre et al., 2006). Some cells were able to detect Lyr al at concentrations as low as 10 nM, while others did not respond until 1 μ M or 10 μ M were applied (Gros maitre et al., 2006). These differences were also observed for acetophenone and benzaldehyde in M71 OSNs (Bozza et al., 2002), and 2-phenylethyl alcohol in S1 OSNs (Lam and Mombaerts, 2013).

The sensitivity of 2-heptanone and (+/-) carvone were compared between SR1 and MOR256-17 OSNs (Figure 4.17). The insignificant statistical in EC50 between the two populations, was maybe obscured by the relative low number of OSNs examined.

MOR256-17 neurons are expressed in the MOE, and the SO, an odorant responsiveness comparison of MOR256-17 cells was conducted in the two olfactory subsystems. MOR256-17 neurons were able to detect 4-tert-butylcyclohexanone (Figure 4.11), menthol, trans-2-hexanal and 1-heptanthiol, in the SO and the MOE.

This finding was previously reported in SR1 OSNs, which are also expressed in the MOE and the SO (Gros maitre et al., 2009). SR1 OSNs showed a response to amyl acetate, (+) camphor, benzaldehyde, octanoic acid, and heptanal in the two olfactory subsystems (Gros maitre et al., 2009). Moreover, dose response-curve analysis to amyl acetate had the same dynamic range in the MOE, and the SO (Gros maitre et al., 2009).

Moreover, profound differences in the response kinetics of the odorant-evoked current recorded in voltage clamp mode within the same OSN subpopulation were observed. This is similar to what was reported for MOR23 OSNs which showed considerable variation among the cells in odorant-evoked current amplitudes and half-widths (Gros maitre et al., 2006).

The response kinetics for all 10 common ligands for SR1 and MOR256-17 were compared (Figure 4.15), and a systematic difference in the latency ($p < 0.0001$), rise time ($p < 0.0001$), peak current ($p < 0.03$) and the total charge area ($p < 0.002$), was observed only in octanoic acid (Figures 4.15B,C, D and F). Differences in OSNs response kinetics are not very understood; the variety in the activation and deactivation phases of the odorant-evoked response may play a role in filtering the odorant signal in the OB, when different OSN subpopulations are activated.

Furthermore, a host of factors could account for these differences. For instance, the size of the cilia (Challis et al., 2015), the number of ORs expressed, the age of the mouse (Lee et al., 2009), but also the age of the OSN itself as a result of ongoing unsynchronized neurogenesis in the MOE (Brann and Firestein, 2014).

5.3 Discrepancies with heterologous systems

The results differ from data obtained by expressing MOR256-17 in heterologous cell expression systems (Saito et al., 2009) (Dahoun et al., 2011) (Goldsmith et al., 2011) (Li et al., 2012). Most importantly, no response was observed to cyclohexanone. Cyclohexanone was reported as a stimulus for human embryonic kidney HEK293T cells that were transfected a rho-tagged MOR-256-17 expression vector (Saito et al., 2009), and for micelle and nanodisc nanotubes in which recombinant MOR256-17 protein produced in Sf9 insect cells was inserted (Goldsmith et al., 2011). However cyclohexanone was not reported as a stimulus in another study (Dahoun et al., 2011) that used the same cell line; however, secreted alkaline phosphatase was measured as a function of activity instead of luciferase and cells were exposed to cyclohexanone for 16h instead of 4h (Saito et al., 2009). Conversely, responses were observed to 2-heptanone, ethyl isobutyrate, (+/-) carvone, dihydrocarvone, heptanal, octanal, and acetophenone; chemicals that were reported as non-activating odorants by Saito et al., 2009. The data for MOR256-17 OSNs were close to those obtained from *Xenopus laevis* oocytes; the exception being that ethyl vanillin and eugenol were not able to elicit a response in the latter (Li et al., 2012) .

These similarities may be attributed to the co-expression of G_{olf} in *Xenopus laevis* oocytes, which provided a similar transduction pathway and hence, response profiles.

In the present study, heptanoic acid and 1-octanethiol failed to elicit a response in SR1 OSNs, and responses to 2-heptanone and acetophenone were observed (Figure 4.12), whereas the opposite results have been reported for HEK293T cells transfected with an SR1 expression plasmid (Yu et al., 2015).

False-negative responses (discrepancies in which a heterologous system fails to detect a response that is observed in native OSNs) can be attributed to lower sensitivity of the heterologous system. However, for false-positive responses towards heptanoic acid and cyclohexanone to be observed in MOR256-17 and 1-octanethiol for SR-1 directly conflicts with results obtained from heterologous systems (Saito et al., 2009) (Goldsmith et al., 2011) (Yu et al., 2015). This may be attributed to perireceptor events *in vivo*, where odorant-binding proteins derived from the mucosa may change the overall structure of the compound and therefore, the ability of the ligand to bind to the receptor.

The expression of the early immediate gene *c-fos* was used in previous studies, to determine glomerular activation by odorant exposure (Guthrie et al., 1993; Lin et al., 2004; Clarin et al., 2010). In MOR256-17-IRES-tauGFP mice exposed to 2,3-hexanedione, there was an increase in the percentage of *c-fos* positive juxtaglomerular cells surrounding the GFP glomeruli (Loch et al., 2013). This was consistent in MOR256-17 OSNs, that were also able to respond to 2,3-hexanedione (Figures 4.10 and 4.14).

While the low-throughput nature of this technique does not allow the screening of a larger odorant panel, it is still a more informative and efficient approach to explore the physiology of OSNs and their putative ligands. Moreover, data from heterologous systems should be interpreted carefully.

The *in vivo* DREAM technique (Weid et al., 2015) is a promising approach to deorphanized the repertoire of OR genes.

5.4 Why does the mouse olfactory system employ broadly responsive ORs?

Both MOR256-17 and SR1 belong to the same OR family, the MOR256 family. With 37 members, it is one of the largest families in the mouse OR gene repertoire (Zhang and Firestein, 2002). A third broadly responsive OR, Olfr263 (Nara et al., 2011; Yu et al., 2015), (formerly known as Olfr42), was previously known as MOR256-31 and thus also belongs to the MOR256 family.

In contrast, other members of the MOR256 family exhibit a narrower odorant response profile, at least when assessed in the heterologous *Xenopus laevis* oocyte system (Liu et al., 2012) or HEK293T cells (Yu et al., 2015). Recently, residues properties analyses of four ORs belonging to MOR256 family (two broadly tuned: SR1, MOR256-31; and two narrowly tuned MOR256-8, MOR256-22) revealed conserved amino acids in the four ORs, with specific ones only in the two broadly ORs (Yu et al., 2015). Substituting SR1 residues by those of MOR256-8 (for instance L107I) dramatically decreased its odorant response (Yu et al., 2015). It will be interesting to determine if the same OR residues are involved in broadening the responsiveness in the case of MOR256-17, to determine whether these sequence homologies are stereotyped among other broadly ORs. Similarly, the narrowly responsive receptor MOR256-8 (also known as Olfr1362) can be converted to a broadly responsive OR by making a single mutation, as assayed in HEK293T cells (Yu et al., 2015).

Pharmacological perturbation of broadly tuned ORs may be a useful tool to elucidate their transduction pathways. Using blockers of the different (cAMP, cGMP) transduction pathways, the responses to different odorants from different chemical classes could be recorded. This would allow one to determine whether ligands activate different transduction pathways in the same population of OSNs.

The integration of odorant mixtures remains a challenge to investigate, as integration can occur at any point from the periphery to higher order processing centers. Therefore, OSNs expressing broadly tuned ORs are a unique tool to investigate mixture integration at the periphery: what is the integration of multiple odorants by a broadly tuned receptor (such as SR1 or Olfr15) compared to a relatively narrowly tuned receptor (such as MOR23 or M71)? What transduction pathway is used by these neurons to integrate mixtures?

Typically, different ensembles of OSNs detect different odorant mixtures. However, to date the combinatorial coding is not very well understood, for instance how two or more OSN subpopulations behave when they are stimulated by a single or a mixture of chemical compounds. While technically difficult to execute, it would be interesting to perform a double patch clamp recordings from two different subpopulations of OSNs at the same time. For instance, performing recordings from a narrowly and broadly tuned OSN, or from two broadly responsiveness subpopulations like SR1 and MOR256-17. The SO is a suitable olfactory subsystem for patch clamping due to dendritic knobs being slightly larger than in the MOE, and most importantly, both SR1 and MOR256-17 receptors are expressed in the SO. Double patch clamping could be conducted from SR1 and MOR256-17 in the SO by generating for instance a cross between SR1-IRES-tauRFP and MOR256-17-IRES-tauGFP.

However, MOR256-17 exhibits a broad responsiveness in both OSNs and other heterologous systems, indicating that broad tuning is a specific feature to this receptor. Therefore, it is possible that these OSNs do not follow the conventional 'one-receptor, one-neuron' theory. Recently, transcriptome analysis of subpopulation of OSNs expressing Olfr73 demonstrated the predominance of this receptor, however, other ORs were detectable (Scholz et al., 2016). It could be interesting to analyze and compare broadly tuned and narrowly OSNs transcriptomes, to determine whether they express different ORs or other proteins.

The evolutionary emergence and biological relevance of broadly responsive ORs within a repertoire of mostly narrowly responsive ORs remain elusive in the absence of any behavioral data. Their role may lie in detecting the mere presence of odorants in the nasal cavity, leaving discrimination to narrowly responsive ORs, or in contributing to the discrimination of structurally similar ligands by increasing the number of responsive neurons (Nara et al., 2011). On the other hand this increase in number of responsive OSNs may blur the actual discriminating signal by increasing the noise.

It will be informative to generate gene-targeted strains with single or combined knockouts of genes that encode broadly responsive ORs such as SR1, MOR256-17, and Olfr263, and to perform behavioral assays that measure olfactory performance in these mice, such as threshold detection and odorant discrimination, to investigate the role of broadly responsive OSNs, in animal behavior.

5.5 Neural activity and axonal guidance

One of the understandable mechanisms in axonal guidance is the implication of neural activity, which includes the spontaneous, the odorant-evoked activity, or the correlation between both of them.

In Chapters 4.3 and 4.4, two channels were investigated to further comprehend their role in OSN axonal guidance, a sodium channel Nav1.7 and a CaCC Tm16b.

Nav1.7 is one of the nine voltage gated isoforms, implicated in the rising phase of action potential in excitable cells (Catterall, 2000). The attention was given to Nav1.7 due his non-redundant role in the transmission of the odorant information to the OB (Weiss et al., 2011).

The generation of mouse expressing or not Nav1.7 in M71-expressing OSNs, permitted the investigation of the axonal guidance in the same OB. However, no influence was seen in axon wiring (Figure 4.21). Both M71 OSNs axons lacking or expressing fNav1.7 were able to navigate, enter the OB, form a glomerulus,

and coalesce in the same position (Figure 4.21B). The result confirms Weiss et al., who reported a normal synapse formation in conditional mutant Nav1.7 mouse (Weiss et al., 2011). Thus, this channel was only important to amplify and conduct the odorant information in OSNs axonal terminals, to the first synapse (Weiss et al., 2011), but had not a necessary role in modulating OSNs map in the OB.

The Tm16b is an important channel in amplifying the odorant signals in OSNs cilia (Billig et al., 2011). The wiring influence of Tm16b channel was investigated by generating a conditional mutant mouse in a subtype of OSNs expressing M71 gene. The axonal guidance and the glomerular formation in Tm16b x M71-IRES-Cre x tdRFP mouse appeared normal (Figure 4.24); the M71 axons converge to the typical M71 glomerulus position. This results is in accordance within a previous study, that also showed normal axonal coalescence of P2-IRES-tauLacZ, and M72-IRES-tauLacZ mice, lacking Tm16b expression (Billig et al., 2011).

The most major effects on axonal guidance occurred by disrupting the OR gene (Mombaerts et al., 1996) or ACIII gene (Zou et al., 2007). Axonal convergence occurred normally in CNG channel mutant mice (Lin et al., 2000), EOG recordings revealed that this mouse was anosmic (Brunet et al., 1996). These data argued that the odorant-evoked activity was not required for establishing the olfactory map in the OB. Moreover, this was consistent in G_{olf} mutant mice that could not detect odorants; however the P2 OSNs lacking G_{olf} expression, could project axons and form normal glomeruli (Belluscio et al., 1998).

Interestingly, the membrane properties were not altered in CNG mutant mouse, and no difference was seen in terms of spontaneous activity, although the number of single OSNs recorded in CNG mutant mice were fewer (Brunet et al., 1996). Remarkably, the olfactory map was altered by silencing the spontaneous activity (Yu et al., 2004). The spontaneous activity was not investigated in the conditional null Nav1.7 mouse (Weiss et al., 2011). Hence, OSNs lacking the expression Nav1.7 or Tm16b could rely on the spontaneous firing to establish the glomerular map.

However, in OCNC1 mice in which a subunit of the CNG channel was knocked-out, show a perturbation of P2 OSNs axons but not in M72 neurons (Zheng et al., 2000). This result suggests that the axonal guidance machinery is not stereotyped over all OSN subpopulations. The Nav1.7 or Tm16b may have axonal guidance effects in other OSNs expressing different OR genes. To confirm the redundant role of Nav1.7 and Tm16b in axonal wiring, other OSN subtypes should be investigated.

5.6 Summary

Despite the progress in the field of olfaction, little is known about the basics of the olfactory coding. OR deorphanization is crucial to better understand this process. This work contributed to the understanding of odorant responsiveness and the olfactory coding in the neuroepithelium, by deorphaning a specific population of OSNs, expressing MOR256-17. The results showed that MOR256-17 reside in one extreme of odorant responsiveness among the ~1100 OR genes repertoire in the mouse. Moreover, investigating the axonal navigation is important to understand the billions of connections in the brain, and repair them when damaged. This thesis shed light on the non-contribution of two channels (Nav1.7 and Tm16b) in OSNs axonal guidance. However, further investigations are needed to confirm this issue.

6 References

- Ahn, H.S., Black, J.A., Zhao, P., Tyrrell, L., Waxman, S.G., and Dib-Hajj, S.D. (2011). Nav1.7 is the predominant sodium channel in rodent olfactory sensory neurons. *Mol. Pain* 7, 32.
- Andersson, M.N., Löfstedt, C., and Newcomb, R.D. (2015). Insect olfaction and the evolution of receptor tuning. *Front. Ecol. Evol.* 3.
- Araneda, R.C., Kini, A.D., and Firestein, S. (2000). The molecular receptive range of an odorant receptor. *Nat. Neurosci.* 3, 1248–1255.
- Bakalyar, H., and Reed, R. (1990). Identification of a specialized adenylyl cyclase that may mediate odorant detection. *Science* 250, 1403–1406.
- Bannister, L.H., and Dodson, H.C. (1992). Endocytic pathways in the olfactory and vomeronasal epithelia of the mouse: ultrastructure and uptake of tracers. *Microsc. Res. Tech.* 23, 128–141.
- Barish, M.E. (1983). A transient calcium-dependent chloride current in the immature *Xenopus* oocyte. *J. Physiol.* 342, 309–325.
- Beites, C.L., Kawauchi, S., Crocker, C.E., and Calof, A.L. (2005). Identification and molecular regulation of neural stem cells in the olfactory epithelium. *Exp. Cell Res.* 306, 309–316.
- Belluscio, L., Gold, G.H., Nemes, A., and Axel, R. (1998). Mice deficient in Golf are anosmic. *Neuron* 20, 69–81.
- Bennett, M.K., Kulaga, H.M., and Reed, R.R. (2010). Odor-evoked gene regulation and visualization in olfactory receptor neurons. *Mol. Cell. Neurosci.* 43, 353–362.
- Billig, G.M., Pál, B., Fidzinski, P., and Jentsch, T.J. (2011). Ca²⁺-activated Cl[−] currents are dispensable for olfaction. *Nat. Neurosci.* 14, 763–769.
- Blankenship, A.G., and Feller, M.B. (2010). Mechanisms underlying spontaneous patterned activity in developing neural circuits. *Nat. Rev. Neurosci.* 11, 18–29.
- Bozza, T., Feinstein, P., Zheng, C., and Mombaerts, P. (2002). Odorant receptor expression defines functional units in the mouse olfactory system. *J. Neurosci.* 22, 3033–3043.
- Bozza, T., Vassalli, A., Fuss, S., Zhang, J.-J., Weiland, B., Pacifico, R., Feinstein, P., and Mombaerts, P. (2009). Mapping of class I and class II odorant receptors to glomerular domains by two distinct types of olfactory sensory neurons in the mouse. *Neuron* 61, 220–233.
- Brann, J.H., and Firestein, S.J. (2014). A lifetime of neurogenesis in the olfactory system. *Front Neurosci* 8, 182.

Brechbühl, J., Klaey, M., and Broillet, M.-C. (2008). Grueneberg ganglion cells mediate alarm pheromone detection in mice. *Science* 321, 1092–1095.

Brechbühl, J., Klaey, M., Moine, F., Bovay, E., Hurni, N., Nenniger-Tosato, M., and Broillet, M.-C. (2014). Morphological and physiological species-dependent characteristics of the rodent Grueneberg ganglion. *Front Neuroanat.* 8, 87.

Bressel, O.C., Khan, M., and Mombaerts, P. (2016). Linear correlation between the number of olfactory sensory neurons expressing a given mouse odorant receptor gene and the total volume of the corresponding glomeruli in the olfactory bulb. *J. Comp. Neurol.* 524, 199–209.

Brunet, L.J., Gold, G.H., and Ngai, J. (1996). General anosmia caused by a targeted disruption of the mouse olfactory cyclic nucleotide-gated cation channel. *Neuron* 17, 681–93.

Buck, L.B. (2004). Olfactory receptors and odor coding in mammals. *Nutr. Rev.* 62, S184–8.

Buck, L., and Axel, R. (1991). A novel multigene family may encode odorant receptors: A molecular basis for odor recognition. *Cell* 65, 175–87.

Cadiou, H., Aoudé, I., Tazir, B., Molinas, A., Fenech, C., Meunier, N., and Grosmaître, X. (2014). Postnatal odorant exposure induces peripheral olfactory plasticity at the cellular level. *J. Neurosci.* 34, 4857–4870.

Caputo, A., Caci, E., Ferrera, L., Pedemonte, N., Barsanti, C., Sondo, E., Pfeffer, U., Ravazzolo, R., Zegarra-Moran, O., and Galletta, L.J.V. (2008). TMEM16A, a membrane protein associated with calcium-dependent chloride channel activity. *Science* 322, 590–594.

Carr, V.M. (2005). Induced and constitutive heat shock protein expression in the olfactory system--a review, new findings, and some perspectives. *J. Neurocytol.* 34, 269–293.

Catterall, W.A. (2000). From ionic currents to molecular mechanisms. *Neuron* 26, 13–25.

Catterall, W.A., Goldin, A.L., and Waxman, S.G. (2005). International Union of Pharmacology. XLVII. Nomenclature and structure-function relationships of voltage-gated sodium channels. *Pharmacol. Rev.* 57, 397–409.

Challis, R.C., Tian, H., Wang, J., He, J., Jiang, J., Chen, X., Yin, W., Connelly, T., Ma, L., Yu, C.R., Pluznick, J.L., Storm, D.R., Huang, L., Zhao, K., and Ma, M. (2015). An olfactory cilia pattern in the mammalian nose ensures high sensitivity to odors. *Curr. Biol.* 25, 2503–2512.

Chess, A., Simon, I., Cedar, H., and Axel, R. (1994). Allelic inactivation regulates olfactory receptor gene expression. *Cell* 78, 823–834.

Clarín, T., Sandhu, S., and Apfelbach, R. (2010). Odor detection and odor discrimination in subadult and adult rats for two enantiomeric odorants supported by c-fos data. *Behav. Brain Res.* 206, 229–235.

Connelly, T., Savigner, A., and Ma, M. (2013). Spontaneous and sensory-evoked activity in mouse olfactory sensory neurons with defined odorant receptors. *J. Neurophysiol.* 110, 55–62.

Connelly, T., Yu, Y., Grosmaître, X., Wang, J., Santarelli, L.C., Savigner, A., Qiao, X., Wang, Z., Storm, D.R., and Ma, M. (2015). G protein-coupled odorant receptors underlie mechanosensitivity in mammalian olfactory sensory neurons. *Proc. Natl. Acad. Sci. USA* 112, 590–595.

Cygnar, K.D., and Zhao, H. (2009). Phosphodiesterase 1C is dispensable for rapid response termination of olfactory sensory neurons. *Nat. Neurosci.* 12, 454–462.

Dahoun, T., Grasso, L., Vogel, H., and Pick, H. (2011). Recombinant expression and functional characterization of mouse olfactory receptor mOR256-17 in mammalian cells. *Biochemistry* 50, 7228–7235.

Gonzalez-Kristeller, D.C., do Nascimento, J.B., Galante, P.A., and Malnic, B. (2015). Identification of agonists for a group of human odorant receptors. *Front. Pharmacol.* 6, 35.

Dauner, K., Lissmann, J., Jeridi, S., Frings, S., and Moehrlen, F. (2012). Expression patterns of anoctamin 1 and anoctamin 2 chloride channels in the mammalian nose. *Cell Tissue Res.* 347, 327–341.

Dewan, A., Pacifico, R., Zhan, R., Rinberg, D., and Bozza, T. (2013). Non-redundant coding of aversive odours in the main olfactory pathway. *Nature* 497, 486–489.

Dib-Hajj, S.D., Yang, Y., Black, J.A., and Waxman, S.G. (2012). The NaV1.7 sodium channel: from molecule to man. *Nat. Rev. Neurosci.* 14, 49–62.

Dulac, C., and Axel, R. (1995). A novel family of genes encoding putative pheromone receptors in mammals. *Cell.* 83,195-206.

Feinstein, P., and Mombaerts, P. (2004). A contextual model for axonal sorting into glomeruli in the mouse olfactory system. *Cell* 117, 817–831.

Feinstein, P., Bozza, T., Rodriguez, I., Vassalli, A., and Mombaerts, P. (2004). Axon guidance of mouse olfactory sensory neurons by odorant receptors and the beta2 adrenergic receptor. *Cell* 117, 833–846.

Firestein, S. (2001). How the olfactory system makes sense of scents. *Nature* 413, 211–218.

Firestein, S., and Werblin, F. (1989). Odor-induced membrane currents in vertebrate-olfactory receptor neurons. *Science* 244, 79–82.

- Firestein, S., and Werblin, F.S. (1987). Gated currents in isolated olfactory receptor neurons of the larval tiger salamander. *Proc. Natl. Acad. Sci. U.S.A.* 84, 6292-6296.
- Firestein, S., Darrow, B., and Shepherd, G.M. (1991). Activation of the sensory current in salamander olfactory receptor neurons depends on a G protein-mediated cAMP second messenger system. *Neuron* 6, 825–835.
- Firestein, S., Picco, C., and Menini, A. (1993). The relation between stimulus and response in olfactory receptor cells of the tiger salamander. *J. Physiol.* 468, 1–10.
- Fleischer, J., Mamasuew, K., and Breer, H. (2009). Expression of cGMP signaling elements in the Grueneberg ganglion. *Histochem. Cell Biol.* 131, 75–88.
- Freitag, J., Krieger, J., Strotmann, J., and Breer, H. (1995). Two classes of olfactory receptors in *xenopus laevis*. *Neuron*. 15, 1383-1392.
- Fuss, S.H., Omura, M., and Mombaerts, P. (2005). The Grueneberg ganglion of the mouse projects axons to glomeruli in the olfactory bulb. *Eur. J. Neurosci.* 22, 2649–2654.
- Fuss, S.H., Omura, M., and Mombaerts, P. (2007). Local and cis effects of the H element on expression of odorant receptor genes in mouse. *Cell* 130, 373–384.
- Gaillard, I., Rouquier, S., and Giorgi, D. (2004). Olfactory receptors. *Cell. Mol. Life Sci.* 61, 456–469.
- Getchell, T.V. (1977). Analysis of intracellular recordings from salamander olfactory epithelium. *Brain Res.* 123, 275–286.
- Getchell, T.V., Margolis, F.L., and Getchell, M.L. (1984). Perireceptor and receptor events in vertebrate olfaction. *Prog. Neurobiol.* 23, 317–345.
- Gimelbrant, A.A., Stoss, T.D., Landers, T.M., and McClintock, T.S. (1999). Truncation releases olfactory receptors from the endoplasmic reticulum of heterologous cells. *J. Neurochem.* 72, 2301–2311.
- Glatz, R., and Bailey-Hill, K. (2011). Mimicking nature's noses: From receptor deorphaning to olfactory biosensing. *Prog. Neurobiol.* 93, 270-296.
- Godfrey, P.A., Malnic, B., and Buck, L.B. (2004). The mouse olfactory receptor gene family. *Proc. Natl. Acad. Sci. U.S.A.* 101, 2156–2161.
- Goldsmith, B.R., Mitala, J.J., Josue, J., Castro, A., Lerner, M.B., Bayburt, T.H., Khamis, S.M., Jones, R.A., Brand, J.G., Sligar, S.G., Luetje, C.W., Gelperin, A., Rhodes, P.A., Discher, B.M., and Johnson, A.T. (2011). Biomimetic chemical sensors using nanoelectronic readout of olfactory receptor proteins. *ACS Nano* 5, 5408–5416.

Graziadei, P.P., and Graziadei GA (1979). Neurogenesis and neuron regeneration in the olfactory system of mammals. I. Morphological aspects of differentiation and structural organization of the olfactory sensory neurons. *J Neurocytol.* 8, 1-18.

Grosmaître, X., Fuss, S.H., Lee, A.C., Adipietro, K.A., Matsunami, H., Mombaerts, P., and Ma, M. (2009). SR1, a mouse odorant receptor with an unusually broad response profile. *J. Neurosci.* 29, 14545–14552.

Grosmaître, X., Santarelli, L.C., Tan, J., Luo, M., and Ma, M. (2007). Dual functions of mammalian olfactory sensory neurons as odor detectors and mechanical sensors. *Nat. Neurosci.* 10, 348–354.

Grosmaître, X., Vassalli, A., Mombaerts, P., Shepherd, G.M., and Ma, M. (2006). Odorant responses of olfactory sensory neurons expressing the odorant receptor MOR23: a patch clamp analysis in gene-targeted mice. *Proc. Natl. Acad. Sci. U.S.A.* 103, 1970–1975.

Grüneberg, H. (1973). A ganglion probably belonging to the N. terminalis system in the nasal mucosa of the mouse. *Z. Anat. Entwicklungsgesch.* 140, 39-52.

Guthrie, K.M., Anderson, A.J., Leon, M., and Gall, C. (1993). Odor-induced increases in c-fos mRNA expression reveal an anatomical “unit” for odor processing in olfactory bulb. *Proc. Natl. Acad. Sci. U.S.A.* 90, 3329–3333.

Hallem, E.A., and Carlson, J.R. (2006). Coding of odors by a receptor repertoire. *Cell* 125, 143–160.

Hansen, A., and Finger, T.E. (2008). Is TrpM5 a reliable marker for chemosensory cells? Multiple types of microvillous cells in the main olfactory epithelium of mice. *BMC Neurosci.* 9, 115.

Hartzell, C., Putzier, I., and Arreola, J. (2005). Calcium-activated chloride channels. *Annu. Rev. Physiol.* 67, 719–758.

Hegg, C.C., Irwin, M., and Lucero, M.T. (2009). Calcium store-mediated signaling in sustentacular cells of the mouse olfactory epithelium. *Glia* 57, 634–644.

Hengl, T., Kaneko, H., Dauner, K., Vocke, K., Frings, S., and Mohrlen, F. (2010). Molecular components of signal amplification in olfactory sensory cilia. *Proc. Natl. Acad. Sci. U.S.A.* 107, 6052–6057.

Herrada, G., and Dulac, C. (1997). A novel family of putative pheromone receptors in mammals with a topographically organized and sexually dimorphic distribution. *Cell* 90, 763–773.

Hodgkin, A.L., and Huxley, A.F. (1952a). A quantitative description of membrane current and its application to conduction and excitation in nerve. *J. Physiol.* 117, 500–544.

Hodgkin, A.L., and Huxley, A.F. (1952b). Currents carried by sodium and potassium ions through the membrane of the giant axon of *Loligo*. *J. Physiol.* 116, 449–472.

Holy, T.E., Dulac, C., and Meister, M. (2000). Responses of vomeronasal neurons to natural stimuli. *Science* 289, 1569–1572.

Imai, T., Suzuki, M., and Sakano, H. (2006). Odorant receptor-derived cAMP signals direct axonal targeting. *Science* 314, 657–661.

Ishii, T., and Mombaerts, P. (2011). Coordinated coexpression of two vomeronasal receptor V2R genes per neuron in the mouse. *Mol. Cell. Neurosci.* 46, 397–408.

Ishii, T., Hirota, J., and Mombaerts, P. (2003). Combinatorial coexpression of neural and immune multigene families in mouse vomeronasal sensory neurons. *Curr. Biol.* 13, 394–400.

Jarriault, D., and Grosmaître, X. (2015). Perforated patch-clamp recording of mouse olfactory sensory neurons in intact neuroepithelium: functional analysis of neurons expressing an identified odorant receptor. *J. Vis. Exp.* e52652.

Jia, C., and Halpern, M. (1996). Subclasses of vomeronasal receptor neurons: differential expression of G proteins ($G_{i\alpha 2}$ and $G_{o\alpha}$) and segregated projections to the accessory olfactory bulb. *Brain Res.* 719, 117–28.

Jones, D.T., and Reed, R.R. (1989). Golf: an olfactory neuron specific-G protein involved in odorant signal transduction. *Science* 244, 790–795.

Kajiya, K., Inaki, K., Tanaka, M., Haga, T., Kataoka, H., and Touhara, K. (2001). Molecular bases of odor discrimination: Reconstitution of olfactory receptors that recognize overlapping sets of odorants. *J. Neurosci.* 21, 6018–6025.

Katoh, M., and Katoh, M. (2003). FLJ10261 gene, located within the CCND1-EMS1 locus on human chromosome 11q13, encodes the eight-transmembrane protein homologous to C12orf3, C11orf25 and FLJ34272 gene products. *Int J Oncol.* 22, 1375–1381.

Keller, A., Zhuang, H., Chi, Q., Vosshall, L.B., and Matsunami, H. (2007). Genetic variation in a human odorant receptor alters odour perception. *Nature* 449, 468–472.

Keverne, E.B. (1999). The vomeronasal organ. *Science* 286, 716–20.

Kim, D.G., Kang, H.M., Jang, S.K., and Shin, H.S. (1992). Construction of a bifunctional mRNA in the mouse by using the internal ribosomal entry site of the encephalomyocarditis virus. *Mol. Cell. Biol.* 12, 3636–3643.

Krautwurst, D., Yau, K.W., and Reed, R.R. (1998). Identification of ligands for

olfactory receptors by functional expression of a receptor library. *Cell* 95, 917–926.

Kuhlmann, K., Tschapek, A., Wiese, H., Eisenacher, M., Meyer, H.E., Hatt, H.H., Oeljeklaus, S., and Warscheid, B. (2014). The membrane proteome of sensory cilia to the depth of olfactory receptors. *Mol. Cell Proteomics* 13, 1828–1843.

Lam, R.S., and Mombaerts, P. (2013). Odorant responsiveness of embryonic mouse olfactory sensory neurons expressing the odorant receptors S1 or MOR23. *Eur. J. Neurosci.* 38, 2210–2217.

Lee, A.C., Tian, H., Grosmaître, X., and Ma, M. (2009). Expression patterns of odorant receptors and response properties of olfactory sensory neurons in aged mice. *Chem. Senses* 34, 695–703.

Lévai, O., Feistel, T., and Breer, H. (2006). Cells in the vomeronasal organ express odorant receptors but project to the accessory olfactory bulb. *J. Comp. Neurol.* 498, 476–90.

Li, J., Haddad, R., Chen, S., Santos, V., and Luetje, C.W. (2012). A broadly tuned mouse odorant receptor that detects nitrotoluenes. *J. Neurochem.* 121, 881–890.

Liberles, S.D. (2015). Trace amine-associated receptors: ligands, neural circuits, and behaviors. *Curr. Opin. Neurobiol.* 34, 1–7.

Liberles, S.D., and Buck, L.B. (2006). A second class of chemosensory receptors in the olfactory epithelium. *Nature* 442, 645–650.

Liman, E.R., Corey, D.P., and Dulac, C. (1999). TRP2: A candidate transduction channel for mammalian pheromone sensory signaling. *Proc. Natl Sci. U.S.A.* 96, 5791–5796.

Lin, D.M., Wang, F., Lowe, G., Gold, G.H., Axel, R., Ngai, J., and Brunet, L. (2000). Formation of precise connections in the olfactory bulb occurs in the absence of odorant-evoked neuronal activity. *Neuron* 26, 69–80.

Lin, W., Arellano, J., Slotnick, B., and Restrepo, D. (2004). Odors detected by mice deficient in cyclic nucleotide-gated channel subunit A2 stimulate the main olfactory system. *J. Neurosci.* 24, 3703–3710.

Liu, C.Y., Xiao, C., Fraser, S.E., and Lester, H.A. (2012). Electrophysiological characterization of Grueneberg ganglion olfactory neurons: spontaneous firing, sodium conductance, and hyperpolarization-activated currents. *J. Neurophysiol.* 108, 1318–34.

Lledo, P.M., Gheusi, G., and Vincent, J.D. (2005). Information processing in the mammalian olfactory system. *Physiol. Rev.* 85:281–317

- Loch, D., Heidel, C., Breer, H., and Strotmann, J. (2013). Adiponectin enhances the responsiveness of the olfactory system. *PLoS ONE* 8, e75716.
- Lowe, G., and Gold, G.H. (1991). The spatial distributions of odorant sensitivity and odorant-induced currents in salamander olfactory receptor cells. *J. Physiol.* 442, 147–168.
- Lowe, G., and Gold, G.H. (1993). Nonlinear amplification by calcium-dependent chloride channels in olfactory receptor cells. *Nature* 366, 283–286.
- Luch, H., Weber O., Nageswara Rao., Blum C T., and Fehling HJ (2007). Faithful activation of an extra-bright red fluorescent protein in knock-in Cre-reporter ideally suited for lineage tracing studies. *Eur. J. Immunol.* 37, 43-53.
- Luxenhofer, G., Breer, H., and Strotmann, J. (2008). Differential reaction of outgrowing olfactory neurites monitored in explant culture. *J. Comp. Neurol.* 509, 580–593.
- Lynch, J.W., and Barry, P.H. (1989). Action potentials initiated by single channels opening in a small neuron (rat olfactory receptor). *Biophys. J.* 55, 755–768.
- Lynch, J.W., and Barry, P.H. (1991). Properties of transient K⁺ currents and underlying single K⁺ channels in rat olfactory receptor neurons. *J. Gen. Physiol.* 97, 1043–1072.
- Ma, M., and Shepherd, G.M. (2000). Functional mosaic organization of mouse olfactory receptor neurons. *Proc. Natl. Acad. Sci. U.S.A.* 97, 12869–12874.
- Ma, M., Chen, W.R., and Shepherd, G.M. (1999). Electrophysiological characterization of rat and mouse olfactory receptor neurons from an intact epithelial preparation. *J. Neurosci. Methods* 92, 31–40.
- Ma, M., Grosmaître, X., Iwema, C.L., Baker, H., Greer, C.A., and Shepherd, G.M. (2003). Olfactory signal transduction in the mouse septal organ. *J. Neurosci.* 23, 317–324.
- Malnic, B., Godfrey, P.A., and Buck, L.B. (2004). The human olfactory receptor gene family. *Proc. Natl. Acad. Sci. U.S.A.* 101, 2584-2589.
- Malnic, B., Hirono, J., Sato, T., and Buck, L.B. (1999). Combinatorial receptor codes for odors. *Cell* 96, 713–723.
- Maue, R.A. (1987). Patch-clamp studies of isolated mouse olfactory receptor neurons. *J. Gen. Physiol.* 90, 95–125.
- McClintock, T.S., Adipietro, K., Titlow, W.B., Breheny, P., Walz, A., Mombaerts, P., and Matsunami, H. (2014). In vivo identification of eugenol-responsive and muscone-responsive mouse odorant receptors. *J. Neurosci.* 34, 15669-15678.

Menco, B., and Morrison, E.E. (2003). Morphology of the mammalian olfactory epithelium: form, fine structure, function, and pathology. 2nd ed. Marcel Dekker, New York.

Mombaerts, P. (1996). Targeting olfaction. *Curr. Opin. Neurobiol.* 6, 481-486.

Mombaerts, P., Wang, F., Dulac, C., Chao, S.K., and Nemes, A. (1996). Visualizing an olfactory sensory map. *Cell* 87, 675-86.

Mombaerts, P. (2006). Axonal wiring in the mouse olfactory system. *Annu. Rev. Cell Dev. Biol.* 22, 713-737.

Munger, S.D., and Leinders-Zufall, T. (2009). Subsystem organization of the mammalian sense of smell. *Annu. Rev. Physiol.* 71, 115-140.

Munger, S.D. (2009). Olfaction: Noses within noses. *Nature* 459, 521-522.

Klugbauer, N., Lacinova, L., Flockerzi, V., and Hofmann, F. (1995). Structure and functional expression of a new member of the tetrodotoxin-sensitive voltage-activated sodium channel family from human neuroendocrine cells. *J. Neurosci.* 14, 1084-7568.

Nakamura, T., and Gold, G.H. (1987). A cyclic nucleotide-gated conductance in olfactory receptor cilia. *Nature* 325, 442-444.

Nara, K., Saraiva, L.R., Ye, X., and Buck, L.B. (2011). A large-scale analysis of odor coding in the olfactory epithelium. *J. Neurosci.* 31, 9179-9191.

Nassar, M.A., Stirling, L.C., Forlani, G., Baker, M.D., Matthews, E.A., Dickenson, A.H., and Wood, J.N. (2004). Nociceptor-specific gene deletion reveals a major role for Nav1.7 (PN1) in acute and inflammatory pain. *Proc. Natl. Acad. Sci. U.S.A.* 101, 12706-12711.

Nef, P., and Hermans-Borgmeyer, I. (1992). Spatial pattern of receptor expression in the olfactory epithelium. *Proc. Natl. Acad. Sci. U.S.A.* 89, 8948-8952.

Ogura, T., Szebenyi, S.A., Krosnowski, K., Sathyanesan, A., Jackson, J., and Lin, W. (2011). Cholinergic microvillous cells in the mouse main olfactory epithelium and effect of acetylcholine on olfactory sensory neurons and supporting cells. *J. Neurophysiol.* 106, 1274-1287.

Oka, Y., Katada, S., Omura, M., Suwa, M., Yoshihara, Y., and Touhara, K. (2006). Odorant receptor map in the mouse olfactory bulb: in vivo sensitivity and specificity of receptor-defined glomeruli. *Neuron* 52, 857-869.

Omura, M., and Mombaerts, P. (2014). Trpc2-expressing sensory neurons in the main olfactory epithelium of the mouse. *Cell Rep.* 8, 583-595.

Omura, M., and Mombaerts, P. (2015). Trpc2-expressing sensory neurons in the mouse main olfactory epithelium of type B express the soluble guanylate cyclase Gucy1b2. *Mol. Cell. Neurosci.* 65, 114-124.

- Omura, M., Grosmaître, X., Ma, M., and Mombaerts, P. (2014). The β 2-adrenergic receptor as a surrogate odorant receptor in mouse olfactory sensory neurons. *Mol. Cell. Neurosci.* 58, 1–10.
- Pacifico, R., Dewan, A., Cawley, D., Guo, C., and Bozza, T. (2012). An olfactory subsystem that mediates high-sensitivity detection of volatile amines. *Cell Rep.* 2, 76–88.
- Partridge, S.R., Tsafnat, G., Coiera, E., and Iredell, J.R. (2009). Gene cassettes and cassette arrays in mobile resistance integrons. *FEMS Microbiol. Rev.* 33, 757–784.
- Pasterkamp, R.J., De Winter, F., Holtmaat, A.J., and Verhaagen, J. (1998). Evidence for a role of the chemorepellent semaphorin III and its receptor neuropilin-1 in the regeneration of primary olfactory axons. *J. Neurosci.* 18, 9962–9976.
- Pelosi, P. (2001). The role of perireceptor events in vertebrate olfaction. *Cell. Mol. Life Sci.* 58, 503–509.
- Pinching, A.J., and Powell, T.P.S. (1971). The neuropil of the glomeruli of the olfactory bulb. *J. Cell Sci.* 9, 347–377.
- Reisert, J., and Matthews, H.R. (1999). Adaptation of the odour - induced response in frog olfactory receptor cells. *J. Physiol.* 515, 801–813.
- Reisert, J., and Matthews, H.R. (2001). Response properties of isolated mouse olfactory receptor cells. *J. Physiol.* 530, 113–122.
- Reisert, J. (2010). Origin of basal activity in mammalian olfactory receptor neurons. *J. Gen. Physiol.* 136, 529–540.
- Rivière, S., Challet, L., Flügge, D., Spehr, M., and Rodriguez, I. (2009). Formyl peptide receptor-like proteins are a novel family of vomeronasal chemosensors. *Nature* 459, 574–577.
- Rodriguez, I., Feinstein, P., and Mombaerts, P. (1999). Variable patterns of axonal projections of sensory neurons in the mouse vomeronasal system. *Cell* 97, 199–208.
- Saito, H., Chi, Q., Zhuang, H., Matsunami, H., and Mainland, J.D. (2009). Odor coding by a Mammalian receptor repertoire. *Sci Signal* 2, ra9.
- Saito, H., Kubota, M., Roberts, R.W., Chi, Q., and Matsunami, H. (2004). RTP family members induce functional expression of mammalian odorant receptors. *Cell* 119, 679–691.
- Sanz, G., Schlegel, C., Pernollet, J.-C., and Briand, L. (2005). Comparison of odorant specificity of two human olfactory receptors from different phylogenetic classes and evidence for antagonism. *Chem. Senses* 30, 69–80.
- Schäfer, B.W., Fritschy, J.M., Murmann, P., Troxler, H., Durussel, I.,

Heizmann, C.W., and Cox, J.A. (2000). Brain S100A5 is a novel calcium-, zinc-, and copper ion-binding protein of the EF-hand superfamily. *J. Biol. Chem.* 275, 30623–30630.

Schild, D., and Restrepo, D. (1998). Transduction mechanisms in vertebrate olfactory receptors cells. *Physiol Rev.* 78, 429-66.

Schmid, A., Pyrski, M., Biel, M., Leinders-Zufall, T., and Zufall, F. (2010). Grueneberg Ganglion Neurons Are Finely Tuned Cold Sensors. *J. Neurosci.* 30, 7563–7568.

Scholz, P., Kalbe, B., Jansen, F., Altmueller, J., Becker, C., Mohrhardt, J., Schreiner, B., Gisselmann, G., Hatt, H., and Osterloh, S. (2016). Transcriptome analysis of murine olfactory sensory neurons during development using single cell RNA-Seq. *Chem. Senses* 10-1093.

Schroeder, B.C., Cheng, T., Jan, Y.N., and Jan, L.Y. (2008). Expression cloning of TMEM16A as a calcium-activated chloride channel subunit. *Cell* 134, 1019–1029.

Schwarting, G.A., and Raitcheva, D. (2004). Semaphorin 3A - mediated axon guidance regulates convergence and targeting of P2 odorant receptor axons. *Eur. J. Neurosci.* 19, 1800-1810.

Schwarzenbacher, K., Fleischer, J., and Breer, H. (2006). Odorant receptor proteins in olfactory axons and in cells of the cribriform mesenchyme may contribute to fasciculation and sorting of nerve fibers. *Cell Tissue Res.* 323, 211–219.

Schwarzenbacher, K., Fleischer, J., Breer, H., and Conzelmann, S. (2004). Expression of olfactory receptors in the cribriform mesenchyme during prenatal development. *Gene Expr. Patterns* 4, 543–552.

Scott, J.W., and Scott-Johnson, P.E. (2002). The electroolfactogram: a review of its history and uses. *Microsc. Res. Tech.* 58, 152–160.

Serizawa, S., Miyamichi, K., Takeuchi, H., Yamagishi, Y., Suzuki, M., and Sakano, H. (2006). A neuronal identity code for the odorant receptor-specific and activity-dependent axon sorting. *Cell* 127, 1057–1069.

Sicard, G., and Holley, A. (1984). Receptor cell responses to odorants: similarities and differences among odorants. *Brain Res.* 292, 283–296.

Silvotti, L., Moiani, A., and Gatti, R. (2007). Combinatorial co - expression of pheromone receptors, V2Rs. *J. Neurochem.* 103, 1753-63.

Sinnarajah, S., Dessauer, C.W., Srikumar, D., Chen, J., Yuen, J., Yilma, S., Dennis, J.C., Morrison, E.E., Vodyanoy, V., and Kehrl, J.H. (2001). RGS2 regulates signal transduction in olfactory neurons by attenuating activation of adenylyl cyclase III. *Nature* 409, 1051–1055.

Solbu, T.T., and Holen, T. (2012). Aquaporin pathways and mucin secretion of

Bowman's glands might protect the olfactory mucosa. *Chem. Senses* 37, 35–46.

Stephan, A.B., Shum, E.Y., Hirsh, S., Cygnar, K.D., Reisert, J., and Zhao, H. (2009). ANO2 is the cilia calcium-activated chloride channel that may mediate olfactory amplification. *Proc. Natl. Acad. Sci. U.S.A.* 106, 11776–11781.

Strotmann, J., Levai, O., Fleischer, J., Schwarzenbacher, K., and Breer, H. (2004). Olfactory receptor proteins in axonal processes of chemosensory neurons. *J. Neurosci.* 24, 7754–7761.

Su, C.-Y., Menuz, K., and Carlson, J.R. (2009). Olfactory perception: receptors, cells, and circuits. *Cell* 139, 45–59.

Takahashi, T., Fournier, A., Nakamura, F., Wang, L.H., Murakami, Y., Kalb, R.G., Fujisawa, H., and Strittmatter, S.M. (1999). Plexin-neuropilin-1 complexes form functional semaphorin-3A receptors. *Cell* 99, 59–69.

Taniguchi, M., Nagao, H., Takahashi, Y.K., Yamaguchi, M., Mitsui, S., Yagi, T., Mori, K., and Shimizu, T. (2003). Distorted odor maps in the olfactory bulb of semaphorin 3A-deficient mice. *J. Neurosci.* 23, 1390–7.

Tazir, B., Khan, M., Mombaerts, P., and Grosmaître, X. (2016). The extremely broad odorant response profile of mouse olfactory sensory neurons expressing the odorant receptor MOR256-17 includes TAAR ligands. *Eur. J. Neurosci.* 43, 608–17.

Tian, H., and Ma, M. (2004). Molecular organization of the olfactory septal organ. *J. Neurosci.* 24, 8383–8390.

Toledo-Aral, J.J., Moss, B.L., He, Z.-J., Koszowski, A.G., Whisenand, T., Levinson, S.R., Wolf, J.J., Silos-Santiago, I., Haleboua, S., and Mandel, G. (1997). Identification of PN1, a predominant voltage-dependent sodium channel expressed principally in peripheral neurons. *Proc. Natl. Acad. Sci. U.S.A.* 94, 1527–1532.

Touhara, K., Sengoku, S., Inaki, K., Tsuboi, A., Hirono, J., Sato, T., Sakano, H., and Haga, T. (1999). Functional identification and reconstitution of an odorant receptor in single olfactory neurons. *Proc. Natl. Acad. Sci. U.S.A.* 96, 4040–4045.

Trombley, P.Q., and Westbrook, G.L. (1991). Voltage-gated currents in identified rat olfactory receptor neurons. *J. Neurosci.* 11, 435–444.

Trotier, D., and Døving, K.B. (1998). “Anatomical Description of a New Organ in the Nose of Domesticated Animals” by Ludvig Jacobson (1813). *Chem Senses* 23, 743–754.

Vogalis, F. (2005). Electrical Coupling in Sustentacular Cells of the Mouse Olfactory Epithelium. *J. Neurophysiol.* 94, 1001–1012.

Vogalis, F., Hegg, C.C., and Lucero, M.T. (2005). Ionic conductances in

- sustentacular cells of the mouse olfactory epithelium. *J. Physiol.* 562, 785-99.
- Wang, F., Nemes, A., Mendelsohn, M., and Axel, R. (1998). Odorant receptors govern the formation of a precise topographic map. *Cell* 93, 47–60.
- Wang, G., Carey, A.F., Carlson, J.R., and Zwiebel, L.J. (2010). Molecular basis of odor coding in the malaria vector mosquito *Anopheles gambiae*. *Proc. Natl. Acad. Sci. U.S.A.* 107, 4418–4423.
- Weid, von der, B., Rossier, D., Lindup, M., Tuberosa, J., Widmer, A., Col, J.D., Kan, C., Carleton, A., and Rodriguez, I. (2015). Large-scale transcriptional profiling of chemosensory neurons identifies receptor-ligand pairs in vivo. *Nat. Neurosci.* 18, 1455–1463.
- Weiss, J., Pyrski, M., Jacobi, E., Bufe, B., Willnecker, V., Schick, B., Zizzari, P., Gossage, S.J., Greer, C.A., Leinders-Zufall, T., et al. (2011). Loss-of-function mutations in sodium channel Nav1.7 cause anosmia. *Nature* 472, 186–190.
- Wong, S.T., Trinh, K., Hacker, B., Chan, G., and Lowe, G. (2000). Disruption of the type III adenylyl cyclase gene leads to peripheral and behavioral anosmia in transgenic mice. *Neuron*. 27, 487-97.
- Wysocki, C., Wellington, J., and Beauchamp, G. (1980). Access of urinary nonvolatiles to the mammalian vomeronasal organ. *Science* 207, 781–783.
- Yang, Y.D., Cho, H., Koo, J.Y., Tak, M.H., Cho, Y., Shim, W.-S., Park, S.P., Lee, J., Lee, B., Kim, B.-M., et al. (2008). TMEM16A confers receptor-activated calcium-dependent chloride conductance. *Nature* 455, 1210–1215.
- Yu, C.R., Power, J., Barnea, G., O'Donnell, S., Brown, H.E.V., Osborne, J., Axel, R., and Gogos, J.A. (2004). Spontaneous neural activity is required for the establishment and maintenance of the olfactory sensory map. *Neuron* 42, 553–566.
- Yu, Y., de March, C.A., Ni, M.J., Adipietro, K.A., Golebiowski, J., Matsunami, H., and Ma, M. (2015). Responsiveness of G protein-coupled odorant receptors is partially attributed to the activation mechanism. *Proc. Natl. Acad. Sci. U.S.A.* 112, 14966–14971.
- Zapiec, B., and Mombaerts, P. (2015). Multiplex assessment of the positions of odorant receptor-specific glomeruli in the mouse olfactory bulb by serial two-photon tomography. *Proc. Natl. Acad. Sci. U.S.A.* 112, E5873–E5882.
- Zhang, J., Huang, G., Dewan, A., Feinstein, P., and Bozza, T. (2012). Uncoupling stimulus specificity and glomerular position in the mouse olfactory system. *Mol. Cell. Neurosci.* 51, 79–88.
- Zhang, J., Pacifico, R., Cawley, D., Feinstein, P., and Bozza, T. (2013). Ultrasensitive detection of amines by a trace amine-associated receptor. *J. Neurosci.* 33, 3228–3239.

Zhang, X., and Firestein, S. (2002). The olfactory receptor gene superfamily of the mouse. *Nat. Neurosci.* 5, 124–133.

Zhang, X., Rogers, M., Tian, H., Zhang, X., Zou, D.-J., Liu, J., Ma, M., Shepherd, G.M., and Firestein, S.J. (2004). High-throughput microarray detection of olfactory receptor gene expression in the mouse. *Proc. Natl. Acad. Sci. U.S.A.* 101, 14168–14173.

Zhao, H., Ivic, L., Otaki, J.M., Hashimoto, M., and Mikoshiba, K. (1998). Functional expression of a mammalian odorant receptor. *Science*. 279, 237–242.

Zheng, C., Feinstein, P., Bozza, T., Rodriguez, I., and Mombaerts, P. (2000). Peripheral olfactory projections are differentially affected in mice deficient in a cyclic nucleotide-gated channel subunit. *Neuron* 26, 81–91.

Zippel, H.P., and Lüthje, L.G.C. (2003). Recent Progress in Aquatic Vertebrate Olfaction. In *Sensory Processing in Aquatic Environments*, (New York, NY: Springer New York), pp. 283–300.

Zou, D.-J., Chesler, A.T., Le Pichon, C.E., Kuznetsov, A., Pei, X., Hwang, E.L., and Firestein, S. (2007). Absence of adenylyl cyclase 3 perturbs peripheral olfactory projections in mice. *J. Neurosci.* 27, 6675–6683.

Zufall, F., Shepherd, G.M., and Firestein, S. (1991). Inhibition of the olfactory cyclic nucleotide gated ion channel by intracellular calcium. *Proc. Biol. Sci.* 246, 225–230.

7 Publications and acknowledgments

7.1 Publication

Tazir, B., Khan, M., Mombaerts, P., and Grosmaître, X. (2016). The extremely broad odorant response profile of mouse olfactory sensory neurons expressing the odorant receptor MOR256-17 includes TAAR ligands. *Eur. J. Neurosci.* 43, 608-617.

7.2 Acknowledgments

At the end of my thesis I would like to thank all those people who made this thesis possible.

First of all, I would like to express my very sincere gratitude to my advisor Dr. Peter Mombaerts, who offered me the opportunity to do a Ph.D. in his group, and to make progress in my scientific career. I thank him for trusting me, by giving me the freedom to collaborate and work outside the lab.

Many thanks must go to my Doktorvater Professor Frank Zufall at the Universität des Saarlandes, who accepted me to be attached to his group.

I would like to express my deepest gratitude to my co-advisor Dr. Xavier Grosmaître at Centre du Goût et de l'Alimentation, Dijon, France. I thank him for support, encouragement, and precious advice. I thank him for giving me the opportunity to work in his group and for his availability. I did not remember how many times I knocked at your office door, what I remember that I always had an answer to my questions. I also thank him for all the effort and the time he put into training me in the scientific field, for all the pleasant moment inside and outside the lab. Xavier, it was always a pleasure working with you.

I would also like to express my sincere gratitude to my co-advisor Dr. Mona Khan at the Max Planck Research Unit for Neurogenetics, for her encouragement at the hardest moment during this thesis, for guidance, and for all the effort she put into training me.

I am very thankful to my colleague Dr. Masayo Omura for support and guidance.

I am also very thankful to Erwin Lewitzki and Gabriele Mörschbacher for all the paper work to make my registration at Universität des Saarlandes.

I am thankful to our lab manager Dr. Guido Haschke for advice and rich scientific discussion.

I am very thankful to my colleague Dr. Sheryl Tan for the thesis proofreading, discussion and advice to improve the quality of the manuscript. Thanks to Dr.

Martin Vogel and Dr. Olaf Bressel for support and advice.

I am thankful to all my colleagues in the Grosmaître group especially to Dr. David Jarrillaut for his support, advice and scientific discussion; and to all my colleagues in our group for all the lovely moments we spend inside and outside the lab. Also many thanks to all my colleagues in the Zufall group.

I am thankful to Ali and our animal caretakers; and to all our technicians in the lab for help, support and for the nice moment in the lab.

I am thankful to Anne our animal caretaker at Centre du Goût et de l'Alimentation, Dijon, France, for excellent animal care.

I am thankful to Professor Laurent Brondel at Centre du Goût et de l'Alimentation, Dijon, France, who often generously accommodated me and made me feel home. I thank him for the precious advice and for all the pleasant moments.

I acknowledge my gratitude to the generous funding support of the Max Planck Society.

Finally, I want to express the profound gratitude from my deep heart to my grandmother Zohra, my parents, my wife, my cousin Ameer and my siblings for their love and continuous support; for my anti-stress my lovely daughter Myriam.

